Automated Measurement of Neuromuscular Jitter Based on EMG Signal Decomposition

By

KUN HE

A thesis
presented to the University of Waterloo
in fulfillment of the
thesis requirement for the degree of
Master of Applied Science
in
Systems Design Engineering

Waterloo, Ontario, Canada, 2007

I hereby declare that I am the sole author of this thesis. This is a true copy of the thesis, including any required final revisions, as accepted by my examiners.

I understand that my thesis may be made electronically available to the public.

Abstract

The quantitative analysis of decomposed electromyographic (EMG) signals reveals information for diagnosing and characterizing neuromuscular disorders. Neuromuscular jitter is an important measure that reflects the stability of the operation of a neuromuscular junction. It is conventionally measured using single fiber electromyographic (SFEMG) techniques. SFEMG techniques require substantial physician dexterity and subject cooperation. Furthermore, SFEMG needles are expensive, and their re-use increases the risk of possible transmission of infectious agents. Using disposable concentric needle (CN) electrodes and automating the measurment of neuromuscular jitter would greatly facilitate the study of neuromuscular disorders. An improved automated jitter measurment system based on the decomposition of CN detected EMG signals is developed and evaluated in this thesis.

Neuromuscular jitter is defined as the variability of time intervals between two muscle fiber potentials (MFPs). Given the candidate motor unit potentials (MUPs) of a decomposed EMG signal, which is represented by a motor unit potential train (MUPT), the automated jitter measurement system designed in this thesis can be summarized as a three-step procedure: 1) identify isolated motor unit potentials in a MUPT, 2) detect the significant MFPs of each isolated MUP, 3) track significant MFPs generated by the same muscle fiber across all isolated MUPs, select typical MFP pairs, and calculate jitter. In Step one, a minimal spanning tree-based 2-phase clustering algorithm was developed for identifying isolated MUPs in a train. For the second step, a pattern recognition system was designed to classify detected MFP peaks. At last, the neuromuscular jitter is calculated based on the tracked and selected MFP pairs in the third step. These three steps were simulated and evaluated using synthetic EMG signals independently, and the whole system is preliminary implemented and evaluated using a small simulated data base.

Compared to previous work in this area, the algorithms in this thesis showed better performance and great robustness across a variety of EMG signals, so that they can be applied widely to similar scenarios. The whole system developed in this thesis can be implemented in a large EMG signal decomposition system and validated using real data.

Acknowledgements

I would like to express my sincere gratitude to my supervisor, Dr. Daniel Stashuk, for providing me with the opportunity to do this research. His inspiring guidance, patient instruction, and continuous encouragement throughout my graduate study and research work make this thesis possible.

I would also like to thank my thesis readers, Dr. Catherine Burns and Dr. Chris Eliasmith for reviewing of this thesis, and their most helpful comments and valuable suggestions.

I take this opportunity to express my appreciation to Marzieh Abdollahi and other members in Biomedical Signal Processing Lab in University of Waterloo, for their support and help.

Finally, my appreciation goes to my parents and my husband, Shen Luo. Thanks to their love, help, understanding, and support throughout my study and work.

Contents

List of Tables

List of Figures

Acronyms

CN:	concentric needle
EMG:	electromyography
IPI:	inter potential interval
ISO-MUP:	isolated motor unit potential
MCD:	mean consecutive difference
MFP:	muscle fiber potential
MN:	monopolar needle
MU:	motor unit
MUP:	motor unit potential
MUPT:	motor unit potential train
NMJ:	neuromuscular junction
SFN:	single fiber needle
SUP-MUP:	superimposed motor unit potential

Chapter 1

Introduction

Electromyographic (EMG) signals can reflect the electrical properties and activities of a contracting muscle. The analysis of EMG signals provides important information for the diagnosis and characterization of neuromuscular disorders. Depending on the electrode used, EMG signals basically consist of the electrical activities of one or multiple motor units (MUs) within the detection area of the electrode, which are called motor unit potentials (MUPs). To study the electrical activity of individual muscle fibers, the technique of single fiber (SF) EMG is used for investigating the neuromuscular jitter phenomena [Stalberg 1971]. SF-EMG techniques use the most precise and fine electrodes -- single fiber needle electrodes (SFN) -- to identify individual muscle fiber potentials (MFPs).

Neuromuscular jitter reflects the transmission stability of neuromuscular junctions (NMJs). It is a sensitive clinical test for evaluation of the NMJ dysfunction. The measurement of jitter has been conventionally completed using SFN electrodes. However, using SFN electrodes is time-consuming since it requires the dexterity of an experienced physician and the cooperation of the patient. In addition, SFN electrodes are expensive, and their re-use increases the risk of possible transmission of infectious agents. Recently, researchers have found that neuromuscular jitter can be measured from EMG signals detected using concentric needle (CN) electrodes with comparable accuracy as SFEMG. Adopting disposable CN electrodes for the automated measurement of jitter would greatly facilitate the study and diagnosis of neuromuscular junction disorders.

Neuromuscular jitter is expressed as the variability of time intervals between two MFPs of the same MUP. To measure jitter from an EMG signal, individual MFP contributions (or MFPs) have to be detected accurately from an MUP, and at least one specific MFP pair has to be identified consistently from the same motor unit. The process of EMG signal decomposition can resolve a routine EMG signal into individual MUPs and assign MUPs generated by the same motor unit to an MUPT. Previous research has shown that MFPs can be detected by 2nd order filtering of an MUP signal, and some tentative work has been done to select the MFPs and MFP

pairs. In this thesis, a three-step procedure has been developed for measuring jitter from decomposed CN detected EMG signals. The three-step procedure includes a preprocessing step to identify the isolated MUPs (ISO-MUPs) in an MUPT, a major step to detect the significant MFPs of each ISO-MUP, and a final step to select typical MFP pairs and calculate jitter. Evaluated by simulated, the performance of each step as well as the whole procedure is improved compared to former work. The whole system developed in this thesis can be integrated to any EMG signal decomposition tool as a jitter measurement system or as an independent application. The well-modularized system allows each step operated and adjusted independently, which makes it easy to modify or reuse these modules for a wide range of applications in the biomedical signal processing area.

The remainder of this thesis is organized as follow. Chapter 2 reviews the background knowledge of neuromuscular electrophysiology, EMG signal composition, and jitter measurement. Chapter 3 provides an overview of CN-detected EMG-signal-decomposition-based automated neuromuscular jitter measurement. The basic ideas of filtering are explained, previous research is discussed, and the three-step procedure is described briefly. For algorithm evaluation, the data simulation method is introduced as well. The following Chapters 4 to 6 are dedicated to the three steps of the procedure respectively. Chapter 7 presents the conclusions and discussions regarding this research.

Chapter 2

Background

"Electromyography is the study of muscle function through the inquiry of the electrical signal the muscles emanate" [Basmajian 1985]. Following the birth of neurophysiology in 1953, the study of electromyographic (EMG) signals has fascinated a wide variety of researchers and grown rapidly. Since Adrian and Bronk's introduction of the concentric needle electrode in 1929, electromyography has developed into a fundamental technique of electrodiagnostic medicine consultation [Dumitru 2002].

Technological advances in electronics and microcomputers have enabled the development of methods for investigating the electrical activity generated by a muscle. For example, the needle EMG examination has been a routine evaluation procedure in the clinical diagnosis of nerve and muscle disease. Signals are acquired using a CN needle or a monopolar needle electrode and recorded by a cable-connected instrument. However, the recorded EMG waveform is traditionally assessed subjectively from its appearance and corresponding sound from the monitors by an electromyographer with trained eyes and ears. When abnormalities of the routine EMG are equivocal and serial assessments of disease progression are required, a statistically valid sample of EMG signals is quantified and characterized manually or using automated computer-based methods, which is called the quantitative analysis of EMG. EMG signal decomposition is a type of quantitative analysis. It helps not only to detect abnormalities more accurately, but also to evaluate their severity, status, duration, etc. With the rapid development of computers and modern signal processing technologies and their dramatically decreasing cost, the integration of automated quantitative analysis and the routine examination is tending to be the standard function of some EMG equipment. From the 1980s, interest has been focused on the ability to analyze EMG signals quantitatively and automatically. [Guiheneuc 1983, Stalberg 1983, Antoni 1983, Stewart 1989, Stashuk 1999, Dumitru 2002]

The SF-EMG technique was developed by Stalberg and Ekstedt in the early 1960s. Exploiting a fine needle with small pickup radius, SFEMG signals provide physiological information about just one or a few muscle fibers. SFEMG has become

a major tool in the electrodiagnosis of disorders of the neuromuscular junction, which are the focal abnormalities of motor unit architecture. Neuromuscular jitter is one of the main measurements of quantified SFEMG analysis which still has to be measured manually in most clinical applications. In addition, SFEMG requires a special electrode which is expensive, and its reuse increases the risk of transmission of infectious agents. Many attempts have been made to measure jitter using standard EMG electrodes, and some of them have produced encouraging results [Payan 1978, Weichers 1985, Buchman 1992, Ertas 2000, Sarrigiannis 2006, and Benatar 2006.

This background chapter briefly describes topics about neuromuscular physiology, the generation of EMG signals, SFEMG and jitter measurement, and EMG signal decomposition.

2.1 Neuromuscular Physiology

The practice of electromyography as well as electrodiagnostic medicine in general is based on knowledge of nerve and muscle physiology. In short, any voluntary movement is produced by a hierarchical procedure: a stimulus initiates from the cortex, passes along the spinal cord, goes through the neurons, transmits to muscle fibers through neuromuscular junctions, and finally results in muscle fiber contractions. The major consequence of the elaborate information processing within the brain is the contraction of skeletal muscle.

A typical skeletal muscle is composed of many thousands of muscle fibers working in parallel and organized into a smaller number of motor units. Muscle fibers are multinucleated cells with diameters from 10 to 100 μm, and lengths from a few mm up to 30 cm [Basmajian 1985]. Like all living cells, a muscle fiber is enclosed by a plasma membrane and has an electrical potential across its membrane. When the electrical signal from the nerve arrives at the muscle fiber, membrane depolarization occurs. Subsequently, an action potential is generated and propagates along the membrane. As a result of electrochemical interactions, muscle fiber contraction then takes place. [Dumitru 2002]

A typical muscle is controlled by about 100 motoneurons whose cell bodies lie in the spinal cord or brain stem, and whose axons bifurcate widely to innervate from several

to 1000 muscle fibers scattered over a part of the muscle. Each muscle fiber is normally connected to only one motoneuron in only one position, usually near its midpoint. The ensemble of muscle fibers innervated by an individual motoneuron together with the motoneuron itself is referred to as a motor unit (see Figure 2.1). MU architecture varies considerably among different muscles and is diversified by various neuromuscular disease processes. [Kandel 2000, Dumitru 2002]

The functional connection between a motoneuron and a target muscle fiber is a synapse called the endplate or neuromuscular junction (NMJ). For each action potential in the motoneuron, the synapse releases sufficient transmitter to depolarize the membrane of the muscle fiber to its threshold for a muscle fiber action potential (MFAP). All of the muscle fibers belonging to the same motor unit respond synchronously to each discharge of the motoneuron, and the MFAPs summate to a motor unit action potential (MUAP). [Kandel 2000, Dumitru 2002]

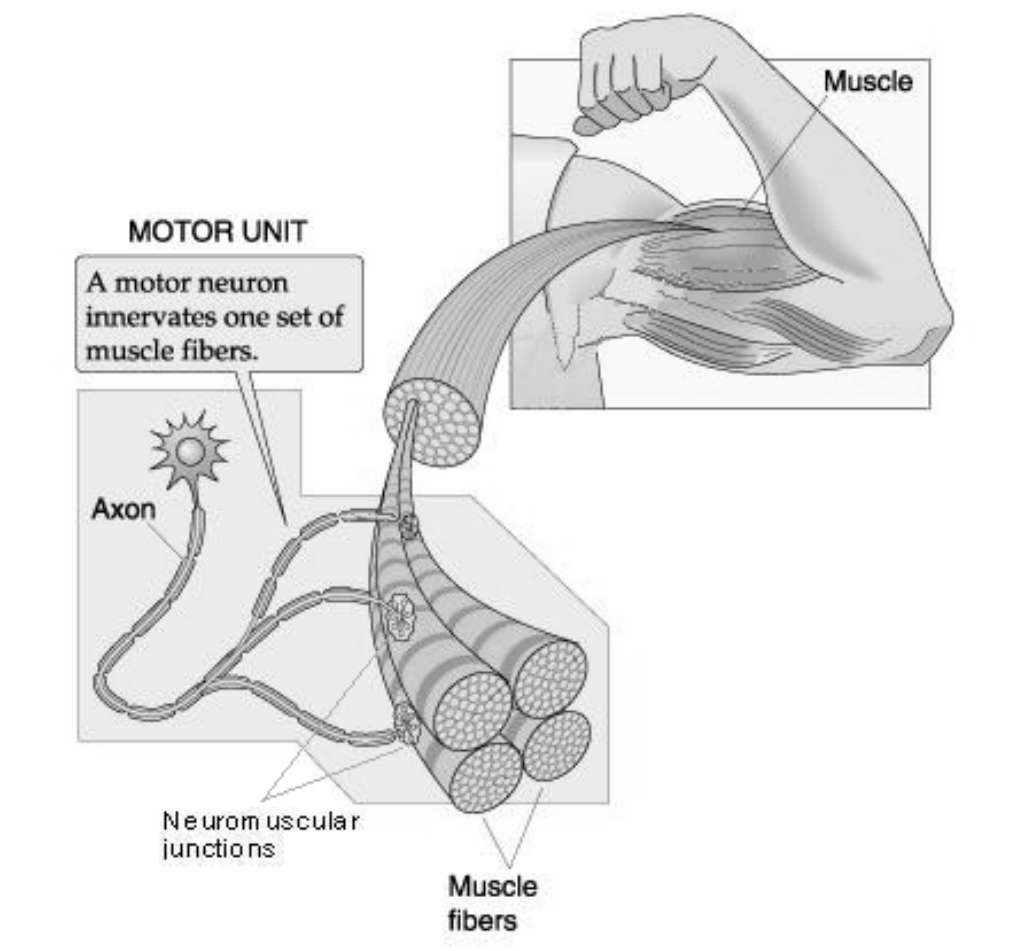

Figure 2.1: Motor Unit [Boron 2003]

Once the membrane of an NMJ is depolarized to its threshold, an action potential propagates along the membrane of the muscle fiber, which gives rise to relatively large potential gradients in the extracellular fluid around the muscle fiber. All muscle fibers of a motor unit are activated in synchrony, so the resulting currents sum to generate an electrical signal that can be readily detectable even outside the muscle. Furthermore, the asynchronous barrage of action potentials from many motoneurons produces overlapping action potentials arising from multiple motor units. The resulting complex pattern of electrical potentials can be recorded as an electromyographic (EMG) signal using electrodes in the muscle or on the overlying skin. The relative timing and amplitude of these patterns recorded in or over particular muscles reflect closely the aggregate activity of motoneurons innervating these muscles.

2.2 Acquisition and Decomposition of EMG Signals

2.2.1 Needle Electrodes for EMG

EMG signals can be detected by electrodes inserted in the muscle tissue or located on the skin surface over the interested muscle, where these electrodes are referred to as needle electrodes or surface electrodes respectively. Although surface electrodes can be conveniently used to detect gross EMG signals, by far the most popular electrode category for electrodiagnosis is the needle electrode [Basmajian 1985]. These needle electrodes are commonly used in clinical practice: standard concentric needle (CN), monopolar needle (MN), and single-fiber needle (SFN), while CN and MN electrodes are used in routine clinical EMG examination. [Dumitru 2002] (see Figure 2.2).

As shown in Figure 2.2, the SFN electrode is the most selective type of electrode among these three. The central 25 μm diameter platinum wire exits approximately 4 mm from the beveled tip through a side port in the cannula. With an uptake radius of about 300 μm, it is possible to detect a single MFP using a SFN electrode. The SFN electrode, specially constructed for detecting SFEMG signals, primarily reflects the activity of only one (with probability of 70%) or two (around 25%) muscle fibers.

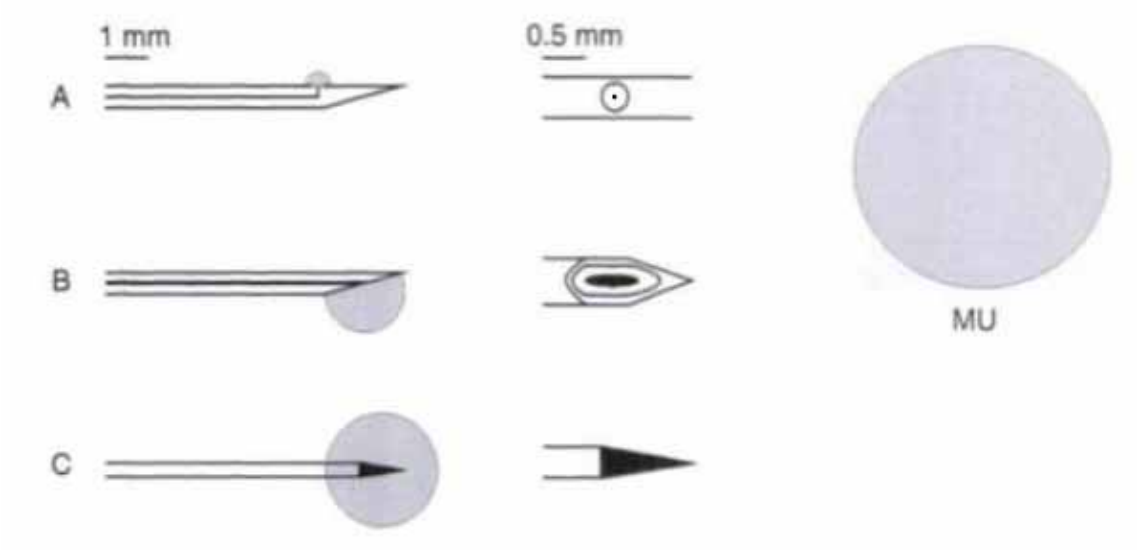

Figure 2.2: Three types of EMG needle electrodes. A schematic view of the pickup area (grey part in the 1st column) and the recording surface (black part in the 2nd column) of different electrodes are shown compared to a typical motor unit territory (inset). (A): SFN electrode, (B): CN electrode, (C): MN electrode. [Merletti 2004]

The CN electrode has an elliptical (150 x 580 μm) detection surface located in the beveled tip of a cannula. Signals detected by the 0.07 mm^2 recording surface are referenced to the cannula so that interference from distant muscle fibers is reduced in the detected signals. On average, CN-EMG signals are derived from 15 to 20 muscle fibers that lie within the uptake area of the needle electrode using standard filter settings of 10 – 10 kHz. The CN electrode is one of the routine electrodes used for clinical detection of EMG signals.

The MN electrode consists of a solid insulated pin, and the detection area is the denuded cone tip, where the standard recording surface is between 0.15 and 0.20 mm^2. A separate surface electrode is needed as a reference for an MN electrode. Compared to CN electrodes, MNs tend to detect larger electrical signals including greater amounts of baseline noise. Therefore, MNs are not as sensitive as CNs for detecting the activity of a motor unit; however, they are more comfortable and economical. The MN electrode is also one of the standard electrodes used for clinical applications.

Differences in the size and construction of CN, MN, and SF electrodes and their reference setups give them various detection characteristics, especially between the SFN and routine electrodes (i.e., CN and MN). In this thesis, the CN was chosen as the representative standard electrode. Comparison of SFN EMG and CN-EMG based neuromuscular jitter measurement will be made based on work in this thesis.

2.2.2 Composition of a EMG Signal: Muscle Fiber Potential (MFP), Motor Unit Potential (MUP), and Motor Unit Potential Train (MUPT)

The electrical activity of a skeletal muscle cell is a transmembrane action potential spikes, which can be perceived extracellularly. To distinguish the membrane action potential generated by a muscle fiber (MFAP) from the corresponding potential detected by an electrode, the latter is called a muscle fiber potential (MFP) in this thesis. Following in the same way, a motor unit potential (MUP) refers to the detected potential of a motor unit in contrast with an MUAP. The detected potential can be considered the corresponding filtered action potential which is filtered by the intermediate tissue and the electrode itself.

An MFP is a primary component of an EMG signal; in addition, an EMG signal results from electrical contributions from all active muscle fibers. Typically, the shape of a MFP is a triphasic voltage waveform, and it corresponds to the procedure that (i) an action potential propagates along the fiber towards the electrode, (ii) moves away from the electrode, and (iii) decays. The duration usually ranges from 2 to 6 ms (see Figure 2.3). The characteristics of the waveform depend on the size of the muscle fiber, the speed of action potential propagation, the configuration of the electrode, and the distance between the muscle fiber and the detection surface. Generally, the magnitude and high frequency content of a MFP decrease exponentially as the distance between the fiber and the detection surface increases. For example, the peak-to-peak amplitude may decrease approximately 75% if the electrode is moved 100 μm away from a fiber. Thus, the contribution of any individual muscle fiber to an MUP crucially depends on its distance from the detection surface. Decreases of amplitude with distance vary with the different types of electrode. As shown in Figure 2.4, needles with a small detection surface show a steep decline of MFP amplitude with increasing distance, therefore they are more selective and detect primarily activity of the closest muscle fibers. Conversely, electrodes with large detection surfaces are less selective, picking up potentials over a larger area. [Brown 1984, Merletti 2004]

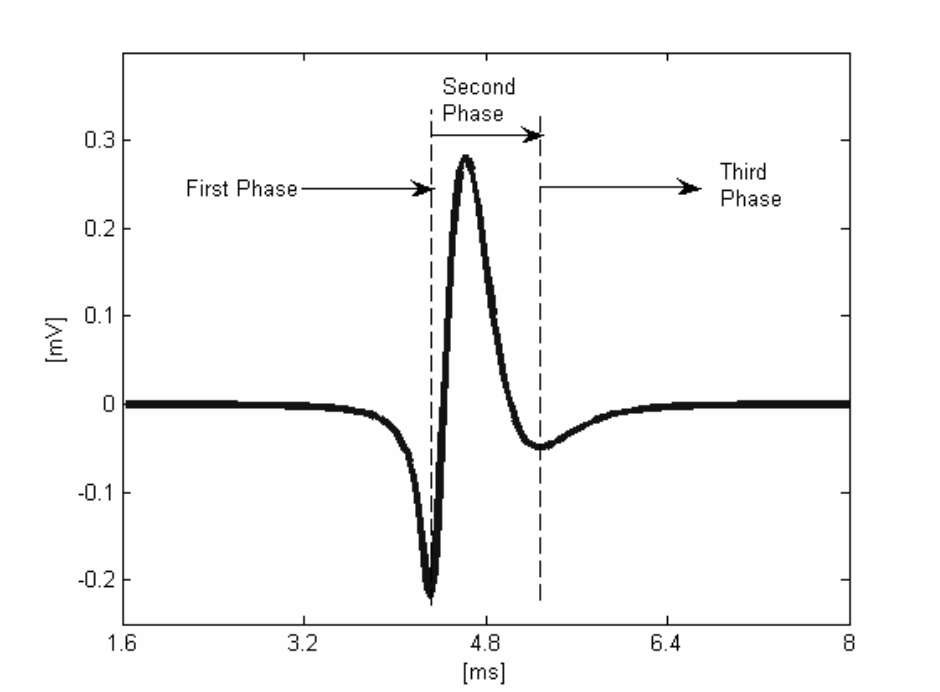

Figure 2.3: Typical MFP waveform

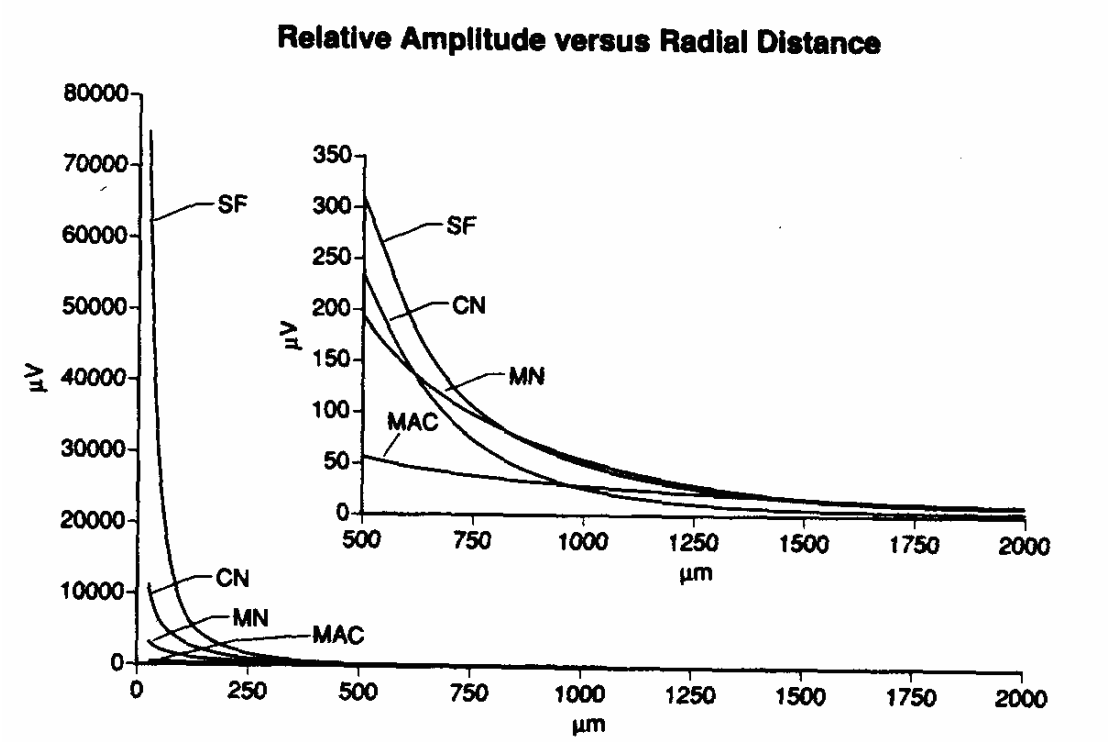

Figure 2.4: Amplitude versus electrode type and distance [King 1997] (SF: single fiber, CN: concentric, MN: monopolar, MAC: macro needle)

Summation of the synchronized activity of muscle fibers belonging to the same motor unit, an MUP, is the linear superposition of MFPs with some temporal delay:

$$\mathrm{MUP}_j = \sum_{i=1}^{N_j} \mathrm{MFP}_{ij}(t-\tau_i)s_i \,, \tag{2.1}$$

where, $\mathrm{MUP}_j(t)$ is the j^{th} MUP detected; $\mathrm{MFP}_{ij}(t)$ is the i^{th} MFP belonging to the j^{th} motor unit; N_j is the number of fibers of the j^{th} motor unit; t is the temporal variable of the waveforms; τ_i is the conduction delay of $\mathrm{MFP}_{ij}(t)$ at the detection site; s_i is a binary flag for muscle fiber i firing ($s_i = 1$) or blocking (i.e., does not fire) ($s_i = 0$) [Stashuk 2001]. The summating MFPs for a motor unit are not perfectly aligned due to the fact that conduction times from the NMJs to the electrode vary with different fibers (i.e., τ_i differs with i). Consequently, MUP amplitude may be affected by the partial phase differences of the contributing MFPs, and the shape could be serrated or polyphasic. Although the size of an MUP is theoretically determined by the number of fibers for that motor unit (i.e., N_j), it mostly depends on the location and diameter of the closet few fibers.

The voluntary discharges of a motor unit are repetitive so as to maintain or increase the force output of a muscle. In the order of firing time, the collection of MUPs generated by the same motor unit is known as a motor unit potential train (MUPT). Following the definition in (2.1), an MUPT can be expressed as:

$$\mathrm{MUPT}_k(t) = \sum_{i=1}^{M_k} \mathrm{MUP}_{ik}(t-\delta_{ki}), \tag{2.2}$$

where, $\mathrm{MUPT}_k(t)$ is the MUPT for the k^{th} motor unit; $\mathrm{MUP}_{ik}(t)$ is the MUP corresponding to the i^{th} firing of the k^{th} motor unit; M_k is the number of firings of the k^{th} motor unit; δ_{ki} is the time of i^{th} firing of the k^{th} motor unit.

Ultimately, the superposition of the MUPTs of all active motor units results in a composite EMG signal:

$$\mathrm{EMG}(t) = \sum_{k=1}^{L} \mathrm{MUPT}_k(t) + n(t), \tag{2.3}$$

where, L is the number of active motor units; $n(t)$ is instrumentation noise. The composition of an EMG signal can be represented as in Figure 2.5. In fact, the composition is associated with the target muscle, the detection site, the contraction

level, and the configuration of the electrode. Using an electrode with a very small pickup area, such as a SFN electrode, EMG signals may primarily detect the electrical activity of only one or a few of the closet fibers.

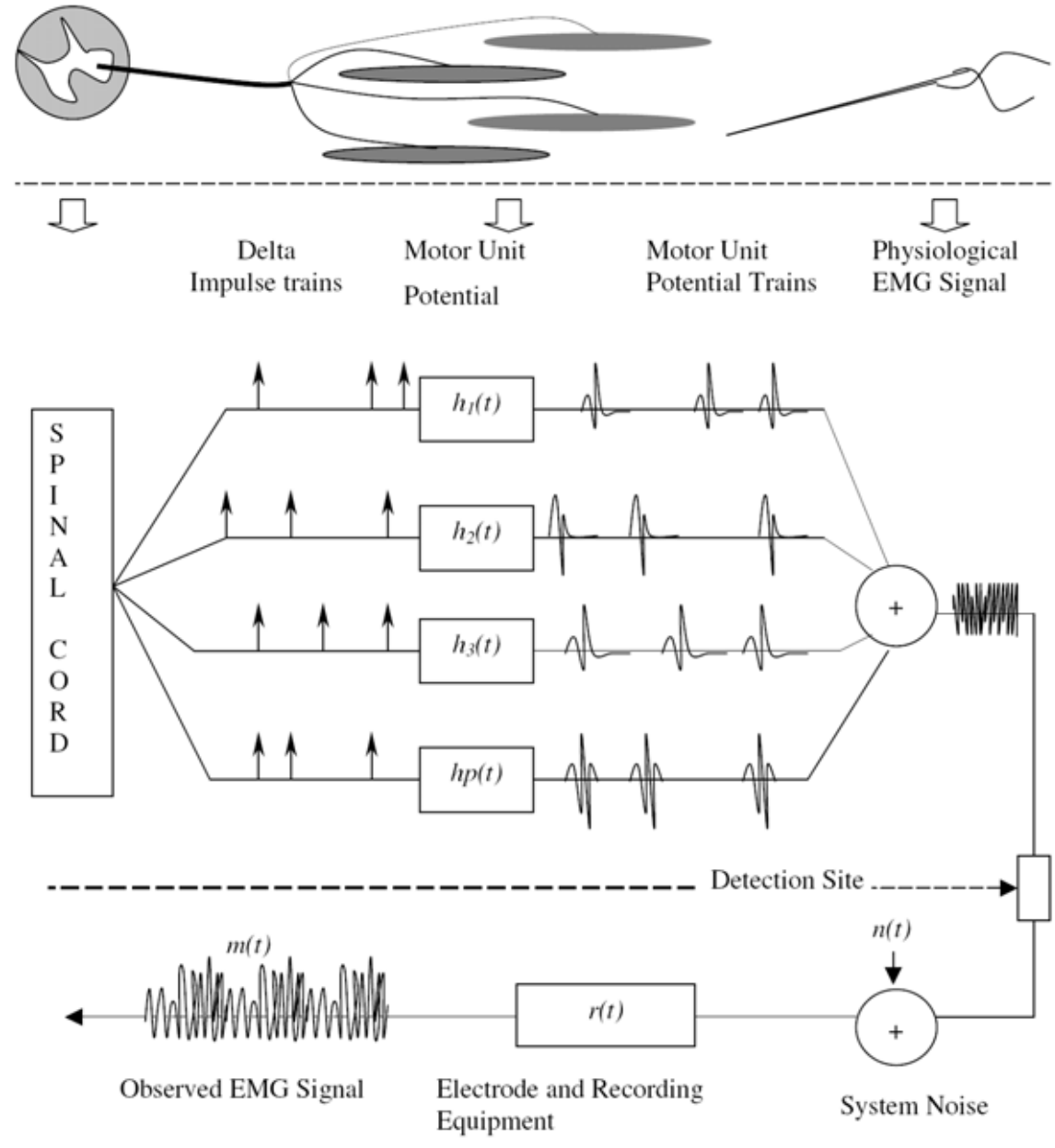

Figure 2.5: Models of the generation of an EMG signal [Basmajian 1985]

2.3 Single Fiber EMG and Neuromuscular Jitter

Since its development in the early 1960s, SFEMG has provided insight into details of motor unit structure and function and become a major tool in the electrodiagnosis of neuromuscular junction disorders. Using the specially constructed SFN electrode, SFEMG allows single and multiple MFPs to be measured with an accuracy of 1 μs or less. Owing to high spatial resolution, MFPs of individual motor units can be reliably recognized selectively. SFEMG signals are quantified mainly by measuring fiber density and neuromuscular jitter. Fiber density provides information about the innervation patterns of MUs. It is measured as the average number of potentials that are recognized as MFPs over 20 tests at different sites within the muscle. Neuromuscular jitter measurement by SFEMG is considered the most sensitive method for detecting disordered neuromuscular transmission, and is widely used to diagnose myasthenia gravis and other diseases of the NMJ. [Brown 2002, Dumitru 2002]

Even in healthy NMJs of a motor unit, there is a certain fluctuation in the time interval between the arrival time of the neuron impulse and the subsequent generation of an MFAP. In a motor unit, the amount of variability in the operation of a pair of NMJs can be assessed if two MFPs can be consistently detected and individually identified. Normally, by carefully positioning a SFN electrode close to the fibers of an MU, and high-pass filtering the detected suitable potentials with a cutoff frequency of 500 to 1,000 Hz, the activity of individual muscle fibers can be consistently identified.

Usually, the subject is asked to voluntarily recruit the associated motor unit or is stimulated repetitively, and successive sweeps are triggered off one MFP of the fiber pairs. With reference to the triggering MFP, the variability in transmission time at both NMJs is defined as the variation in latency of the other potential, which has been termed neuromuscular jitter (see Figure 2.6). When this jitter is greatly increased, indicating a pronounced NMJ disturbance, one fiber may fail to generate a potential with some MU discharges. This is seen when some potentials are missing in some MU discharges, and this phenomenon is called blocking.

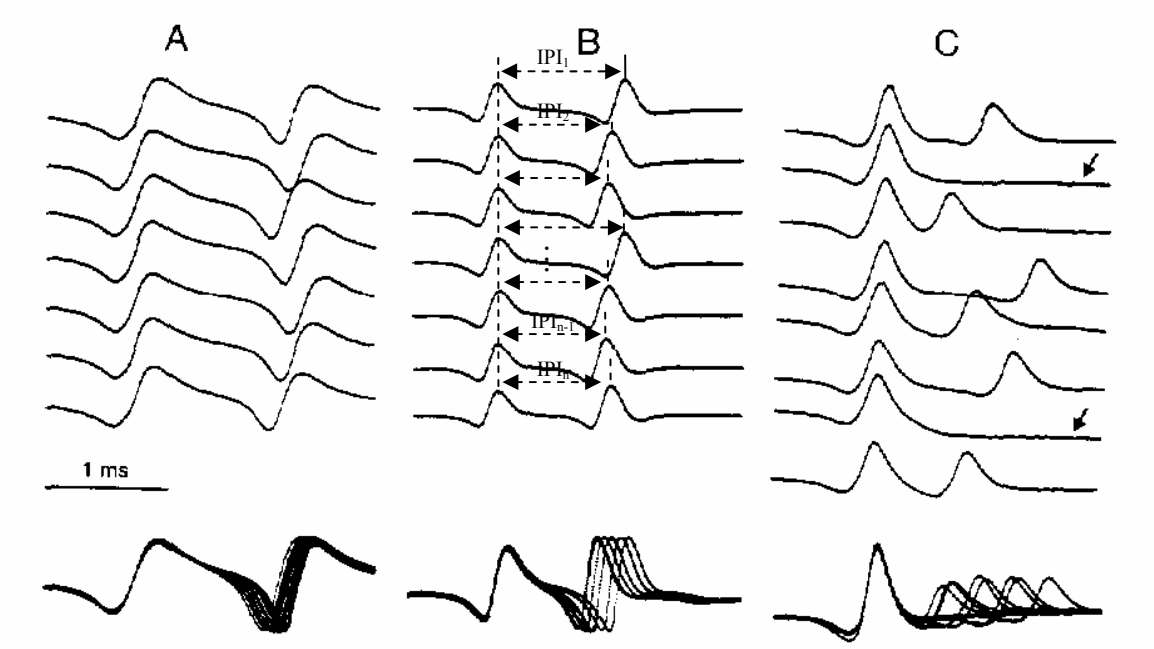

Figure 2.6: Neuromuscular jitter and blocking. A: normal jitter, B: increased jitter but no blocking, and C: increased jitter and occasional blocking (arrows). In the lower part, discharges are superimposed. [Stalberg 1997]

The time interval between the two MFPs, called the interpotential interval (IPI) (see Figure 2.6), varies from one discharge to another. Defined as in formula (2.4), the statistic typically used to quantify neuromuscular jitter is the mean consecutive difference (MCD) which is relatively unaffected by any trends in the mean value of the time interval between the MFPs. At least 50 IPIs should be analyzed to compute the MCD. Jitter can be also calculated on the ordered set of IPIs, which is called the mean sorted difference (MSD). Usually, the smaller of the MCD and MSD values is used to represent jitter in the pair of potentials. The reference value for normal neuromuscular jitter is from 5 to 55 μs for different muscles [Brown 2002].

$$MCD = \frac{\left|IPI_1 - IPI_2\right| + \left|IPI_2 - IPI_3\right| + \cdots + \left|IPI_{n-1} - IPI_n\right|}{n-1}. \qquad (2.4)$$

Neuromuscular jitter analysis can be quite tedious, time-consuming, and subject to errors when several MUs are active. In addition, the SF electrode is quite expensive and vulnerable, and its reuse has raised concern regarding the risk of accidental transmission of infectious agents such as prions. These limitations have prompted researchers to evaluate the possibility of employing some disposable needles with alternate filtering methods to detect single MFPs. Experiments have shown that

accuracies obtained using CN and MN-EMG for measuring neuromuscular jitter are comparable with SFEMG. Investigators still face the challenges of measuring jitter automatically from decomposed CN or MN-EMG signals. [Wiechers 1985, Clarke 1985, Buchman 1992, Stashuk 1999b, Ertas 2000, Sarrigiannis 2006, Benatar 2006].

2.4 EMG Signal Decomposition

EMG signal decomposition is a quantitative analysis process of identification and classification of individual MUPs in the interference pattern detected so as to determine the MUPTs that make up the signal. Despite some nonlinear effects such as temperature and very high lever of muscle contraction which can be ignored clinically, the decomposition of EMG signals is a linear signal process according to Formula 2.1 – 2.3. However, this practical process is complex for needle EMG because different MUPs may overlap in time to different degrees, and their shapes may deviate with motor unit property changes or electrode movements. Since the 1980s, many techniques have been developed to implement this process for intramuscularly detected signals with various degrees of automation [Merletti 2004, Stashuk 1999a]. A clinical quantitative EMG analysis system has been developed in the Biomedical Signal Processing Lab of the University of Waterloo, which would be the basic experimental environment for this research in practice.

To resolve a composite EMG signal into its significant and constituent MUPTs, EMG signal decomposition involves the two major steps of detecting MUPs and recognizing detected MUPs (See Figure 2.7). The detailed procedure includes signal acquisition, signal segmentation for detecting MUPs, MUP representation or feature extraction, MUPs clustering, supervised MUP classification, resolution of superimposed MUPs, and discovery of temporal relationships between MUPTs.

Following the decomposition of needle detected EMG signals, once the MUPs in an MUPT are resolved into MFPs accurately and consistently, neuromuscular jitter can be measured based on the decomposition of a routine EMG signal. In Chapter 3, the method of decomposing an MUP into its constituent MFPs for jitter measurement is described in detail.

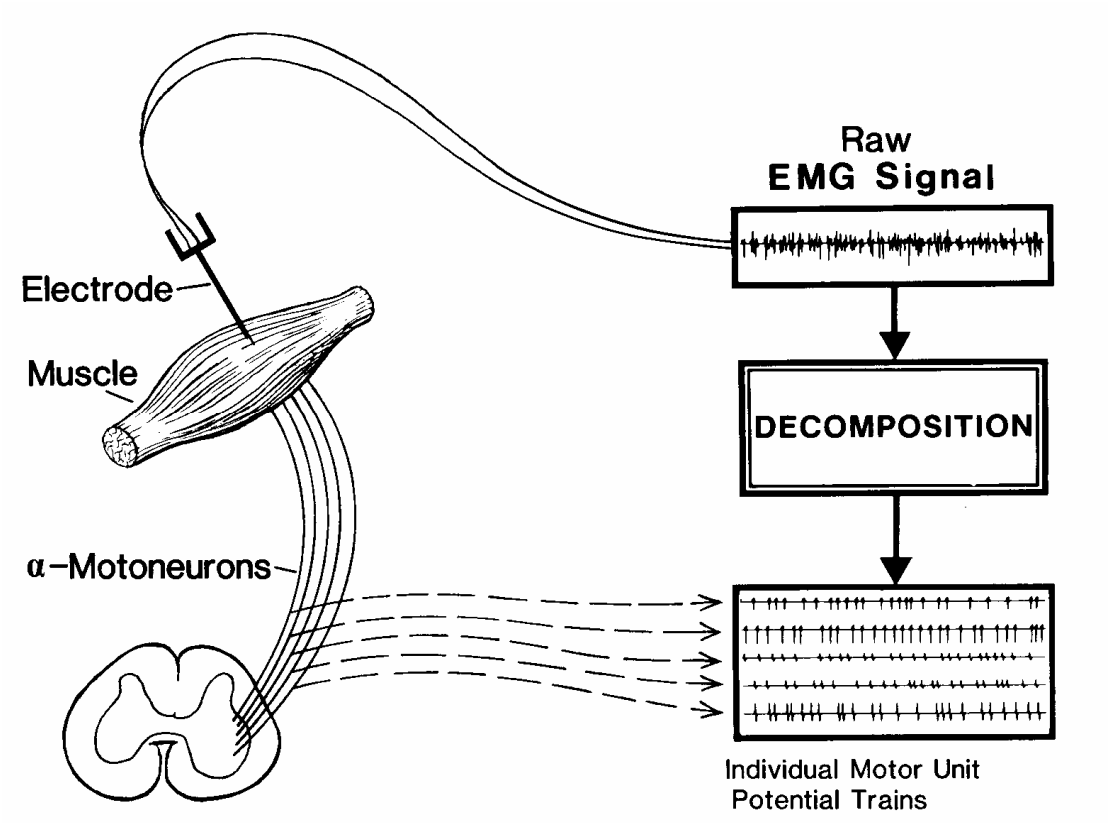

Figure 2.7: Schematic representation of the detection and decomposition of the intramuscular EMG signals [Merletti 2004]

Chapter 3

Measuring Neuromuscular Jitter based on Concentric EMG Signal Decomposition

As introduced in Chapter 2, neuromuscular jitter is usually measured using a SFN electrode either manually or automatically. Attempts have been made to study jitter in MUPs detected with CN or MN electrodes, some of which give values that are similar to those obtained using a SFN electrode. However, due to the much larger uptake area of CN and MN electrodes, the spike components of the detected MUPs are the superimposition of multiple MFPs. This may lead to an underestimation of jitter if superimposed MUPs are recognized as single MFPs. To measure jitter automatically based on CN and MN detected EMG signals, a strict procedure must be followed.

This chapter introduces methods for measuring neuromuscular jitter from a decomposed EMG signal in detail. The first section presents a review of related work on this topic, followed by two sections describing different aspects of the methods. Section 3.4 gives an overview of the three-step system developed for this research with further details coming in Chapters 4 – 6, while section 3.5 introduces the EMG signal simulator used for evaluating the developed system.

3.1 Review of Former Works

By removing low-frequency energy from CN or MN detected MUPs, the underlying complexity and instability of MUs can be revealed. Payan was the first one to show this theory in his 'blanket principle' where he used a 3.2 kHz cutoff frequency and demonstrated that the high-pass filtered MUPs contained useful stability information [Payan 1978]. Wiechers removed frequencies below 500 Hz from MUPs detected using an MN electrode, and assessed neuromuscular jitter and blocking qualitatively [Wiechers 1985]. Buchman and Garratt also filtered MN detected EMG signals with a cutoff frequency of 500 Hz, and quantitatively proved that MN-based jitter measurements are reproducible and able to distinguish between normals and patients with myasthenia gravis (MG), an NMJ disease [Buchman 1992]. Recently, Tutkavul et al. evaluated jitter measured using an MN electrode and a 3 kHz high-pass filter,

and concluded that jitter measurements with an MN electrode can be superior to those obtained using an SFN electrode [Tutkavul 2006].

At the same time, many researches have focused on jitter measurement using the more popular standard electrodes, CN electrodes. A simulation study on this topic using a line-source model was done by Tvrdon and Stashuk [Tvrdon 1995]. Processed by an 'inverse average-current filter', it was found that the measured jitter varied approximately linearly with the expected jitter with the correlation coefficients around 0.96. Stashuk did more simulations comparing the abilities of detect MFPs contributing to MUPs measured using SFN and CN electrodes [Stashuk 1999b]. The results suggested that the filtered acceleration of CN detected MUPs can strongly correspond to individual fiber activity and may be useful for measuring fiber density and jitter. Ertas et al. [Ertas 2000] applied a 2 kHz to 10 kHz band-pass filter to measure jitter, and compared the results to those using an SFN electrode. For two muscles during voluntary contraction and electrical stimulation respectively, jitter values using CN and SFN electrodes were found highly comparable, which demonstrated that CN electrodes could be used instead of SFN electrodes for neuromuscular jitter analysis. Ma presented an algorithm for automated jitter measurement in MUPs in his thesis [Ma 2003]. Choosing an acceleration filter, the algorithm demonstrated acceptable performance and could consistently measure jitter in a variety of EMG signals with the average error of 8.37%. Extending Ma's work, Wang improved this algorithm by applying a McGill filter [Wang 2005]. Recently, studies done by Sarrigiannis et al. [Sarrigiannis 2006], Benatar et al. [Benatar 2006], and Cattaneo et al. [Cattaneo 2007] have also confirmed that a CN electrode is a justifiable alternative to an SFN electrode for measuring neuromuscular jitter or other statistics related to NMJ disease. Stalberg [Stalberg 2006] concluded that jitter values measured from CN-based MUPs may not be as accurate as those obtained using a SFN electrode due to the relatively large pickup area of a CN electrode, but that the deviation would not usually lead to misdiagnosis of NMJ disease. More specifically, using the peak trigger measurement algorithm, reference values for measurements made with a CN electrode are about 5 μs lower than those obtained using a SFN electrode.

Based on the above studies and following Ma and Wang's work, this thesis is dedicated to the design of an automated neuromuscular jitter measurement system

based on CN-EMG signal decomposition. The method developed for measuring jitter is introduced as follows: (i) definition of significant or near MFPs, (ii) MUP filter selection, (iii) system architecture design, and (iv) data simulation.

3.2 Significant or Near MFPs

As introduced in section 2.2.2, the amplitude of detected potentials steeply declines with distance from the detection surface. In fact, no matter what type of electrode is used, only muscle fibers very close to the detection surface contribute significant MFPs to an MUP. Compared to the 5 to 10 mm MU territory, only those muscle fibers within approximately 0.5 mm range around the electrode make significant contributions to the detected MUPs, which are called significant or near MFPs (or MFP contributions). The spike components of an MUP detected by a CN electrode are produced predominantly by the closest 2 to 12 muscle fibers [Wang 2005].

It may be hard to distinguish all MFPs from muscle fibers within the CN electrode pickup area. However, if one is only interested on the focal area very close to the detection surface like when using an SFN electrode, jitter can be measured from only those significant MFPs once they are accurately and consistently identified. Referring to the characteristics of individual MFPs detected using an SFN electrode, a significant MFP has a stable shape with no bifurcation, a short rise time, and adequate amplitude across the ensemble of detected MUPs from the same MU. For measuring jitter automatically based on CN detected MUPs and evaluating an algorithm, significant or near MFPs have to be quantitatively defined. In [Ma 2003], near MFPs were defined arbitrarily as MFPs that had amplitudes above 150 μV. Stashuk used a threshold of peak acceleration to distinguish near and distant MFPs, where the best threshold values were found to range from 2.5 to 7.5 kV/s^2 for MUPs detected using a CN electrode [Stashuk 1999b]. In the research of this thesis, two threshold values of peak acceleration of a MFP were used for defining a significant or near MFP: 5 and 7.5 kV/s^2.

Significant MFPs usually can not be recognized directly in a CN detected MUP since they may be a superposition of more than 2 MFPs. Proper filtering has to be applied to the MUP to distinguish the significant MFP contributions, which is discussed in the next section.

3.3 Methods for Detecting Significant MFPs in MUPs

In clinical settings, a CN detected MUP may consist of up to 50 individual MFP contributions [Stashuk 1999a]. However, a considerable portion of them are created by muscle fibers that are relatively distant from the detection surface of the electrode, which are defined as distant MFPs. In fact, distant MFPs consist mostly of relatively lower frequency components compared to near MFPs. Consequently, distant MFPs can be essentially removed by proper filtering techniques so that near MFP contributions can be more distinguishable.

3.3.1 Filtered MUPs

As reviewed before, the principle of measuring jitter using a CN or MN electrode is to differentiate individual MFPs by filtering the detected MUPs, though different filters with various cutoff frequencies have been exploited by researchers. As for CN-based detection, Stashuk [Stashuk 1999b] compared two band-pass filters with bandwidths of 500 Hz to 10 kHz: a 16^{th} order zero-phase Butterworth filter and a McGill filter [McGill 1984]; The filter settings used by Ertas et al [Ertas 2000] were 500 Hz to 10 kHz for SFN electrode recordings and 2 kHz to 10 kHz for CN electrode recordings, which were also employed in [Sarrigiannis 2006], [Benatar 2006] and [Cattaneo 2007].

In his thesis [Ma 2003], Ma completed a detailed frequency spectrum analysis of MFPs and MUPs. It was found that for an MUP, the peak of the spectral density corresponds to contributions of almost all MFPs in the low frequency bandwidth, i.e. below 2000 Hz. These contributions contain mostly distant MFPs with relatively low frequency components. In the high frequency zone ranging from 3500 Hz to 10 kHz, an MUP's spectral density is low and approximately constant. Since the spectral density of individual MFPs is relatively low and rapidly falls off over 3500 Hz, the contributions of MFPs to an MUP in the high frequency bandwidth would be subtle and the energy may mainly come from noise. So in order to distinguish near or significant MFPs for measuring neuromuscular jitter, the frequency section between 2000 Hz and 3500 Hz, which mainly contains contributions from near MFPs, was selected as the bandwidth of a band-pass filter.

Several kinds of digital filters satisfying the bandwidth requirement were discussed and evaluated in Ma's thesis, for example, a McGill filter which is a specific 2nd order symmetric differentiator (shown as in Equation (3.1)), a 1st order differentiator which was called a 'Slope' filter (Equation (3.2)), and a 2nd order differentiator which was called a 'Acceleration' filter (Equation (3.3)).

McGill filter:
$$Y_n = \frac{1}{3}X_{n+6} - \frac{1}{3}X_{n+3} - \frac{1}{3}X_n + \frac{1}{3}X_{n-3}; \tag{3.1}$$

Slope filter:

$$\begin{aligned} Y_n \;=\; & 0.0371(X_{n+1} - X_{n-1}) + 0.1002(X_{n+2} - X_{n-2}) + 0.1338(X_{n+3} - X_{n-3}) \\ & + 0.1283(X_{n+4} - X_{n-4}) + 0.0861(X_{n+5} - X_{n-5}) + 0.0205(X_{n+6} - X_{n-6}); \\ & - 0.049(X_{n+7} - X_{n-7}) - 0.1016(X_{n+8} - X_{n-8}) \end{aligned} \tag{3.2}$$

Acceleration filter:

$$\begin{aligned} Y_n \;=\; & -0.2158X_n - 0.1521(X_{n+1} + X_{n-1}) - 0.0444(X_{n+2} + X_{n-2}) \\ & + 0.0427(X_{n+3} + X_{n-3}) + 0.0884(X_{n+4} + X_{n-4}) + 0.1040(X_{n+5} + X_{n-5}) \\ & + 0.0757(X_{n+6} + X_{n-6}) + 0.0175(X_{n+7} + X_{n-7}) - 0.0155(X_{n+8} + X_{n-8}), \\ & - 0.0122(X_{n+9} + X_{n-9}) + 0.0037(X_{n+10} + X_{n-10}) \end{aligned} \tag{3.3}$$

where, X_n is the sampled data of the original MUPs, and Y_n is the data of the filtered MUP.

The criteria of designing or choosing the optimal filter is that it should be sensitive to the rapid rising edges of MFPs and able to suppress low frequency content and the false peaks efficiently. The 'Acceleration' filter was chosen for his algorithm due to its best performance, and the average detection, false, and miss rates were 75.1%, 4.6%, and 24.9% respectively.

3.3.2 MUP acceleration

Another filtering method is to use MUP acceleration directly [Stashuk 1999b, Wang 2005]. The sharp peaks of the MUP acceleration with sufficient amplitude and short rise time are corresponding to significant MFPs. Stashuk asserted that analyzing MUP acceleration is a powerful technique for detecting major fiber contributions to MUPs compared to a 16th order zero-phase Butterworth filtered MUP.

The MUP acceleration can be considered as another version of a McGill filtered MUP with different step length and divided by a constant which only depends on the sampling rate. For example, the zero-phase acceleration of an MUP can be calculated using the following 2nd order difference equation:

$$Y_n = \frac{X_{n+2} - X_n - X_{n+1} + X_{n-1}}{2\Delta^2}, \tag{3.4}$$

where, Δ is the sampling time interval of the detected MUP. Meanwhile, MUP accelerations and filtered MUPs have different units like kV/s^2 versus μV, so also different detection thresholds for significant MFPs.

In this thesis, the MUP acceleration calculated using equation (3.4) was used to differentiate significant MFPs. However, no matter which filtering method is applied, a key problem is how to identify false peaks produced by the filter. Ma did some initial work on this problem by characterizing true peaks which correspond to individual MFPs with features of the peaks of the filtered MUPs. Discussion on this problem is contained in the next section and later chapters.

3.4 The Three-Step System for Automated Neuromuscular Jitter Measurement from an MUPT

Needle-detected EMG signal decomposition is commonly a supplementary function for a clinical EMG analysis system in diagnosing myopathies and neuropathies. The decomposition process is complex since different MUPs overlap to various degrees in time, the shape of an MUP may vary because of changing MU properties or MU-electrode relative position, and the firing intervals of an MU deviate to some extent depending on the stability of NMJ transmission [Merletti 2004]. By applying complex signal processing and pattern recognition techniques, a needle-detected EMG signal can be decomposed into MUPTs, and summarized as MUP templates and corresponding statistics suggesting the physiological status of a muscle.

From an MUPT, significant or near MFPs can be identified in each of the filtered MUPs or MUP accelerations of the train. Neuromuscular jitter can then be calculated based on the IPIs of significant MFP pairs in the MUPs of an MUPT. To measure

jitter accurately, near MFPs should be identified precisely and consistently for each MUP of the MUPT. However, in order to keep complete firing information of an MU, a decomposed MUPT may contain superimposed MUPs which are contaminated with MUPs from other MUs. Filtering or using the acceleration of superimposed MUPs may reveal the MFPs of contaminating MUs, or show superimposed MFPs, which would be sources of false detection. To avoid the effect of superimposition, superimposed MUPs have to be removed from decomposed MUPTs before further analysis. Therefore, a preprocessing step that identifies isolated MUPs (i.e., the un-superimposed MUPs) of an MUPT has to be completed before detecting near MFPs and calculating jitter.

To design and evaluate the complex procedure for neuromuscular jitter measurement in decomposed CN-EMG signal hierarchically, a system composed of three functional steps is described:

Preprocessing step:	Identify isolated MUPs in an MUPT;
Major step:	Recognize near MFPs in each isolated MUP;
Final step:	Track near MFPs across an MUPT, select MFP pairs, and calculate jitter.

The identification of isolated MUPs can be addressed as a clustering problem, while the detection of significant MFPs can be solved by a pattern recognition system. Algorithms designed for the three steps are introduced and evaluated independently in detail in the following chapters. Simulated data were generated for evaluation of each step as well as the whole system quantitatively. Real data collected by the Biomedical Signal Processing Lab of University of Waterloo were also used for validating algorithms. An EMG signal simulator was employed to generate synthetic data [Hamilton-Wright 2005], and an EMG signal decomposition system was applied for decomposing the EMG signals. The principles of the EMG signal simulator are introduced in the next section.

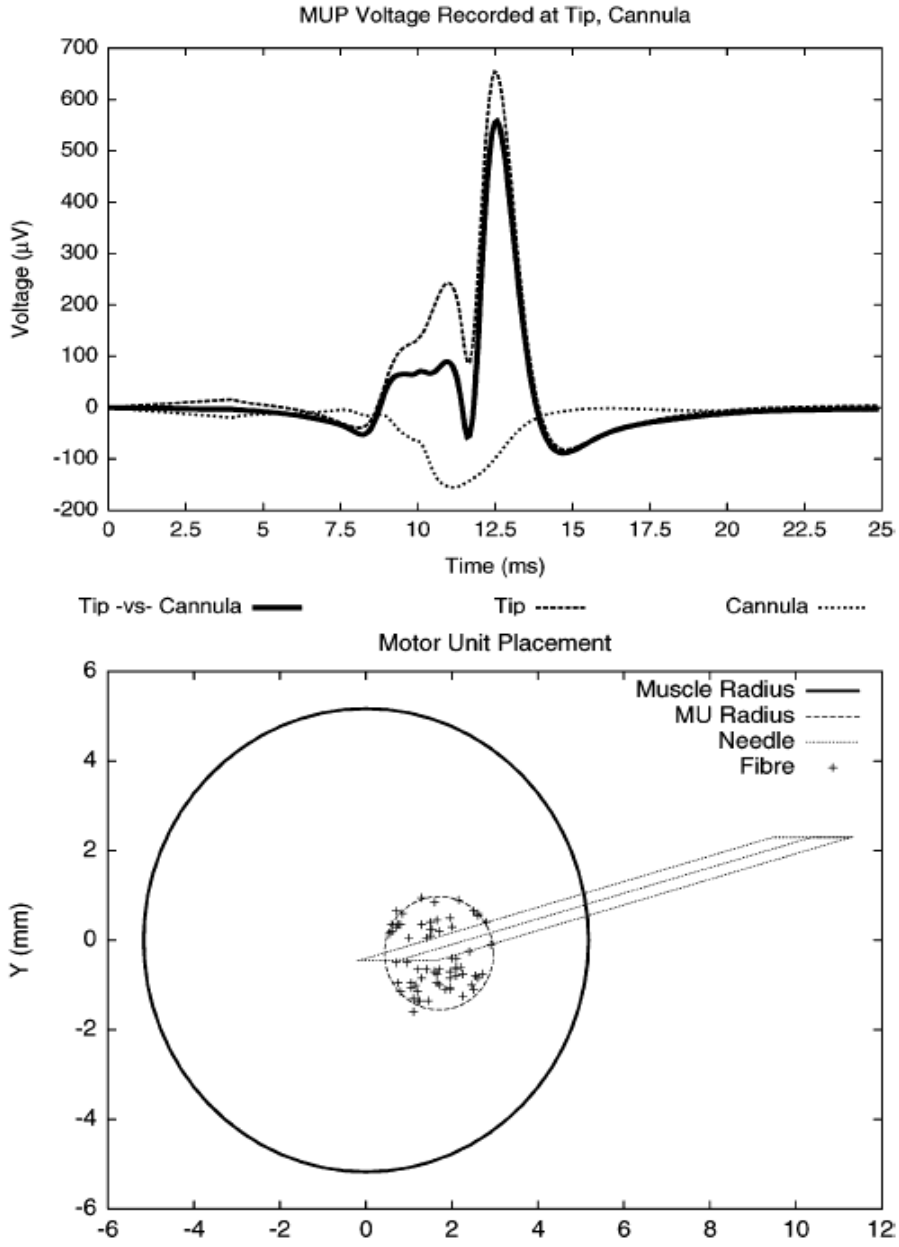

Figure 3.1: An example of muscle fiber distribution in an MU (bottom) and a CN electrode detected MUP (top) [Hamilton-Wright 2005]

3.5 Data Simulation

To evaluate the jitter measurement system, a large dataset which covers a variety of EMG signals with known jitter or known MFPs for each MU detected, i.e. data with a known structure, had be to created. Furthermore, to estimate the accuracy of each step of the procedure, MUPTs with different degrees of superposition and MUPs with various complexities of MFP contributions were required as well as corresponding

pre-known compositions. In practice, it is impossible to establish such a large real EMG dataset with known details at each level. In this thesis, synthetic data were used for quantitative evaluations, while real data can be employed for qualitative checking and validating since the true answer of the composition of the real data is not available.

An EMG signal simulator has been adopted to produce synthetic datasets for evaluation of the designed system [Hamilton-Wright 2005]. The simulator imitates the generation of EMG signal at each detailed level from bottom to top, and is mainly based on four models: a muscle model, an MU recruitment model, a MFP and MUP model, and a composite EMG signal model [Stashuk 1993]. The muscle model defines MU organization and muscle fiber layout based on a "seed" scattering algorithm and possible developmental mechanisms. The MU recruitment model is applied to mimic the repetitive neural stimulus of each MU during muscle contraction. It determines which MUs of a muscle are active for a specific contraction level, and simulates firing times for the individual active MUs. A line source volume conductor model is then used to create MFPs and MUPs for a specific electrode configuration, a physical layout of the fibers, and relative positions of the muscle fibers and the MU to the detection surface of the electrode. MUPTs are produced using the firing times of the corresponding MUs. Finally, a simulated EMG signal is generated using the composite EMG signal model considering the setting of signal to noise ratio, sampling rate, etc. Because the simulator builds up the signal based on physiological and morphological models of the muscle with proper statistical distribution of random variables, simulated EMG signals are credible, rational and closely resemble real EMG signals.

Using data generated by this simulator, the effects of MU morphology, activation, and neuromuscular junction activity on acquired signals can be analyzed at the fiber, MU, and muscle level (exemplified in Figure 3.1). The intermediate results of the simulator include individual MFPs and MUPs, which are useful for evaluating the individual steps of the system developed in this thesis. The simulator also incorporates the variability of MUPs due to the deviation of NMJ transmission delay, i.e. neuromuscular jitter (see Figure 3.2), which makes the simulated data suitable for evaluating the whole jitter measurement system. Details of how the simulator was

used for evaluating each step as well as the whole system are presented in the experimental parts of the corresponding chapters.

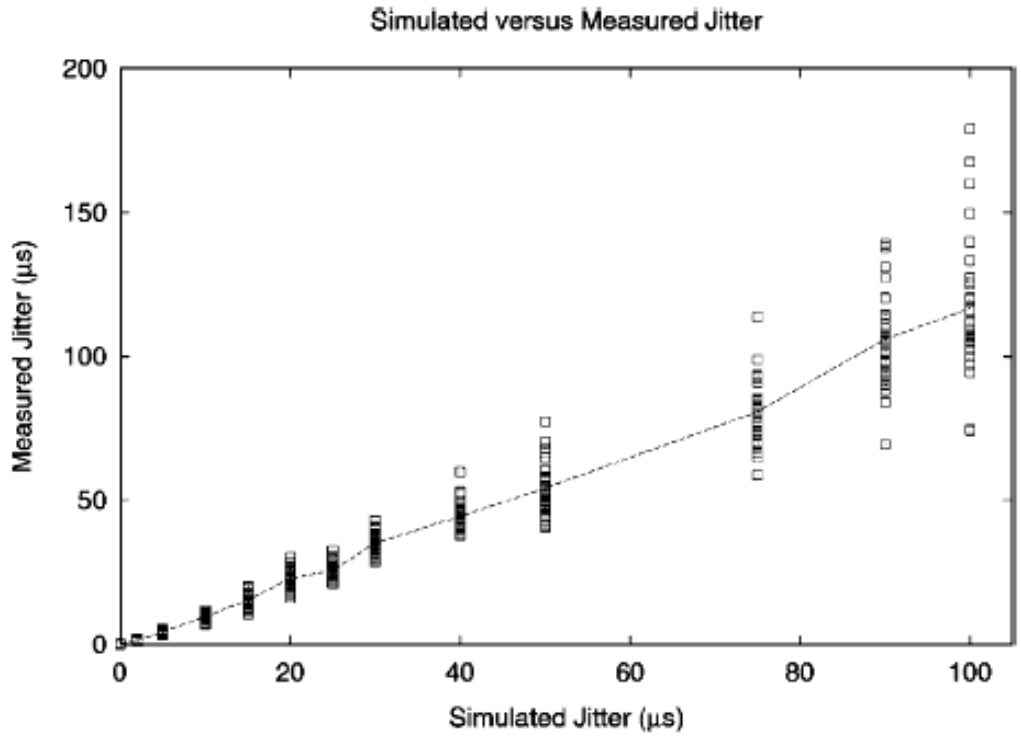

Figure 3.2: Simulated neuromuscular jitter values versus measured values with correlation coefficient of 0.97. [Hamilton-Wright 2005]

Chapter 4

Identifying Isolated MUPs from an MUPT

Identifying isolated MUPs is not only crucial for jitter measurement, it also is the initial task for resolving superimposed MUPs which is important for the detailed analysis of MU firing patterns [Merletti 2004]. In this chapter, interrelationships between/among isolated and superimposed MUPs were exploited, methods for classifying MUPs were discussed, and a two-phase clustering algorithm is presented theoretically and experimentally compared with a minimum spanning tree (MST) clustering algorithm and a template-based clustering algorithm.

4.1 Isolated MUPs versus Superimposed MUPs

During muscle contraction, MUs discharge asynchronously at variable firing rates, depending on an MU's recruitment threshold and the contraction level. When two or more MUs discharge at the same time or in close temporal succession, a superimposed MUP (abbreviated as SUP-MUP in this thesis), which is the algebraic summation of individual MUPs, is detected (as exemplified in Figure 4.1). On the contrary, those MUPs whose waveforms are not contaminated by any other MUPs are termed isolated MUPs (noted as ISO-MUPs). Technically, a MUP is superimposed when its waveform is overlapped with other MUPs and the interfered energy of other MUPs is larger than some threshold. For example, the MUP drawn with solid line in Figure 4.1 is definitely an SUP-MUP comparing to MUP 1 (dashed curve) since the interfered energy is more than 100% of the individual energy of MUP 1, but it is not differ from MUP 2 (dotted waveform) too much, so may not be declared as an SUP-MUP in MUPT 2 depending on the energy interference threshold used. In this thesis, the energy interference of simulated MUPs are checked using information from the gold standard file, a document generated by the simulator containing the true firing times and shapes of all individual MUPs of each EMG signal, which allows us to define SUP-MUPs correctly.

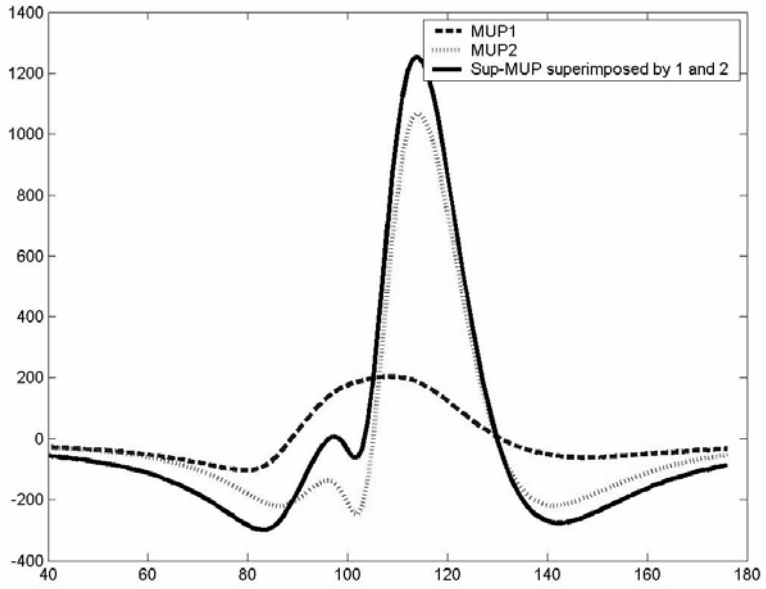

Figure 4.1: An example of SUP-MUPs

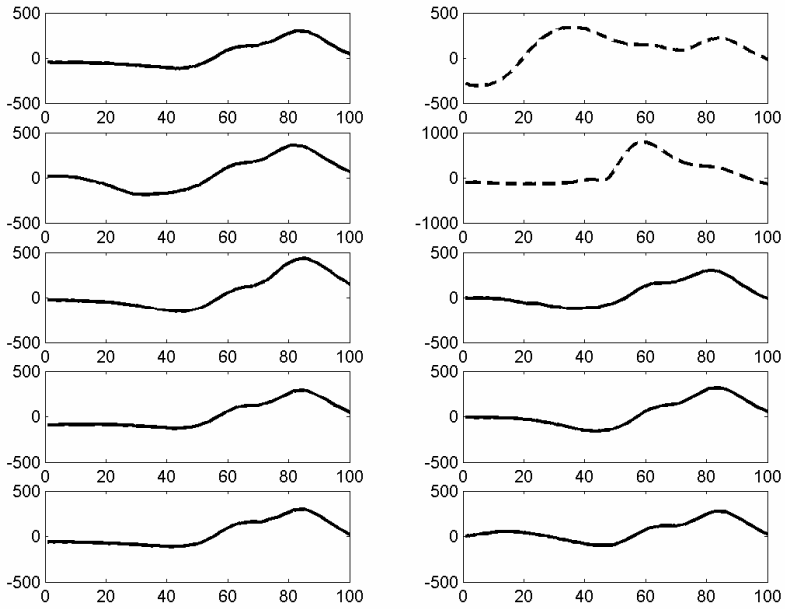

Figure 4.2: Raster graphs of MUPs in an MUPT with SUP-MUPs (dashed lines)

Compared to various compositions of SUP-MUPs, ISO-MUPs of an MUPT usually consist of the same MFPs of that MU. From Figure 4.2, the SUP-MUPs can be easily identified visually, since isolated ones look similar to each other. To identify ISO- or SUP-MUPs automatically, classification techniques especially clustering algorithms have been exploited.

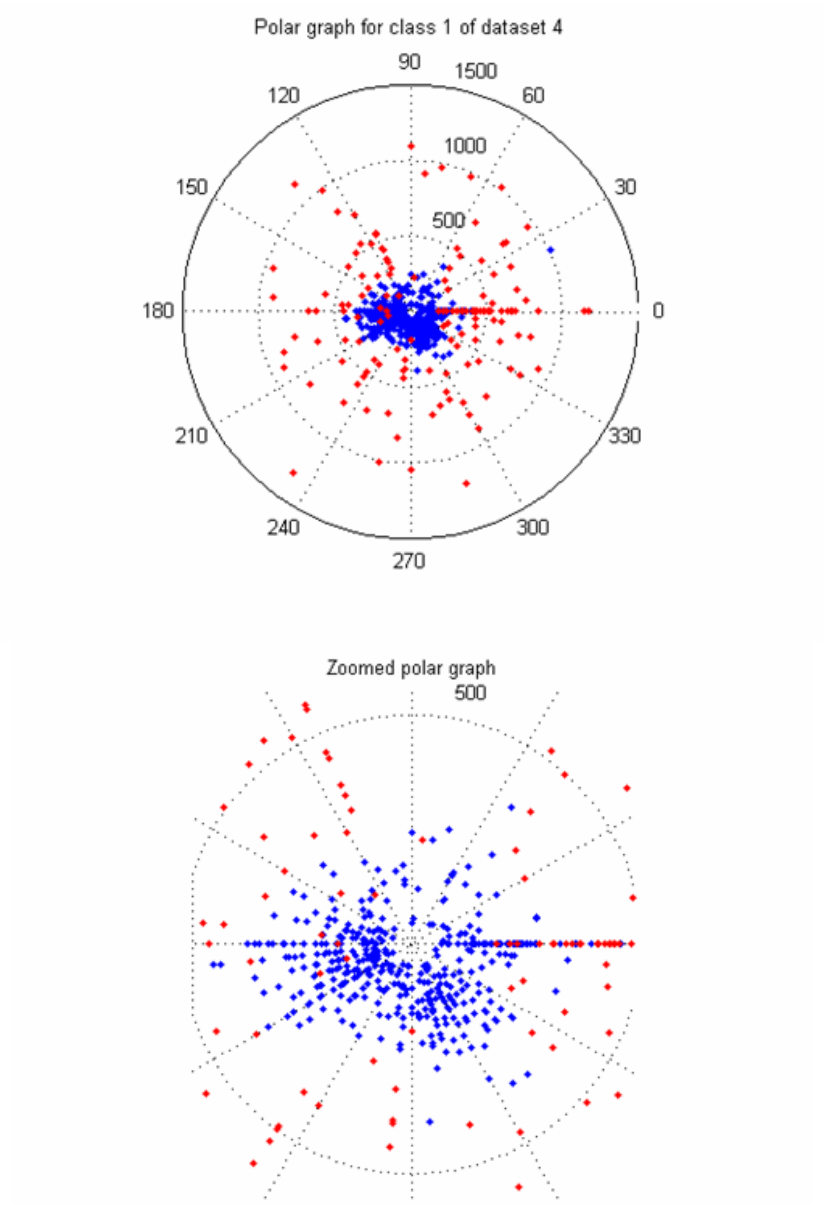

Figure 4.3: A 2-dimentsional expression of ISO- (blue) and SUP- (red) MUPs in an MUPT

4.2 Classification Algorithms for Detecting ISO-MUPs

As a two-class classification question essentially, the problem of identifying ISO-MUPs in an MUPT can be solved in two ways: classifying ISO-MUPs or detecting SUP-MUPs. Since SUP-MUPs are scattered relative to the major cloud of ISO-MUPs in a multi-dimensional feature space, in the former way identifying ISO-MUPs can be addressed as a one-class classification problem, while in the later way, detecting SUP-

MUPs can be solved by outlier detection algorithms where SUP-MUPs are outliers and isolated ones are inliers. For both categories of problems, different types of algorithms have been designed based on the model or structure of data, e.g., distance-based types, density-based schemes, and connectivity-based models [Juszczak 2006, Tang 2005].

As exemplified in Figure 4.2, it seems that a SUP-MUP differs a lot from an ISO-MUP in shape so that it may be easily distinguished from isolated ones. However, due to the instability of MUPs and measurement noise, the diversity of ISO-MUPs may be comparable with the dissimilarity between ISO- and SUP-MUPs [Etawil 1996]. This is why some distance-based or template-based algorithms which measure the distance to a template of MUPs may not yield high accuracies of identifying ISO-MUPs especially when jitter is large.

In fact, ISO-MUPs usually do not form a compact spherical class in a high dimensional feature space. Statistically observing an ISO-MUP in a train which usually contains hundreds of MUPs, though an ISO-MUP may be far away from the center of the isolated ones, it can be expected to be close to at least one other ISO-MUP. Expressed in the terms of graph theory, one can image that in a graph whose vertices are MUPs in a train, the connectivity among ISO-MUPs is much better than between SUP- and ISO-MUPs or among SUP-MUPs. According to this assumption, some researchers have applied connectivity-based classification algorithms for similar problems. For example, a ‘nearest neighbor clustering’ technique was adopted by Slawnych et al. to classify MUPs based on the statistical distance between isolated and superimposed classes with 5% false alarm rates [Slawnych 1996]; Wang selected a minimal spanning tree (MST) algorithm to identify ISO-MUPs with less than 10% miss detection error [Wang 2005].

Nevertheless, in practical operation, low false classification error is always obtained at the cost of high miss classification error, because the ISO- and SUP-MUP data are not well separated especially when high contraction level or large jitter exists (as shown in Figure 4.3). To identify MUPs robustly, the MST clustering algorithm developed by Wang was extended to include a template based refining phase in this thesis.

4.2.1 The Minimal Spanning Tree (MST) Clustering Algorithm

4.2.1.1 MST and MST Curve

In graph theory, a spanning tree is a sub-graph spanning a set of vertices such that every pair of points is connected without closed loops. Each edge in the tree is associated with the distance between the linked vertices. An MST is the spanning tree such that the sum of all the distances is a minimum. An example of a MST is shown by the points and solid line segments in Figure 4.4. The MST algorithm is actually a single-link hierarchical clustering method in statistics [Webb 1999].

A clustering algorithm based on Kruskal's MST [Kruskal 1956] was used in Wang's thesis. MUPs of a train and their interrelationship can be expressed in a graph where each vertex refers to an MUP and each edge between two vertices represents the distance between two corresponding MUPs. Starting from the nearest pair of MUPs of an MUPT which are assumed as ISO-MUPs, a MST can be generated to express the inter sample connectivity. For an MUPT, the root of a tree is one of the closest MUPs of the train. Then it grows by linking to the nearest unconnected MUP to the tree one by one until all MUPs are connected. The distance of an MUP to the tree is defined as the smallest distance from the MUP to all MUPs in the tree, i.e.,

$$D\,(\mathrm{MUP}_i, \mathrm{MST}) = \min_{MUP_j \in MST} (\mathrm{MUP}_i, \mathrm{MUP}_j), \text{ for } \forall\ \mathrm{MUP}_i \notin \mathrm{MST}. \qquad (4.1)$$

If MUPs are indexed in the order of generation of a MST, any MUP to MST distance can be expressed as:

$$D\,(\mathrm{MUP}_i, \mathrm{MST}) = \min_{i>j} (\mathrm{MUP}_i, \mathrm{MUP}_j), \text{ for } \forall\ \mathrm{MUP}_i \text{ in an MUPT}, \qquad (4.2)$$

where the subscripts i and j are indexes of MUPs ordered by the generation of the MST. Since the connectivity of a MST decreases along with its generation, an MUP with a small index tends to be an ISO-MUP and one with a large index is apt to be a SUP-MUP. Compared to a complete graph where each pair of vertices is linked by one edge, a MST is a simple but meaningful graph representing the connectivity or interrelationship of MUPs.

If distances of MUPs to MST are plotted in the order of generating the MST (i.e., a piecewise linear curve of MUP to MST distance versus MUP index), the inter-MUP connectivity can be conveniently displayed as an approximately increasing curve of MUP to MST distance, which is called a MST curve in this thesis (see Figure 4.5). Generally, a sudden increase in this curve happens at the breaking point where the distance of the next MUP to MST is much larger than those of the former MUPs. Theoretically, this breaking point can be referred as the boundary of ISO- and SUP-MUPs classes in the curve, e.g., the dotted stem which cuts the MST curve and separates the ISO- and SUP-MUPs (marked with dotted stems) as shown in Figure 4.5.

4.2.1.2 MST Clustering Algorithm

The principle of the MST clustering algorithm is to find the proper cutting of the MST curve, e.g., the solid stem in Figure 4.5, or stop generation of the tree when the next MUP to MST distance is larger than some threshold, e.g., four bold lines cutting the MST in Figure 4.4. Depending on the order of the statistics used, this cutoff threshold can be a distance value, a relative increasing of distance or slope of the MST curve, or even an acceleration threshold of the MST curve.

The MST clustering algorithm designed by Wang can be summarized by the following steps:

i. Calculate the distance between each pair of MUPs in an MUPT;

ii. Sort these pair wise distances and generate the MST;

iii. Choose 30 to 50 of the most similar MUPs to calculate the mean and standard deviation (STD) of the MUP to MST distances;

iv. Cut the tree when the distance of an MUP to the MST is larger than 2.4 to 2.9 times the STD plus the mean calculated at step iii, and mark the MUPs before the cut as isolated and the remaining MUPs as superimposed.

The threshold of ‘coefficient × STD + mean’ is robust to the change of jitter to some extent. As the jitter becomes large, the STD of the distances increases accordingly, so the threshold raises as well, which makes the algorithm somehow adaptive to the increased variability of ISO-MUPs.

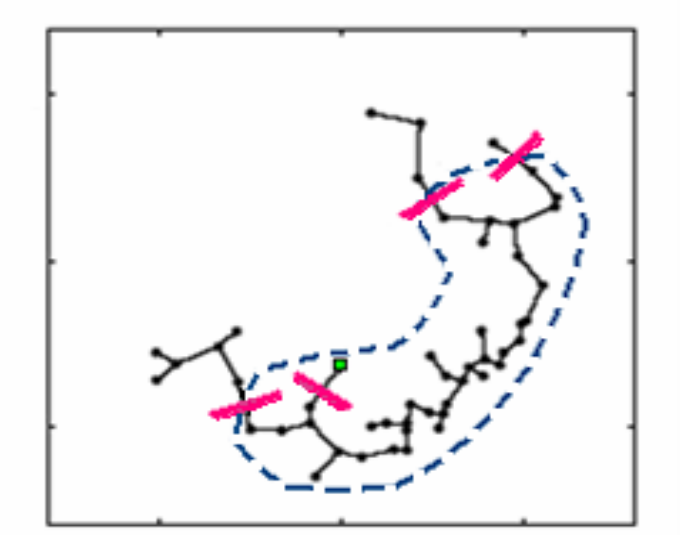

Figure 4.4: An illustration of MST and the two-phase clustering algorithm (MST: points and solid line segments; cutoff: bold sticks; reclassified sample: hollow square point; final clustering result: dashed circle.)

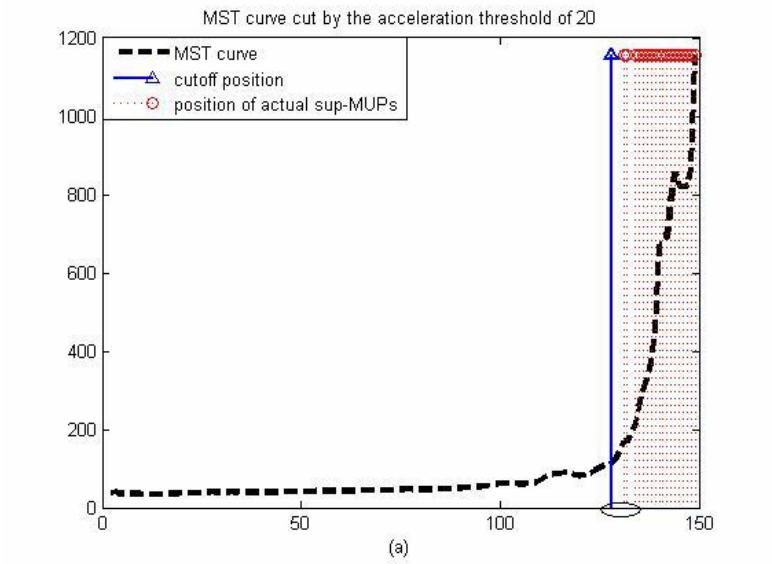

Figure 4.5: An MST curve of a simulated MUPT with SUP-MUPs (dotted stems) according to the gold standard and a cutoff (bold stem)

4.2.1.3 Criteria for Cutting the MST Curve

Cutting the MST around the breaking point of the curve is the main step of the MST algorithm. However, the assumption that there is a sudden change of MUP-MST distance or MST curve slope which can be used to separate ISO-MUPs and SUP-MUPs roughly may not hold true in some situations. With the help of the simulator, MUPTs of the same MU can be detected with different values of jitter and at various contraction levels. The effect of contraction level and jitter on the MST curve and

cutoff position can be clearly demonstrated by comparing two curves of the same MUPT with different contraction level and jitter, e.g. the MST curves in Figure 4.6. Note the curves are smoothed using a median trimmed filter on a moving window along the curve.

The train shown in subplot (a) of Figure 4.6 is a simulated normal MUPT with 25 μs jitter under contraction level of 5% of maximum voluntary contraction (MVC), while subplot (c) shows a MST curve of the same train with 4 times the contraction level, subplot (b) is with 4 times the jitter, and (d) with increased jitter and contraction level simultaneously. Comparing subplot (a) with (b) of Figure 4.6, one can find that larger jitter will make the MUP-MST distances larger because of the variation of MUPs increases with jitter. This is why the absolute distance threshold will not work well for cutting an MST or MST curve since it is not flexible to any change of jitter.

The effect of contraction level or intensity on MUPTs can be learned by contrasting subplot (c) to (a). Besides the increased MUP to MST distance, the breaking position is also less distinct for higher contraction level. Meanwhile, the number of superimposed MUPs goes up with contraction level because the firing frequency of each MU raises with contraction level so MUPs are more overlapped with each other. This is why a cutting criterion which works perfectly in one case may not work well for other situations with different contraction levels.

Besides the distance threshold, two backup criteria for cutting an MST curve were considered: the slope threshold and the acceleration criterion, where each criterion can be absolute or relative. The absolute slope threshold was applied for cutting the MST curves in Figure 4.6, from which one can conclude that the slope criterion is insensitive to jitter but is not adaptive to changes of contraction level. An acceleration threshold 0.1 was used for cutting the curves in Figure 4.7. Though it seems that the acceleration criterion is less sensitive to contraction level than the slope criterion, it is still not flexible enough to cut trees under high contraction level. Since the idea of the acceleration criterion matches the intuition of cutting the curve at a breaking point, the acceleration threshold was selected in this thesis. An adaptive acceleration threshold was designed for the two-phase algorithm based on the inverse relationship between intensity and the proper cutting threshold as shown in Figure 4.8, i.e. when intensity goes up, the cutting threshold should be reduced, and vice versa.

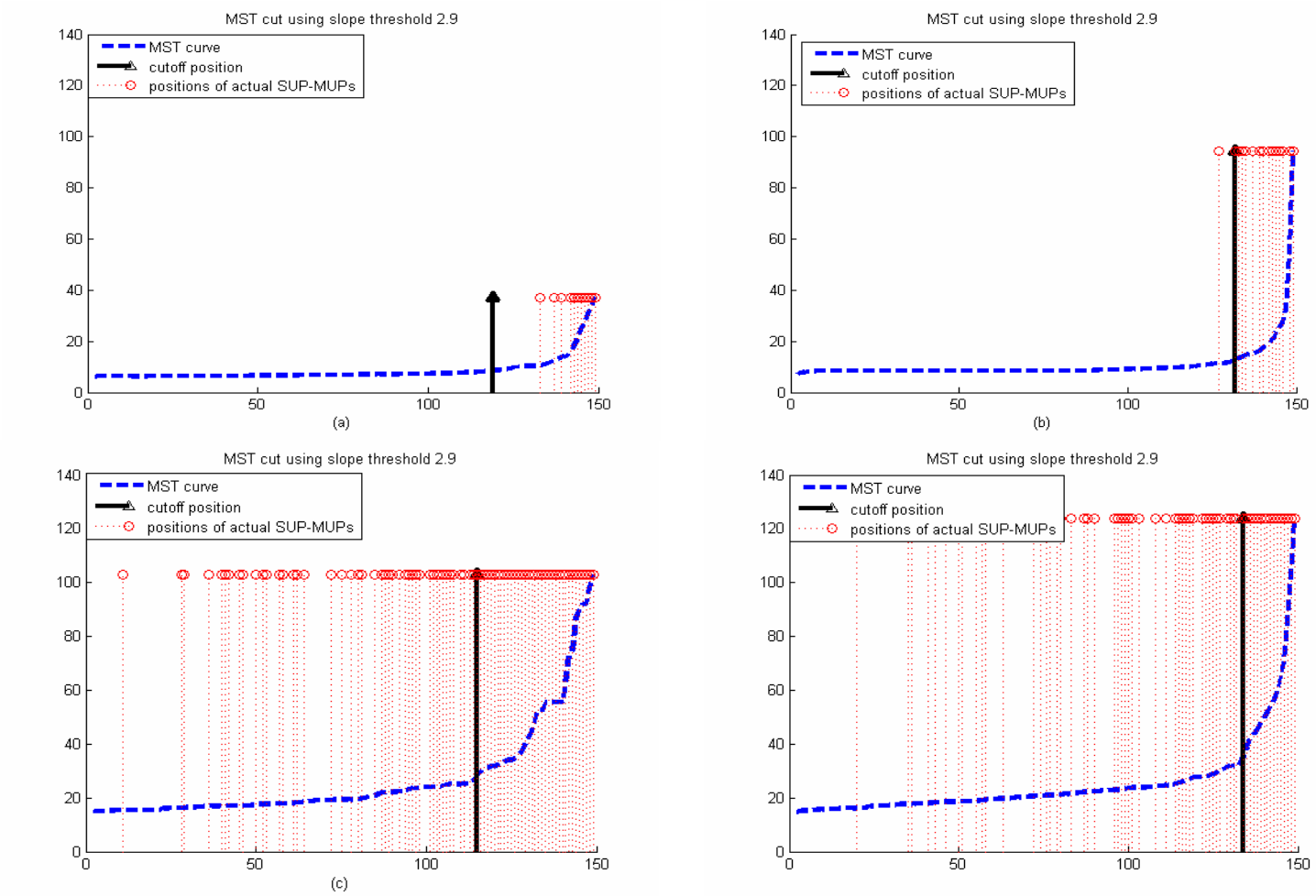

Figure 4.6: Effects of jitter and contraction level on an MST curve cutting by the slope threshold 2.9 ((a) jitter: 25 µs; contraction level: 5% MVC (b) jitter: 100 µs; contraction level: 5% MVC (c) jitter: 25 µs; contraction level: 20% MVC (d) jitter: 100 µs; contraction level: 20% MVC)

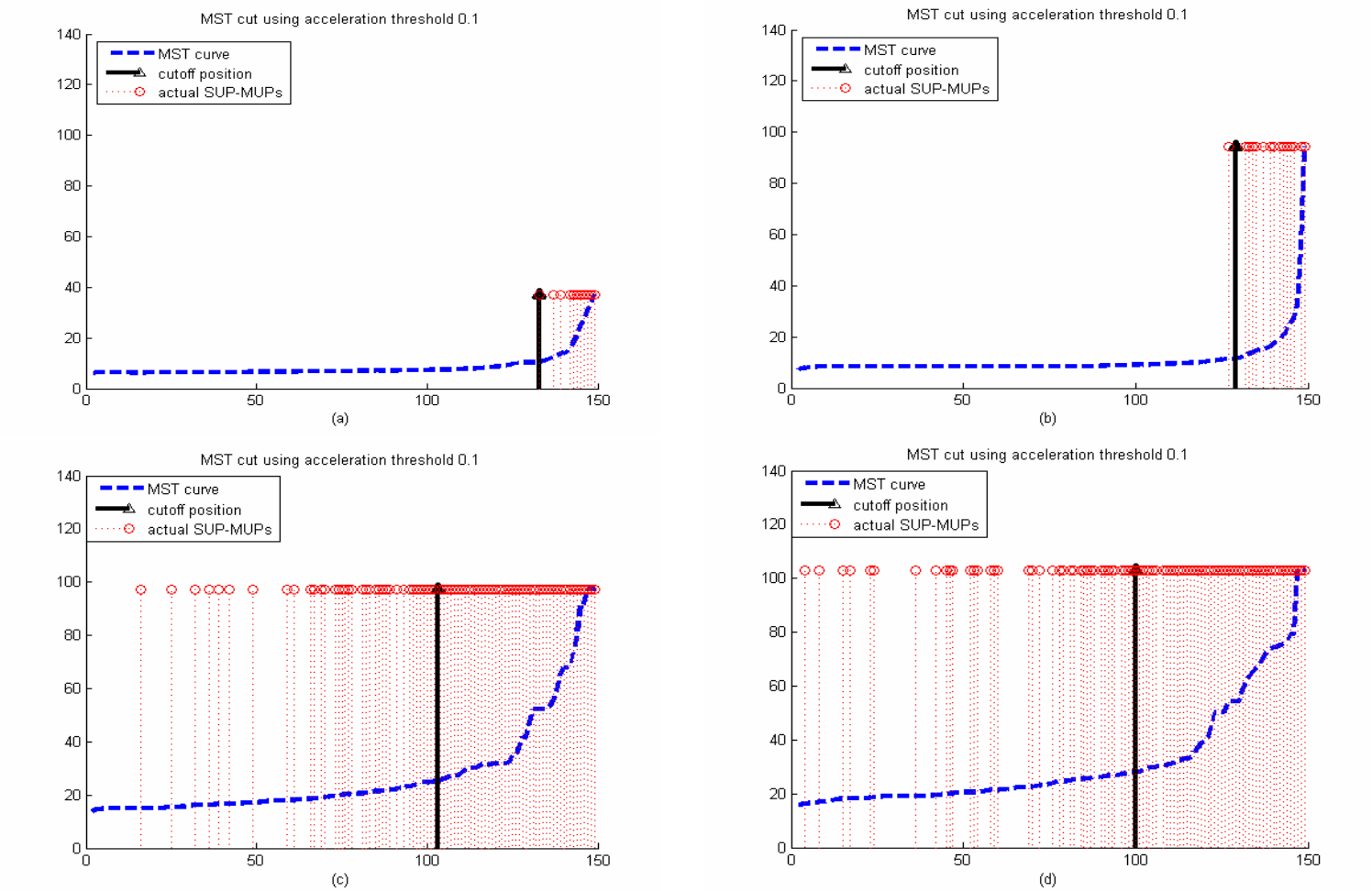

Figure 4.7: Effects of jitter and contraction level on an MST curve and the cutoff position using absolute acceleration threshold of 0.1 (MUPTs are the same as Figure 4.6)

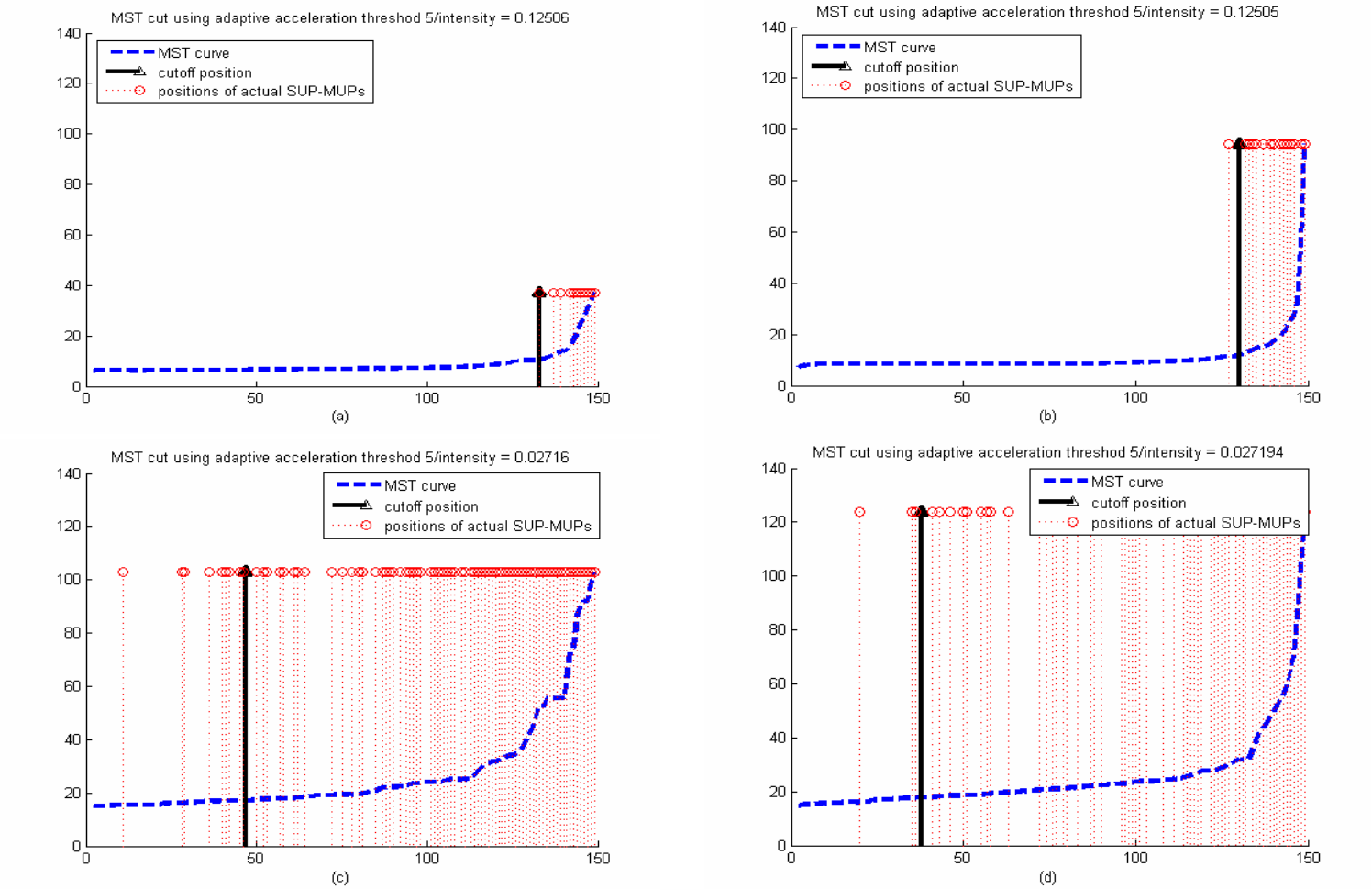

Figure 4.8: Effects of jitter and contraction level on an MST curve and the cutoff position using adaptive acceleration threshold of 5/intensity (MUPTs are the same as Figure 4.6)

4.2.2 The Minimal Spanning Tree-based Two-phase Clustering Algorithm

When adopting 2.4 as the coefficient of STD, the MST algorithm was reported having a false error rate of less than 10% and a relatively low missed error rate of ISO-MUP's identification in [Wang 2005]. The missed detected ISO-MUPs may be still close to the center or template of the ISO-MUPs, though they are not similar to other ISO-MUPs, like the square sample point in Figure 4.4. In practice, both identification errors are important for accurate measurement of jitter. Missed classified ISO-MUPs usually are MUPs with large variation, the losing of which will lead to the underestimation of jitter values. On the other hand, false identifications will cause errors of detection of significant MFPs directly. Furthermore, there is commonly no perfect cutoff of a MST that can separate ISO- and SUP-MUPs completely, since they are intersected around the breaking point on the curve (shown in the ellipse area in Figure 4.5). Therefore, an optimal algorithm for ISO-MUPs identification has to be well balanced for both types of error as well as the stability, robustness, and computation efficiency.

Although the adaptive acceleration cutting criterion exemplified in Figure 4.8 can greatly reduce false errors, the number of missed ISO-MUPs will increase at the same time. In this thesis, a template based classifier was added to the MST algorithm as a second phase to reclassify missed ISO-MUPs. If an MUP was closer the ISO-MUP center compared to some threshold, it would be added into the isolated class; on the contrary, it would be classified as a SUP-MUP.

To achieve a balanced accuracy, a conservative cutting of the MST was made at first trying to ensure that MUPs before the cutoff place are isolated to the fullest extent possible without too much cost of missing. Then MUPs after the cutting point are checked if their distances to the template of ISO-MUPs is within the 'mean + coefficient × STD', where the template, mean and STD of distances to the template are calculated using ISO-MUPs detected during the first phase. The threshold of the second phase represents for the boundary of the ISO-MUPs class well since those statistics are measured from almost all ISO-MUPs. If some robust statistics of average and variance are measured instead of mean and STD, e.g. median or trimmed mean describing average and median absolute deviation or mean absolute deviation

estimating variance, some of the SUP-MUPs falsely detected in the first phase can be correctly identified as ISO-MUPs.

This two-phase solution actually combines the advantages of the connectivity-based scheme and the distance-based model for complex datasets like an MUPT. This combined clustering algorithm is named the MST-based two-phase clustering algorithm in this thesis, with the first phase referred to as the separating phase, and the second phase called the refining phase. Concretely, the two-phase algorithm can be summarized by adding two more steps to the original MST clustering algorithm:

v. Calculate the isolated template, the mean and STD of ISO-MUPs to template distances using the ISO-MUPs identified by the MST clustering;

vi. Check the unidentified MUPs, and reclassify an MUP as isolated if its distance to the ISO-MUP template is smaller than some threshold: 'mean + coefficient × STD' of ISO-MUP to template distances.

Illustrated in the example of Figure 4.4, the square sample point would be reclassified as an ISO-MUP during the refining phase since it is close to the center of the ISO-MUPs. Those ISO-MUPs between the cutoff point and the SUP-MUPs in Figure 4.5 (MUPs located in the ellipse) might be identified as well. The computation complexity of the two-phase algorithm is $n^2 D$, where n is the number of data points and D is the dimension of the feature space, which is the same as the complexity of the MST clustering algorithm.

4.2.3 Other Algorithms

Besides the MST-based algorithms, some other methods have also been tried to identify ISO- or SUP-MUPs by the author, e.g., a customized fuzzy c-means (CFCM) clustering algorithm identifying ISO-MUPs and a robust principle component analysis (RPCA) algorithm detecting SUP-MUPs as outliers. The CFCM clustering algorithm yielded high accuracies with relatively high computation cost. The number of classes (i.e., value of 'c') had to be decided arbitrarily, which was hard to predict since the SUP-MUPs are usually not gathered as one or multiple classes. The RPCA outlier detection algorithm worked very fast, but had relatively high identification error rates compared to the MST algorithm. In this thesis, the two-phase algorithm was compared to the original MST method and a template based classifier, i.e., the

component technique of each phase, to show the improvement of combining the two methods.

4.3 Experiment

Besides listing the experimental results, this experiment section of identifying ISO-MUPs also involves the related topics such as data simulation, experimental procedure design, error cost design, and error analysis.

4.3.1 Data

To evaluate the performance of an algorithm on diverse EMG signals, a small database was created. It is comprised of seven data sets which simulated EMG signals detected during different levels of muscle contraction (qualified as firing intensity) , where each data set includes six EMG signals with MUPs comprised of MFPs with different amounts of jitter, and each EMG signal contains 5 to 13 MUPTs depending on the contraction level. In total 42 EMG signals, 378 trains were generated with different contraction levels and jitter values: the two main parameters affecting ISO-MUP identification. With increasing values of jitter, the variance of ISO-MUPs increases, while the number of the overlapping MUPs in an EMG signal (denoted by the ratio of SUP-MUPs in a train) increases with contraction level. All the data were created using the same needle configuration, in the same muscle, and with the same needle-muscle position, which allowed study of the effects of jitter and intensity independently.

In each simulated data set, jitter values were 25, 50, 75, 100, 125, and 150 μs and ranged from normal to extremely abnormal at each contraction level. Contraction levels are 5, 7.5 10, 12.5, 15, 17.5, and 20 corresponding to the seven data sets. The ratio of SUP-MUPs differed from around 9% to 45% representing simple to very complex EMG signals depending on the contraction level. SUP-MUPs were marked by an energy overlapping criterion based on the gold standard files generated by the simulator, which means MUPs that have at least 15% of their energy overlapping with other MUPs were recognized as actual SUP-MUPs. Other parameters of the simulator were set as normal, e.g., 25% S/N ratio, maximum recruitment threshold of 50, and generating 30 seconds EMG signal per run. The simulated database is summarized in Table 4.1.

Note that in practice the contraction level is usually 5% to 15% of MVC for NMJ measurement, where the simulated range is wider than the practical one. However, with a wide range of contraction levels, the ability of an algorithm to process data with high SUP-MUP ratio can be investigated for other applications, although, the SUP-MUP ratio of a train is normally less than 30% in an EMG decomposition system. Meanwhile, neuromuscular jitter is seldom larger than 100 μs because the possibility of NMJ blocking usually increases with high jitter, and blocked MFPs can not be used to calculate jitter. The process of NMJ blocking is described in Chapter 6.

Table 4.1: Summary of the simulated MUPT data base 1

Data Set	Contraction level (% MVC)	Jitter (μs)	Num. of Train	Ave. Intensity (pulse per sec.)	Ave. SUP-MUPs Ratio (%)
1	5	25	5	40.0	9.1
		50	5		
		75	5		
		100	5		
		125	5		
		150	5		
2	7.5	Same as Data Set 1	7	64.1	15.5
3	10		9	90.7	23.3
4	12.5		9	105.7	27.0
5	15		9	120.8	30.0
6	17.5		11	151.3	38.9
7	20		13	184.2	45.4
AVE	13.75	87.5	10	119.5	30.0

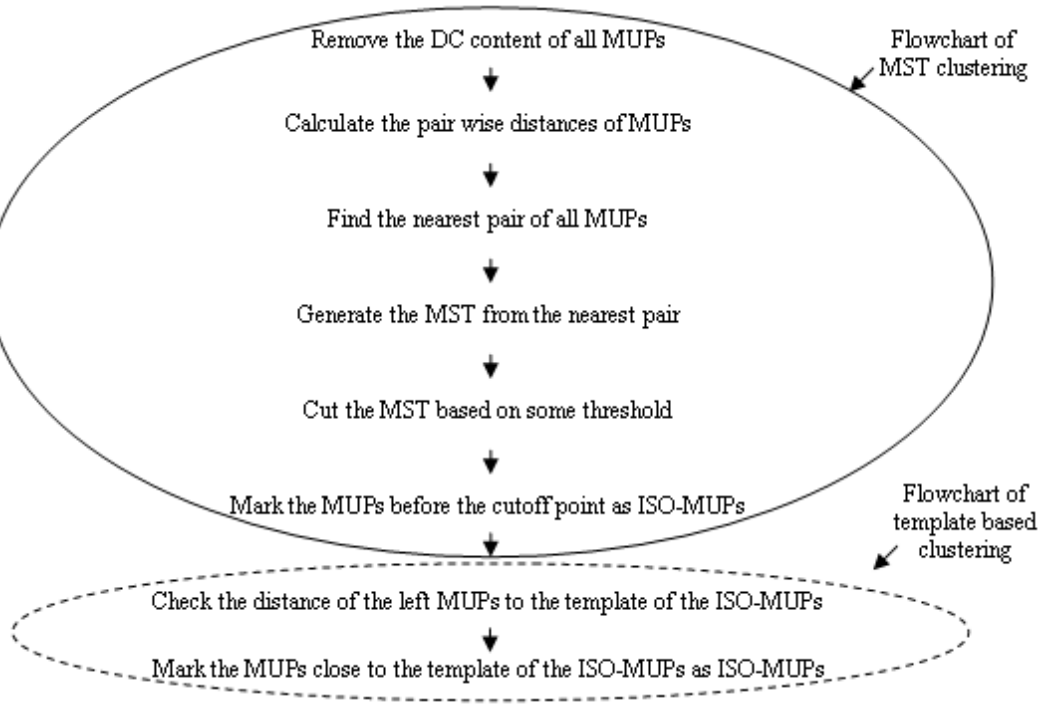

Figure 4.9: Flowcharts of the MST based two-phase clustering (all steps) and two component algorithms (steps in the ellipses)

Multiple real EMG data sets from different muscles of various subjects including controls and patients were visually checked since a gold standard for real data is not available.

4.3.2 Procedures

The flowcharts of the three algorithms are shown in Figure 4.9. For the template-based algorithm, the trimmed mean of all MUPs was calculated as the template of the ISO-MUPs. The classification criteria for this algorithm were the same as the second phase of the two-phase algorithm, except it was applied to all the MUPs in a train.

For the MST clustering algorithm, a 'mean + coefficient × STD' threshold was used for cutting the tree, where the mean and STD are calculated using the 30 MUPs in a moving window which moves along the MST and searches for the cutting position. The statistics of the 30 MUPs in a moving window represents the variability of the distances between ISO-MUPs well, which makes this algorithm somewhat robust to different amounts of jitter.

The two-phase algorithm has two parameters: CAT and COV_3, which are not independent since the result of the separating phase will be used as a reference for the refining phase. The parameter optimization for a problem with multiple dependent parameters can be tedious in order to find the global optimal. However, we simply set an empirical value for CAT which conservatively cuts off the MST, so that the estimated mean and STD can remain relatively constant as jitter and contraction levels change.

The performances of the three algorithms were compared with optimized controlling parameters. For the MST clustering algorithm, the cutoff threshold 'mean + COV_1 (i.e., Coefficient Of Variance) × STD' is controlled by the COV_1. The classification boundary of template-based method, 'median + COV_2 × MAD', is also determined by a coefficient COV_2, where MAD stands for median absolute deviation which is a robust measure of the variability of data with outliers. As for the two-phase clustering algorithm, an adaptive acceleration threshold of 'CAT / intensity' was introduced to cut the MST at the first phase, where CAT stands for a Constant for Acceleration Threshold, and the 'median + COV_3 × MAD' threshold of MUP to template distance was calculated for the refining phase.

A code optimization for speed was made by dividing an MUPT which contains hundreds of MUPs into small groups of MUPs, e.g., small groups of 150 MUPs, in respect that the calculating and sorting of pair wise distances has the computational complexity of $O(n^2)$ where n is the number of MUPs in a group. Generally, it speedups the process more than 3 times without any noticeable effect on the accuracy if a group size of 150 is used.

4.3.3 Error Cost Design

As a two-class classifier, two types of errors were defined for the ISO-MUP identification algorithms: false errors and missed errors. The false error (a.k.a. false positive, false alarm, or type I error) corresponds to the error that classifies SUP-MUPs as ISO-MUPs. On the contrary, a missed error (a.k.a. false negative or type II error) happens when an ISO-MUP is identified as a SUP-MUP. In medical classification problems, the terms sensitivity and specificity are adopted to characterize a rule. They can be defined as follows for the ISO-MUP identification problem:

Sensitivity: the probability of predicting ISO-MUP given true state of an MUP is isolated;

Specificity: the probability of predicting SUP-MUP given true state is superimposed.

Accordingly, we have

$$\text{Sensitivity (\%)} = 1 - \text{missed error rate (\%)}$$

and

$$\text{Specificity (\%)} = 1 - \text{false error rate (\%)}.$$

In practice, identification of ISO-MUPs is an asymmetric problem, where the two types of errors should not be weighted equally. The cost of a missed error is a bit more serious than that of a false error for jitter measurement. The missed ISO-MUPs usually have large jitter, so not including them will lead to an underestimation of jitter. On the other hand, falsely identified SUP-MUPs can be partly excluded during a later stage of the jitter measurement process. Therefore, one simple cost function was defined to assess a classifier:

$$\text{Error cost} = 0.55 \times \text{missed error} + 0.45 \times \text{false error}. \quad (4.2)$$

Unfortunately, the unbalanced cost function of errors may lead to minimizing missed error rates with a relatively large false error rate. Therefore, acceptable ranges of both errors have to be defined as constrain of the cost function. For example, the expected error upper bounds are 10% for missed error rates and 20% for false error rates in this thesis.

4.3.4 Results

Table 4.2 lists the best experimental results (i.e., lowest error cost) obtained with parameters COV_1 = 2.96, COV_2 = 2.70, CAT = 5.00 and COV_3 = 7.00. Note that results of the MST algorithm and template-based algorithm were optimized by minimizing the false error when keeping the missed error smaller than 10%, since they can not satisfy the two constrains for errors at the same time. Summarized in Table 4.3, the experimental results demonstrate that the error costs of two-phase algorithm are less than other two algorithms, and it is also the only method satisfying both error bounds concurrently. In a word, the two-phase algorithm yields higher accuracy and better balance of the two types of errors. Errors of the three algorithms are summarized in Table 4.3.

4.3.5 Error Analysis

The experimental results are analyzed on the aspects of robustness, stability and sensitivity of ISO-MUP identification.

4.3.5.1 Robustness Analysis

Since the three algorithms all have some mechanisms to resist the change of jitter, only the robustness to contraction level (intensity) is investigated for each method.

To investigate the robustness of the three algorithms to contraction level, error details of each data set are averaged and listed in Table 4.4. Contraction level is a quantified intensity level relative to the maximal intensity a muscle can generate. The changes in both error types corresponding to changes in contraction level are clearly shown in Table 4.2, Table 4.4 and the error bars in Figure 4.10. For the two compared techniques, missed errors changed inversely with contraction level, and false errors were positively related to it. For the two-phase algorithm, both missed and false errors increase slowly with contraction level.

Table 4.2: Details of Experimental Errors

Cont level	Jitter (us)	MST clustering				Template-based classifying				Two-phase clustering			
		Missed error		False error		Missed error		False error		Missed error		False error	
		Mean	MAD	Mean	MAD	Mean	MAD	Mean	MAD	Mean	MAD	Mean	MAD
5.0	25	9.3	2.1	0.7	0.4	8.8	0.3	0.5	0.3	2.1	1.2	1.7	0.5
	50	8.1	3.9	0.6	0.7	8.4	0.7	0.7	0.5	1.9	1.4	2.1	1.1
	75	4.9	1.8	1.3	0.1	9.8	0.5	2.0	0.4	0.8	0.7	3.7	0.4
	100	3.5	1.3	3.6	1.3	8.8	1.5	3.9	2.7	1.9	1.6	5.5	2.9
	125	4.8	2.2	1.9	1.4	8.3	3.1	3.1	1.9	1.7	1.2	4.8	2.5
	150	4.3	1.4	2.0	0.5	9.4	3.1	3.5	2.6	2.5	1.8	4.7	2.4
7.5	25	4.7	2.2	3.1	0.3	4.5	0.7	1.9	0.4	1.9	0.8	3.8	0.7
	50	6.2	3.1	2.1	1.3	4.6	0.4	3.3	1.0	2.5	1.1	4.6	1.4
	75	5.0	0.8	4.4	1.8	5.4	1.2	4.5	1.5	2.3	0.9	5.9	1.8
	100	5.4	3.2	3.7	1.3	6.7	1.1	5.0	2.4	4.2	2.8	6.3	2.4
	125	3.8	2.6	5.1	1.4	5.3	1.6	6.6	2.3	2.6	1.0	8.0	3.1
	150	3.3	0.8	5.4	1.8	6.1	1.7	6.1	1.9	3.8	3.5	7.7	3.3
10.0	25	4.3	1.5	6.6	1.8	3.1	0.7	6.0	2.6	2.2	1.3	6.7	2.7
	50	3.9	1.8	6.9	2.9	3.1	1.1	6.9	1.9	2.7	1.4	7.4	1.3
	75	2.5	1.7	8.5	2.9	3.8	0.8	8.2	1.1	2.0	1.3	9.9	1.9
	100	2.4	1.1	9.4	0.9	4.5	2.1	9.2	1.7	1.7	1.1	11.0	2.0
	125	3.2	0.9	9.6	3.4	3.3	1.4	10.4	2.0	3.0	2.8	11.0	2.3
	150	1.6	1.0	11.1	2.0	3.5	1.1	11.4	2.3	5.8	5.2	11.3	1.7
12.5	25	4.2	2.4	11.4	2.1	3.2	0.5	10.6	2.1	3.2	1.1	10.7	3.1
	50	4.6	2.0	10.4	3.3	3.1	1.4	10.9	2.6	3.8	1.5	10.4	2.9
	75	3.8	1.4	11.5	2.3	3.8	1.0	11.4	2.1	5.8	2.1	9.6	2.3
	100	3.7	2.0	12.0	1.7	4.1	1.3	12.4	1.7	4.1	1.9	11.9	1.5
	125	2.5	0.6	14.8	2.6	3.5	1.9	13.6	0.9	5.6	3.5	11.8	2.4
	150	4.0	3.0	12.4	2.3	3.3	0.7	13.5	1.3	4.0	2.8	13.3	3.6
15.0	25	2.2	1.5	14.9	5.0	2.5	0.7	12.2	2.3	4.5	1.3	10.2	2.5
	50	4.5	3.3	11.6	3.9	2.9	0.5	12.1	2.4	4.4	1.1	10.2	2.3
	75	3.0	1.5	14.3	2.5	3.3	1.2	15.0	2.5	4.2	2.1	13.4	3.7
	100	1.6	1.0	16.2	2.1	3.2	1.1	15.3	0.9	6.0	2.2	12.6	2.0
	125	1.1	0.6	16.0	1.3	3.0	1.4	14.7	2.5	5.5	2.1	12.9	2.5
	150	2.2	1.2	17.5	3.9	2.9	1.6	17.7	4.8	6.0	2.8	15.8	4.0
17.5	25	1.8	0.6	20.3	5.9	1.6	0.9	20.1	4.3	5.7	1.6	13.3	3.2
	50	2.9	1.2	19.3	3.3	1.6	0.5	19.7	6.1	5.6	1.6	14.2	2.5
	75	0.9	0.6	24.1	6.3	1.5	0.4	21.4	4.0	5.3	1.7	14.9	3.1
	100	2.1	0.9	20.4	4.8	2.0	0.7	21.3	2.9	5.2	1.9	15.5	3.1
	125	1.6	0.9	23.8	2.9	1.9	0.4	22.8	3.1	6.1	2.2	17.5	3.2
	150	1.3	0.3	25.7	3.9	1.7	0.9	24.9	3.9	5.8	1.8	17.5	5.4
20.0	25	1.5	0.4	26.4	6.3	0.7	0.2	25.9	5.5	6.0	2.4	14.8	2.5
	50	1.0	0.2	27.8	6.7	0.7	0.2	27.2	4.9	5.0	1.4	16.7	4.1
	75	1.1	0.5	26.2	5.4	0.9	0.4	26.1	4.0	5.4	2.6	17.3	3.5
	100	1.7	0.6	28.3	8.4	1.0	0.4	29.2	6.9	5.8	1.9	18.7	3.6
	125	0.7	0.2	30.5	4.8	1.3	0.4	30.1	3.1	5.8	2.3	18.7	4.4
	150	1.2	0.4	30.7	5.5	1.2	0.6	30.0	5.5	6.3	2.0	19.8	5.1

Table 4.3: Best Results Averaged over Whole Database

Algorithm	Missed error rate (%)		False error rate (%)		Error cost (%)	
	Maximum	Average	Maximum	Average	Maximum	Average
MST	9.3	3.2	30.7	13.1	14.5	7.7
Template	9.8	3.9	30.1	13.1	14.2	8.0
Two-phase	6.3	4.1	19.8	10.9	12.4	7.1

Table 4.4: Results of each data set averaged over EMG signals with different jitter*

Cont level	MST clustering				Template-based classifying				Two-phase clustering			
	Missed error		False error		Missed error		False error		Missed error		False error	
	Mean	MAD	Mean	MAD	Mean	MAD	Mean	MAD	Mean	MAD	Mean	MAD
5.0	5.8	1.9	1.7	0.8	8.9	0.5	2.3	1.2	1.8	0.4	3.8	1.3
7.5	4.7	0.8	4.0	1.0	5.4	0.6	4.6	1.3	2.9	0.7	6.1	1.3
10.0	3.0	0.8	8.7	1.4	3.6	0.4	8.7	1.7	2.9	1.0	9.6	1.7
12.5	3.8	0.5	12.1	1.0	3.5	0.3	12.1	1.1	4.4	0.9	11.3	1.1
15.0	2.4	0.9	15.1	1.5	3.0	0.2	14.5	1.6	5.1	0.7	12.5	1.5
17.5	1.8	0.5	22.3	2.3	1.7	0.2	21.7	1.4	5.6	0.3	15.5	1.4
20.0	1.2	0.3	28.3	1.5	1.0	0.2	28.1	1.7	5.7	0.3	17.7	1.4
AVE	3.2	0.8	13.2	1.4	3.9	0.3	13.1	1.4	4.1	0.6	10.9	1.4

* Note that the 'MAD' in this table measures the deviation of errors for each contraction level.

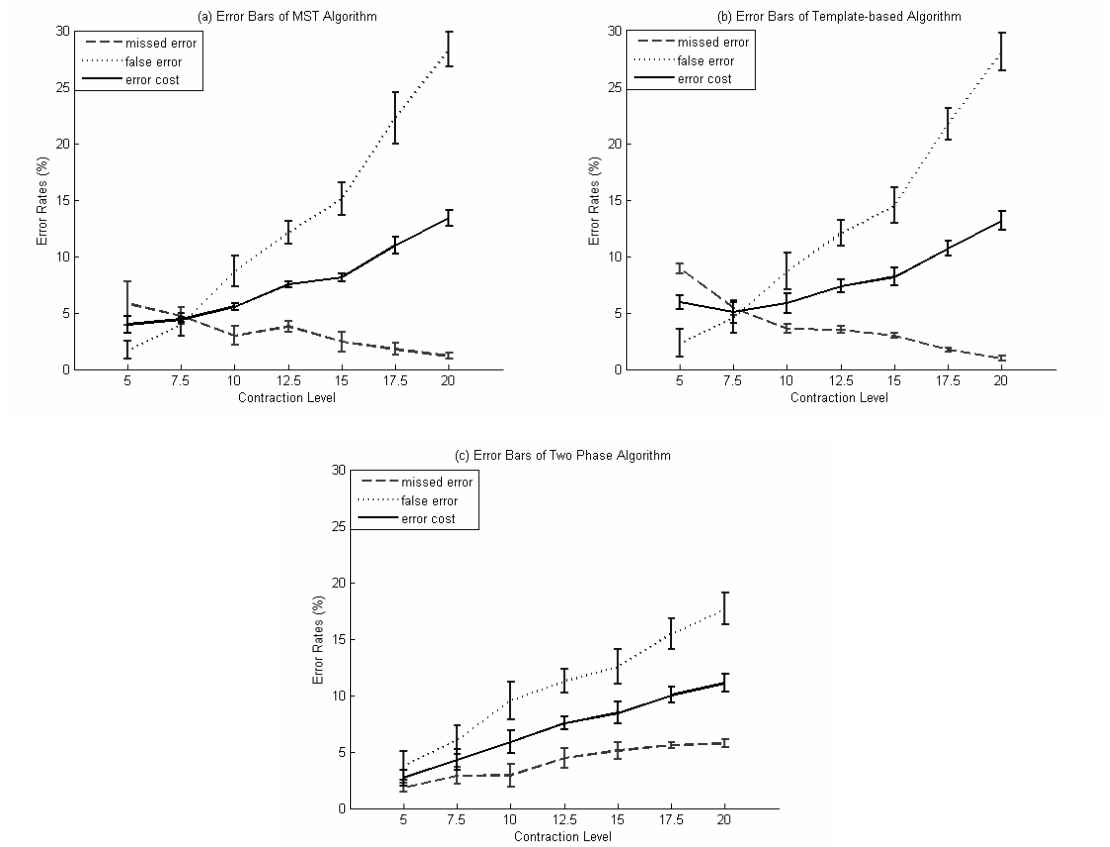

Figure 4.10: Error bars of three algorithms with different contraction levels

The influence of contraction level on ISO-MUP identification errors is reflected through SUP-MUP ratios of an MUPT. The template-based algorithm adopts all MUPs to calculate the ISO-MUP template and the distance threshold to the template. Even if an ISO-MUP template is estimated without the effect of SUP-MUPs using some robust method, the mean and STD of distances to the template may still be overestimated because of the influence of SUP-MUPs especially when the ratio of SUP-MUPs is high. The higher a contraction level is, the larger the difference

between predicted class radius (i.e., 'mean + COV_2 * STD') and the actual radius of the ISO-MUP class will be. Consequently, the missed errors get smaller until all ISO-MUP are included, while false errors increase dramatically with contraction level.

Similar trends are obtained by the MST clustering algorithm. When contraction level increases, more and more ISO-MUPs are contaminated by other MUPs to some extent so that the all MUP-MST distances become larger, the sudden change of distances or the cutting point on the MST curve becomes harder to detect. Like the example shown in subplot (c) of Figure 4.8, there is almost no clear cutting point in the MST curve at a contraction level of 20% MVC. If the MST curve is cut using the 'mean + COV_1 * STD' of the adjacent 30 MUPs on the curve, as the mean and STD estimations both increase with the contraction level, the cutting position would be later than the proper one in the MST. The number of missed errors will go down and the number of false errors will increase as the class radius of ISO-MUPs becomes larger than the actual one.

On the contrary, the two-phase clustering algorithm is designed to be adaptive to the contraction level based on the positive relationship between intensity and the percentage of SUP-MUPs in an MUPT. Figure 4.8 demonstrates the efficiency of the adaptive acceleration threshold for cutting a MST curve. However, since the ISO- and SUP-MUPs become more overlapped along the MST as contraction level increase, the false errors during the separating phase will increase which can not be corrected by the second phase. Alternately, the conservative separating of ISO- from SUP-MUPs causes more ISO-MUPs to be missed during the first phase. Therefore, the ISO-MUP class radius is also underestimated so that fewer ISO-MUPs are reclassified. This is why the number of missed errors slightly increases with contraction level while the number of false errors also increases. However, the degree of influence of contraction level on this algorithm is much lower than that on the other two (see Figure 4.10), which means the two-phase algorithm is more robust to the effect of intensity.

4.3.5.2 Stability Analysis

The MADs calculated in Table 4.4 measure the variability of testing results on multiple EMG signals with different jitter values at certain contraction levels. The stability of the identification results of different trains with the same jitter and contraction level can only be investigated from the detailed Table 4.3, where the

MAD was used for measuring variability within each EMG signal that only has a few trains, in order to reduce the effect of outliers. Though the variations of missed errors are all quite small for the three algorithms, the variations of false errors are large for the first two methods. On the contrary, the results for the two-phase algorithm are more consistent even for some situations where its predictions are not very accurate. It means that the two-phase algorithm is more stable for identifying ISO-MUPs from diverse MUPTs. The same conclusion can be drawn by comparing the ranges of errors across the whole database, i.e., contrasting the maximal values to the averaged ones. As shown in Table 4.3, the differences between the maximum and the average errors made by the first two algorithms are much larger than that of the two-phase method.

4.3.5.3 Sensitivity Analysis

The sensitivity of controlling parameters can be investigated by comparing the drifting of performance with certain adjustment of corresponding parameters. For the two phase algorithm, a robust value 5.00 was chosen as the CAT in this thesis based on some initial experiments. Then the control parameters for searching optimal results are all COV, coefficient of variance for the 'mean + COV * STD' estimation, so the sensitivity of the three algorithms relative to the controlling parameters can be compared by the changes of results during certain parameter adjustment. For example, with the COVs altered in the range of -10% to +10% around their cost optimal values, the errors are compared in Table 4.5.

Table 4.5: Results for different controlling parameters

Algorithm	Change of COV	Missed Error		False Error		Error Cost	
		Maximum	Average	Maximum	Average	Maximum	Average
MST	2.66	13.7	6.2	25.3	10.0	13.1	7.9
	2.96	9.3	3.2	30.7	13.2	14.5	7.7
	3.26	5.9	1.8	34.2	15.5	15.5	7.9
Template	2.43	11.1	4.7	29.0	12.5	14.0	8.2
	2.70	9.8	3.9	30.1	13.1	14.2	8.0
	2.97	8.3	3.2	31.1	13.7	14.5	8.0
Two-phase	4.68	11.2	7.6	14.7	8.1	12.8	7.8
	5.20	10.0	6.6	16.0	8.8	12.7	7.6
	5.72	8.7	5.7	17.2	9.4	12.5	7.4

Comparing the changes of errors in Table 4.5, one can find that the MST algorithm is sensitive to its parameter, since the relative change of errors is up to 50% corresponding to the 10% tuning of the parameter. On the contrary, the template-based method and the two-phase algorithm both have around 10% accuracy shifts with 10% changes of the controlling parameters, which are acceptable as long as the changed errors are still in a proper range.

The sensitivity of the two-phase clustering algorithm on the first parameter, CAT, can also be investigated by checking the optimal range with alternative COVs. As shown in Table 4.6, when CAT increases, the acceptable COVs tend to be small but change relatively slowly, which means COV is not sensitive to changes of CAT if it is kept in a suitable range, e.g., 4 to 5.

Table 4.6: Acceptable ranges of COV and errors with different CAT

CAT	Acceptable range of COV	Missed Error		False Error		Error Cost	
		Maximum	Average	Maximum	Average	Maximum	Average
4	5.9	9.9	6.4	17.3	8.9	12.4	7.5
	7.1	7.6	4.7	19.9	10.3	12.4	7.2
5	5.2	10.0	6.6	16.0	8.8	12.7	7.6
	7.0	6.3	4.1	19.8	10.9	12.4	7.1
6	4.9	9.9	6.4	16.2	9.0	12.6	7.5
	6.5	6.9	4.1	19.9	10.8	12.5	7.2

Table 4.7: Speeds of three algorithms (s)*

Contr. level (% of MVC)	Intensity (p.p.s.)	Ave. num of MUPs in one train	Ave. time processing each train		
			MST clustering	Template-based classification	Two-phase clustering
5.0	40.0	320	2.0	0.0	2.0
7.5	64.1	300	2.4	0.1	2.5
10.0	90.7	296	2.9	0.1	2.9
12.5	105.7	332	3.3	0.1	3.3
15.0	120.8	368	3.9	0.1	3.9
17.5	151.3	396	4.0	0.1	4.0
20.0	184.2	439	4.1	0.1	4.1
AVE	119.5	350	3.2	0.1	3.3

*: Implemented in Matlab 7.0 and tested on a PC with dual core 1.60 GHz CPU and 1 GB of RAM.

4.3.6 Computation Efficiency

The speeds of the three algorithms are listed in Table 4.7, where the two-phase algorithm has almost the same speed as the MST method. By further code optimization, the running time of the two-phase algorithm on a train can be reduced to less than 0.1 s in Visual C++, which is fast enough for the online measurement of jitter.

4.3.7 Algorithm Validation

A real MUPT example validating the two-phase algorithm is shown in Figure 4.11, where the MUPT is decomposed by DQEMG, an EMG signal decomposition and quantitative analysis system developed by Biomedical Signal Processing Lab at the University of Waterloo. Since no prior knowledge of jitter is available, the identification results are visually checked by researchers. The real data checking is completed on some real EMG data detected from normals and patients with neuropathic or myopathic disease, and the automated identification results match the manual results consistently.

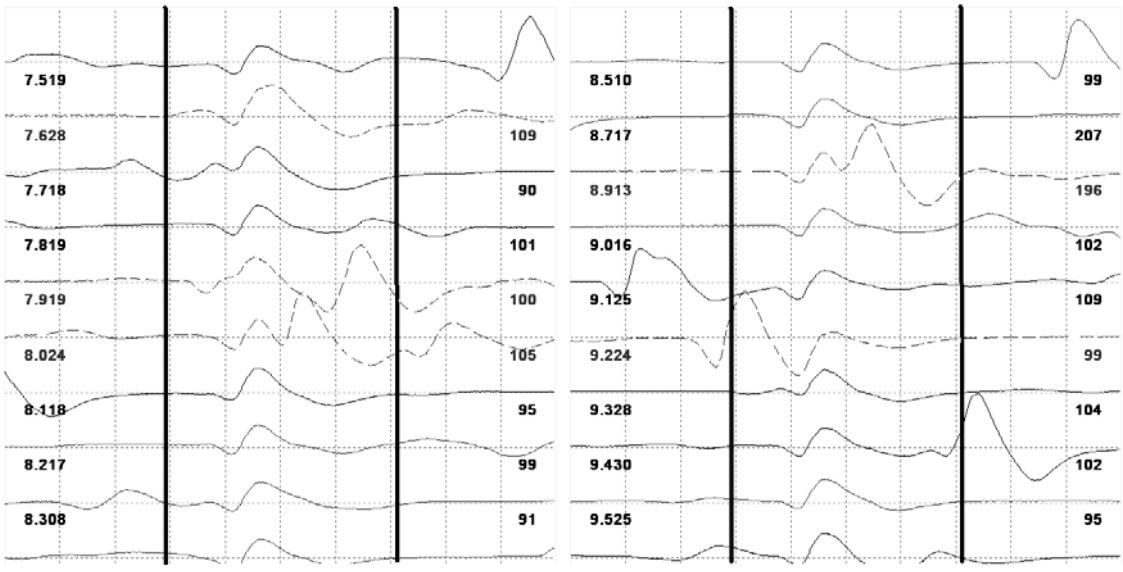

Figure 4.11: An example of the identification results of two-phase algorithm on a real MUPT (detected SUP-MUPs are marked by dashed lines)

4.4 Discussions

To meet the requirements of identifying ISO-MUPs for automated jitter measurement and prepare for other applications in EMG signal detailed decomposition, a MST-based two-phase clustering algorithm was designed and tested compared to a MST clustering technique and a template-based method. Identification accuracies, error balances, robustness, stabilities, speeds, and sensitivities to parameters of the three algorithms were compared using a simulated database. In summary, the two-phase clustering algorithm excels or equals the other two algorithms in most of the investigated aspects. The strongest point of the two-phase algorithm is its robustness to the diversity of EMG signals detected during various contraction levels and (or) with different jitter values. Meanwhile, it keeps both types of errors relatively small simultaneously with stable performance if parameters are in proper ranges.

The effect of jitter is reduced by employing the MST scheme to describe the connectivity among MUPs instead of using the distance scheme. Meanwhile, by introducing an intensity adaptive threshold for cutting the MST curves, the two-phase algorithm is robust to the contraction level as well. The second refining phase helps make a better error balance as a complement process. Moreover, the design idea is that makes a conservative guess first then check the answer with obtained information, which is the reason for the stability of performance and insensitivity with respect to controlling parameters.

Besides being successful to identifying ISO-MUPs in a variety of EMG signals, the two-phase algorithm is also useful for SUP-MUPs resolution for detailed EMG signal decomposition. The proposed algorithm has been implemented in the DQEMG system to accurately estimate MUPT templates with a satisfying performance.

As a suggestion for future work, the optimal value or range of the controlling parameters could be searched using a receiver operating characteristic (ROC) curve [Hastie 2001] for best error balance. Real datasets with gold standard or physician defined SUP-MUPs should be collected for algorithm validation. The connection between this preprocessing step and the next step for automated jitter measurement will be discussed in Chapters 6 and 7.

Chapter 5

Recognizing Near MFP Contributions to Isolated MUPs

Detecting MFP contributions to MUPs is a core step for automated measurement of neuromuscular jitter. After the preprocessing of MUPs, near MFPs can be detected as 'near' peaks in filtered MUP waveforms, while 'distant' peaks correspond to relatively distant MFPs, and 'false' peaks refer to baseline noise or artificial peaks created by the filter. MFP detection can be addressed as a multi-class classification problem and solved using pattern recognition (PR) techniques. The PR system designed for this problem has to be robust, accurate, and computationally efficient. By using simulated MUPs with known MFP components, the performance of two categories of classifiers – discriminant classifiers and nonparametric classifiers have been evaluated and compared in a reduced feature space. A simple PR system employing the quadratic discriminant classifier has been validated as the most appropriate MFP identification system in this thesis.

5.1 Introduction

As reviewed in Chapter 3, previous research has proved that MFP peaks can be detected by band-pass filtering an MUP or by using the acceleration of an MUP directly. Detected acceleration peaks may correspond to near or distant MFP contributions or may not correspond to any MFP contribution. For convenience, these peaks have been named near, distant, and false peaks respectively. Two examples of MUPs and detected peaks are shown in Figure 5.1. The problem in this chapter is how to determine if a detected acceleration peaks is a near, distant, or false peak. It is essentially a pattern recognition problem.

A typical PR system comprises three phases, i.e., data acquisition, feature selection or extraction, and classification. Data are collected using a set of sensors during the data acquisition phase. After some preprocessing, they are passed on to the feature selection or extraction phase, where the dimensionality of measured data is reduced to a few characterizing features. Finally, the data represented by these features are fed to the classification system, and the classifier makes the final decision [Sankar 2004].

Usually, the design procedure for a PR system is an adaptive cycle as shown in Figure 5.2. Feature and classifier selection are key steps for the whole design.

For the specific PR problem in this chapter, the input data are measurements of the detected acceleration peaks of an MUP, and the output of the classifier should be labels of near, distant, or false. To handle the variety caused by different muscles and the noisy measuring channel, the MFP peaks identification system has to be robust and accurate. It is also required to be computationally efficient, since the designed PR system designed will be integrated into a larger EMG signal processing system in the future.

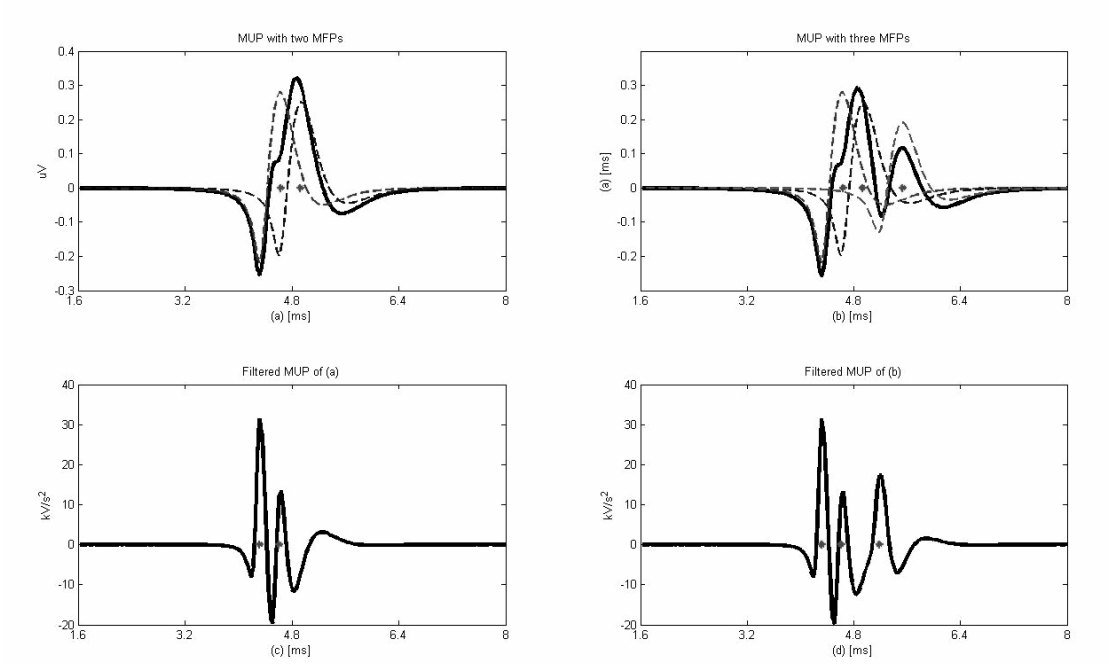

Figure 5.1: MUPs and corresponding acceleration filtered MUPs (solid line) composed by two (left) and three (right) near MFPs (dashed lines). The locations of near MFP contributions and acceleration peaks are marked by asterisks.

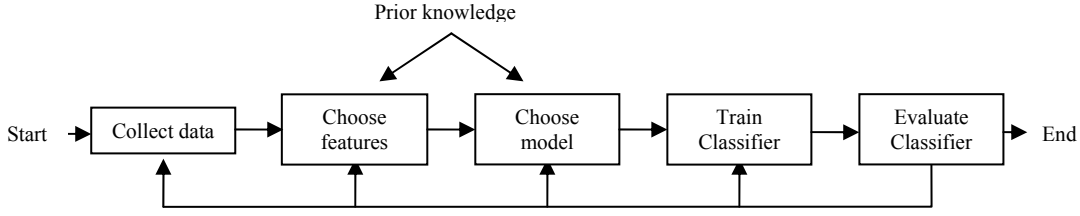

Figure 5.2: The design cycle of a pattern recognition system

5.2 Method

Following the design cycle shown as in Figure 5.2, the method of the near MFP recognition system is discussed in three parts: data collection, feature selection or extraction, and classification designing.

5.2.1 Data Collection

5.2.1.1 Data measuring

As exemplified in Figure 5.3, a peak on an MUP acceleration waveform, or more specifically, a positive peak, can be defined as the local maximum and the monotone increasing and decreasing segments of the waveform at the side of that maximum are called the rising and falling edges respectively. To characterize acceleration peaks, measurements are usually taken from the perspectives of energy, frequency, symmetry, and location of a peak. Six measurements have been considered in this thesis, and their definitions and units are:

- Amplitude [kV/s^2]: magnitude of the detected peak which is the minimal magnitude of the rising and falling edges of that peak;
- Sharpness [kV/s^2/sample interval]: minimal absolute slope of the two edges;
- Slope ratio: the ratio of the two absolute slopes, i.e., the falling slope / the rising slope;
- Peak location [sample index]: the location of the maximal acceleration in the whole MUP;
- Maximal acceleration [kV/s^2]: the maximal acceleration of the peak;
- Rise time [sample interval]: the length of the rising edge of the peak,

where the sample interval is the constant time interval between two sample points in an MUP, and it is the reciprocal of the sample frequency of an EMG signal. The sample interval is 32 μs and the sample index is relative to the 10 ms sampling window of an MUP in the simulated dataset. As shown in Figure 5.3, part of the six measurements can be taken directly from the detected peak, while others are calculated from these basic measurements. Meanwhile, some quantities are also related physically, e.g., amplitude and maximal acceleration are both quantities

measuring energy. It means the six measurements are correlated to some extent. The redundant information as well as the relatively high dimensionality should be reduced by a feature extraction or feature selection process.

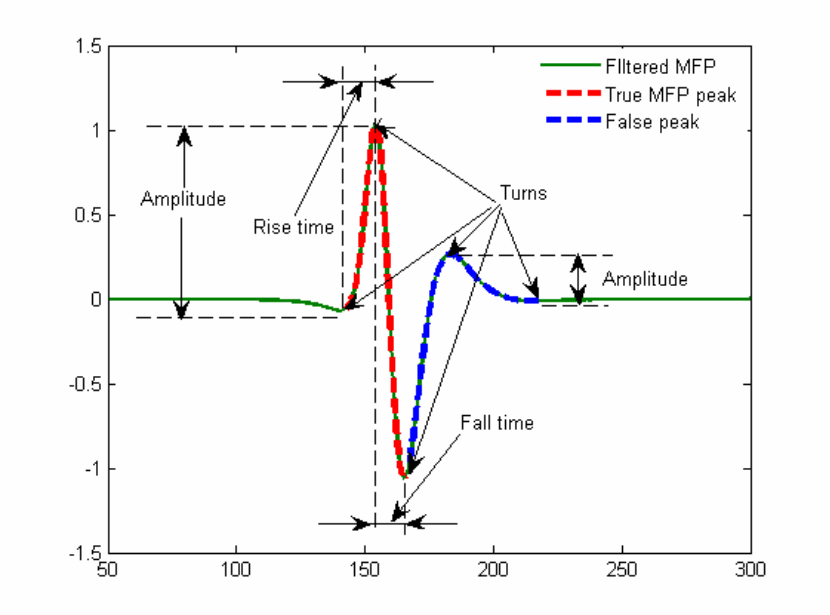

Figure 5.3: Some measurements of a MFP acceleration waveform

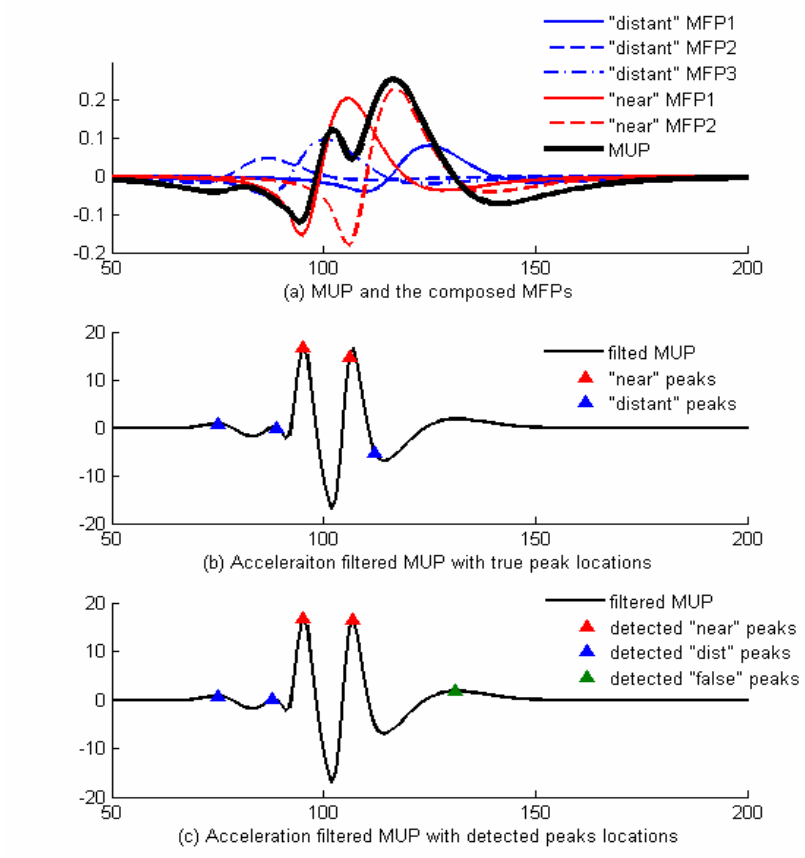

Figure 5.4: An example shows the procedure of MUP simulation and peaks labeling

5.2.1.2 Data simulation and labeling

For the purposes of algorithm evaluation, peaks detected from accelerations of MFPs are collected like the two peaks in the example shown in Figure 5.3. Since the near peaks and distant peaks are just relative categories, in this thesis, three arbitrary criteria were used to define the acceleration peaks for simplicity. One example of a definition criterion, namely '7.5-2.5', is listed as follow:

An isolated acceleration peak is a

$$\begin{cases} \text{"near" peak,} & \text{if it corresponds to a MFP peak and its amplitude} > 7.5\ \text{kV/s}^2; \\ \text{"dist" peak,} & \text{if it corresponds to a MFP peak and its amplitude} < 2.5\ \text{kV/s}^2; \\ \text{"false" peak,} & \text{if it does not correspond to any MFP peak.} \end{cases} \quad (5.1)$$

The blank between the near and distant (or dist in short) categories was left intended for the purpose of making the two peak classes more separable to simplify this classification problem. Two other criteria with smaller or no gap between near and distant peaks have also been employed to evaluate the performance of the designed pattern recognition system.

During EMG signal decomposition of real signals, it is not important to identify a detected MFP peak as near or distant, as the idea of significant MFP is only relative to baseline. However, the error of falsely detecting baseline noise as a significant MFP, and the opposite, the missed detection error, are important for further MFP analysis. Therefore, the PR system designed should be able to distinguish between near and false peaks as accurately as possible.

A variety of individual MFPs were simulated and summated with small random shifting to make a pool of MUPs. The detected acceleration peaks of those simulated MUPs were labeled corresponding to individual peaks, though they have different measurements due to the overlapping with other MFPs. As illustrated in Figure 5.4, the actual labeling rule of a detected peak dataset is:

An detected acceleration peak is a

$$\begin{cases} \text{'near' peak,} & \text{if it is detected close to the relative position of a individual near peak;} \\ \text{'dist' peak,} & \text{if it is detected close to the relative position of a individual dist peak;} \\ \text{'false' peak,} & \text{otherwise.} \end{cases}$$

where the concept of 'close' is quantified as less than 128 μs (i.e., 4 sample intervals) in this research.

A simulated MUP example composed by two near MFPs and three distant MFPs is shown in Figure 5.4. The locations of the isolated peaks corresponding to true MFPs are shown in subplot (b). And the detected peaks labeled using the above rule are shown in subplot (c). Note that one distant MFP peak is not detectable since it is overwhelmed by one near peak.

5.2.2 Feature Selection / Extraction

5.2.2.1 Feature normalization

As discussed before, six measurements have been taken to represent some features of a MFP acceleration peak: Amplitude and maximal acceleration are measurements of energy; sharpness and rise time are quantities related to frequency content; slope ratio inspects the symmetry of a peak; and peak location relates to the temporal distribution of a peak in an MUP. If we simply take each measurement as one feature, the feature space is correlated and has to be normalized. Sample histograms were studied for each measurement taken from a typical simulated dataset. Figure 5.5 shows that the simulated data distributions of the three types of peaks for each measurement. 500 peaks of each type were randomly picked from the dataset defined by criteria of equation (5.1) (see Table 5.1 for the composition of this data set) and counted for the frequencies of the bins in the histograms. Due to the nature of digital measurements, all of these quantities are discrete.

Observing the density histograms in Figure 5.5, it seems that the feature distributions of some classes are non-Gaussian or even bimodal, which makes the classification problem very hard. To avoid the complex classification of non-Gaussian data, the sample distribution of each feature was studied using the distribution fitting tool of Matlab statistics toolbox, 'dfittool'. The lognormal distribution was found to be the best fitting for almost all of the non-normal distributed features. Figure 5.6 has exemplified the lognormal fittings of amplitude distributions with respect to a PDF, while Figure 5.7 shows the CDF, where most of the fitting errors are within the confidence level.

Table 5.1: The composition of the simulated '7.5-2.5' dataset

Classes	Near	Distant	False	Total
Number of data	1280	500	696	2476
Percentage (%)	51.7	20.2	28.1	100

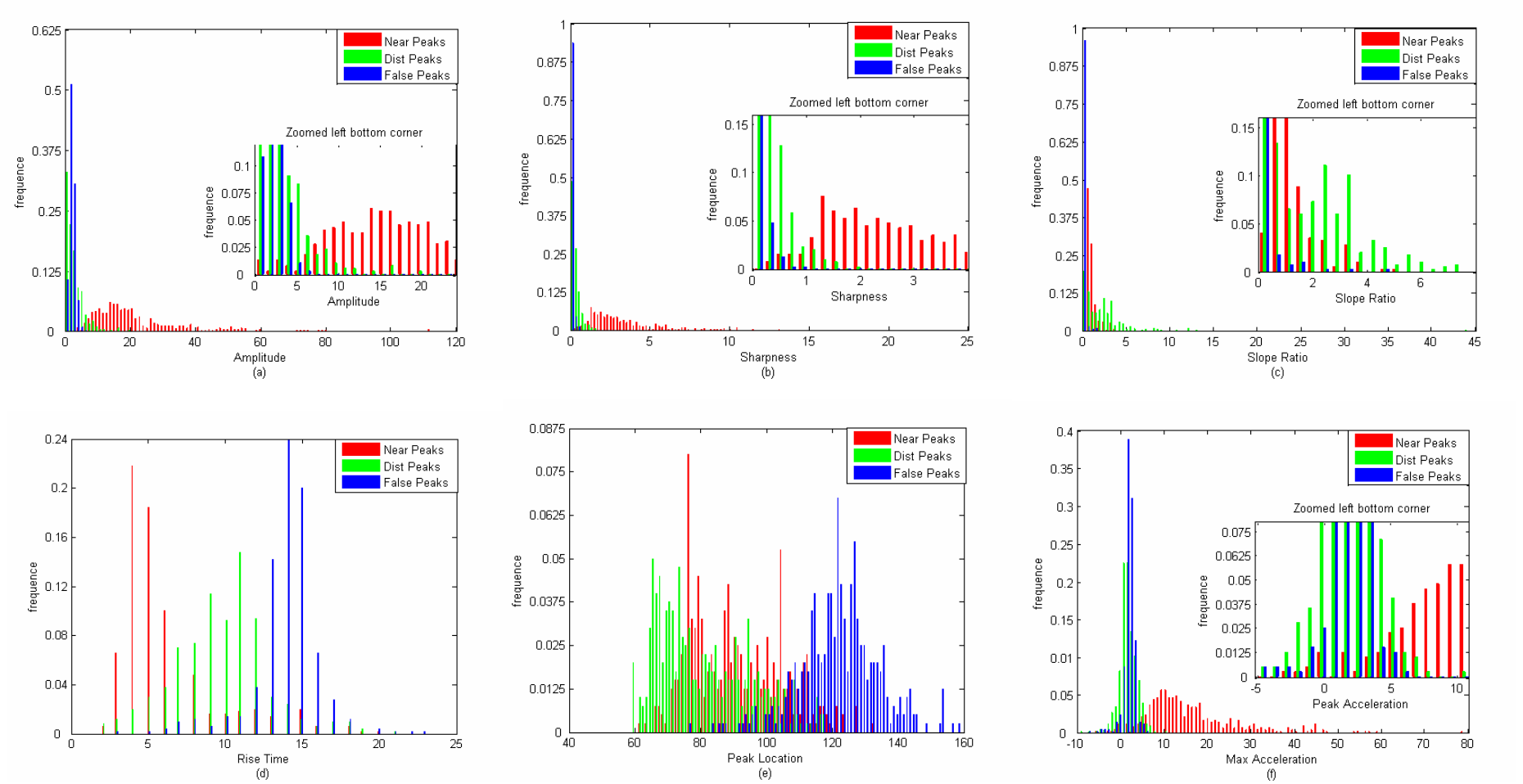

Figure 5.5: Histograms show the measurement distributions of three classes

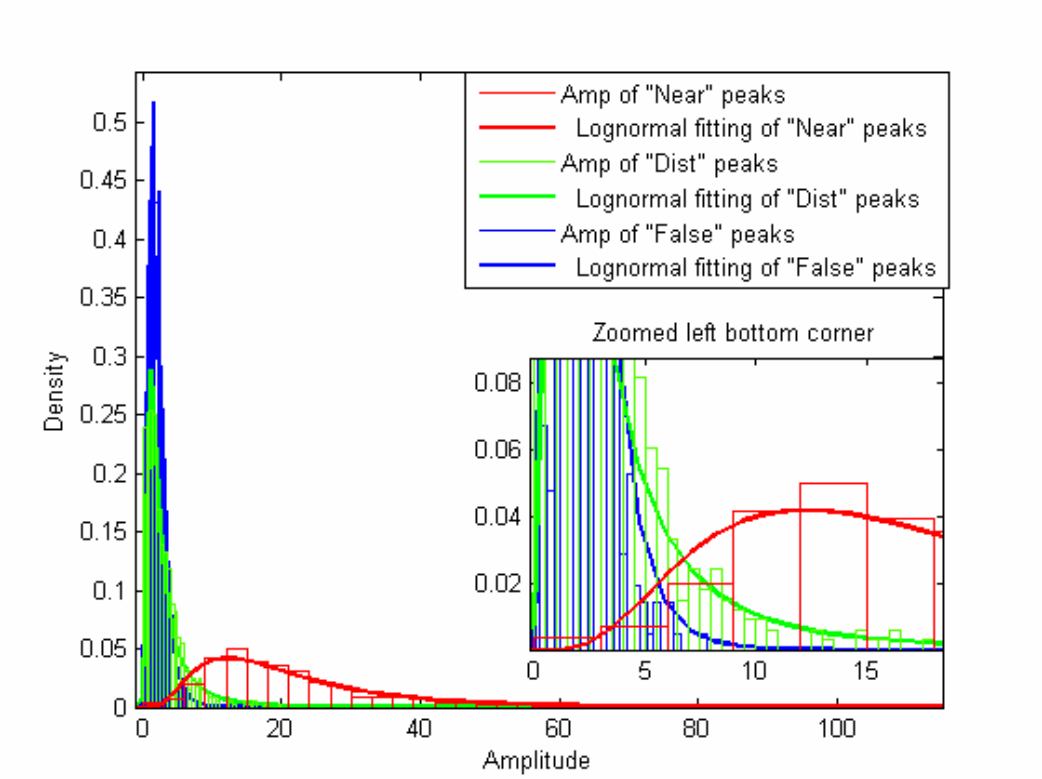

Figure 5.6: The lognormal fitting of three categories of data by density (PDF) display

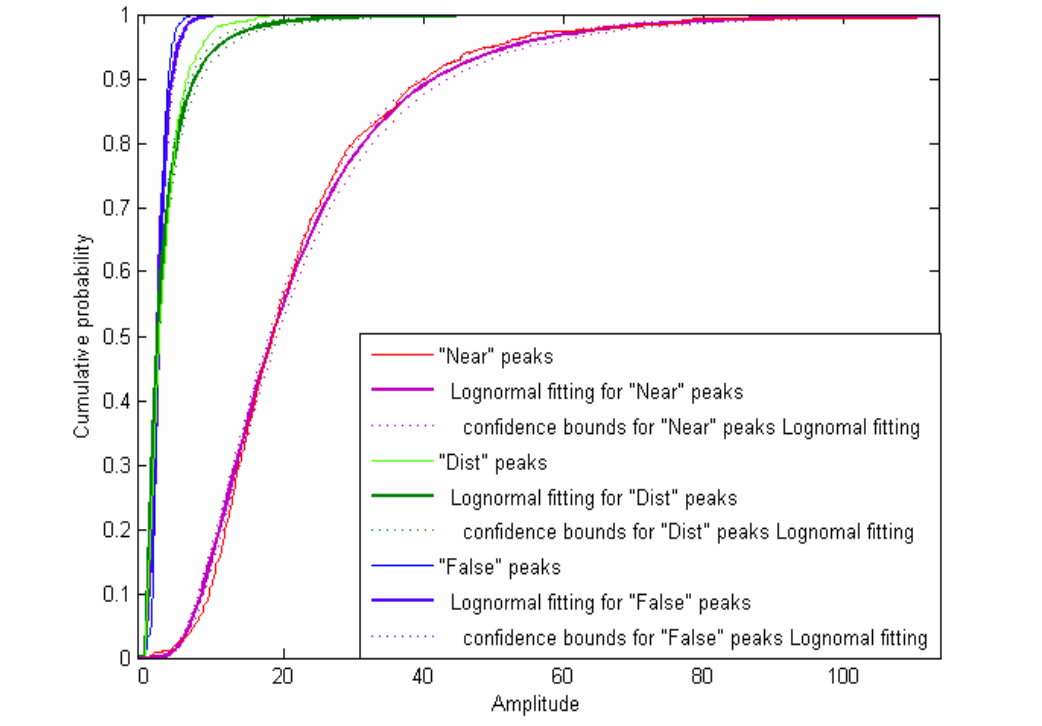

Figure 5.7: The lognormal fitting of three categories of data using the cumulative probability (CDF) display

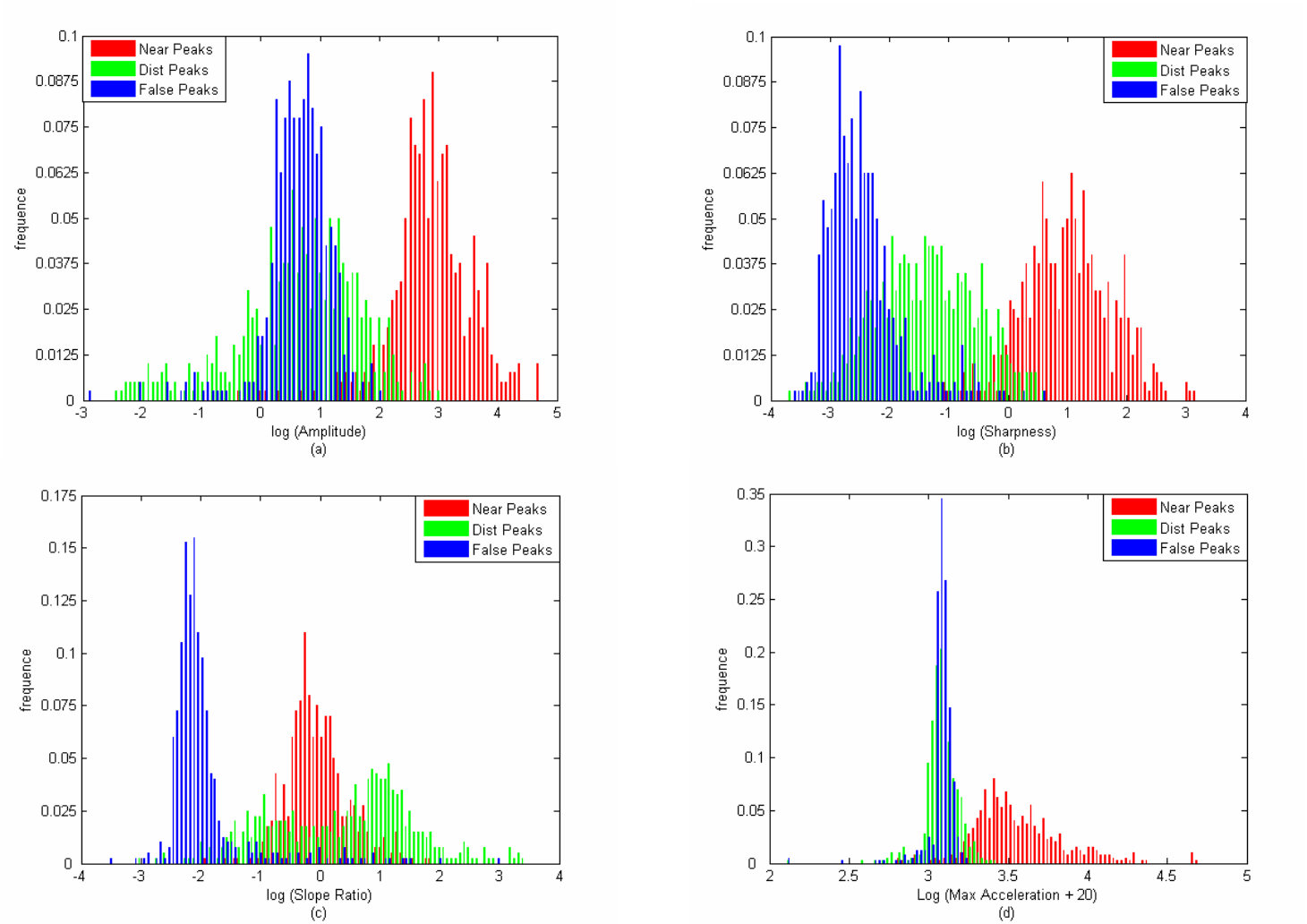

Figure 5.8: Histograms of the logarithmic transformed features

In statistics, the lognormal distribution is the probability distribution of any random variable whose logarithm is normally distributed. It means that if X is log-normally distributed with parameters μ and σ^2, then ln(X) is distributed normally with the same parameters μ and σ^2. So by simply taking the natural logarithm of each non-Gaussian measurement, one can convert the feature space to be normally posed. The results of logarithm transformations of the non-normal features are shown in Figure 5.8.

5.2.2.2 Dimensionality reduction

After feature normalization, dimensionality reduction can be applied to reduce the complexity and information redundancy of a feature space. Two different approaches exist for reducing the dimensionality: one is to discard certain measurements and to select the remaining ones, which is called feature selection; another approach is feature extraction such that the selection takes place in a transformed space.

Transformation for dimensionality reduction can be linear, e.g., principal component analysis (PCA) and independent component analysis (ICA), or nonlinear, e.g., multidimensional scaling and kernel PCA. The eigen-map in Figure 5.9 shows that the first two principal components (PCs) account for most (87%) of the variance of the feature space, thus we can reduce the dimensionality of the feature space to 2. (Although using 3 or 4 may be more accurate, 2-D features can express the near and false peaks separately enough for this practical application.)

However, transformation of original measurements by PCA causes the low dimensional features to lose their physical identity and makes the final decision rule hard to interpret. In addition, the extracted feature subspace is data dependent since the transformation is based on the sample covariance. Alternatively, selecting the best N features does keep the physical units, and does not depend on the training sample dataset. The best separable 2-D subspace observed is the subspace of sharpness and slope ratio shown in Figure 5.10. The effectiveness of feature extraction and feature selection were compared using the classification results of data represented by extracted features or selected features in one course project done by the author. The selected two features: sharpness and slope ratio, were employed to characterize the measured peaks since the performance difference between using extracted feature and

using selected feature was not obvious, and feature selection is much more simple and fast in practice.

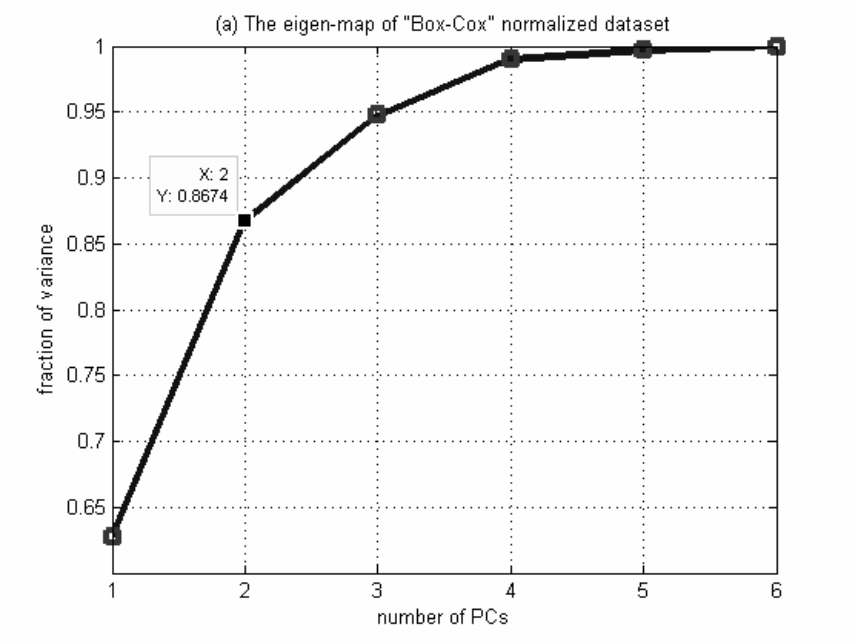

Figure 5.9: The fractions of variance wrt number of PCs

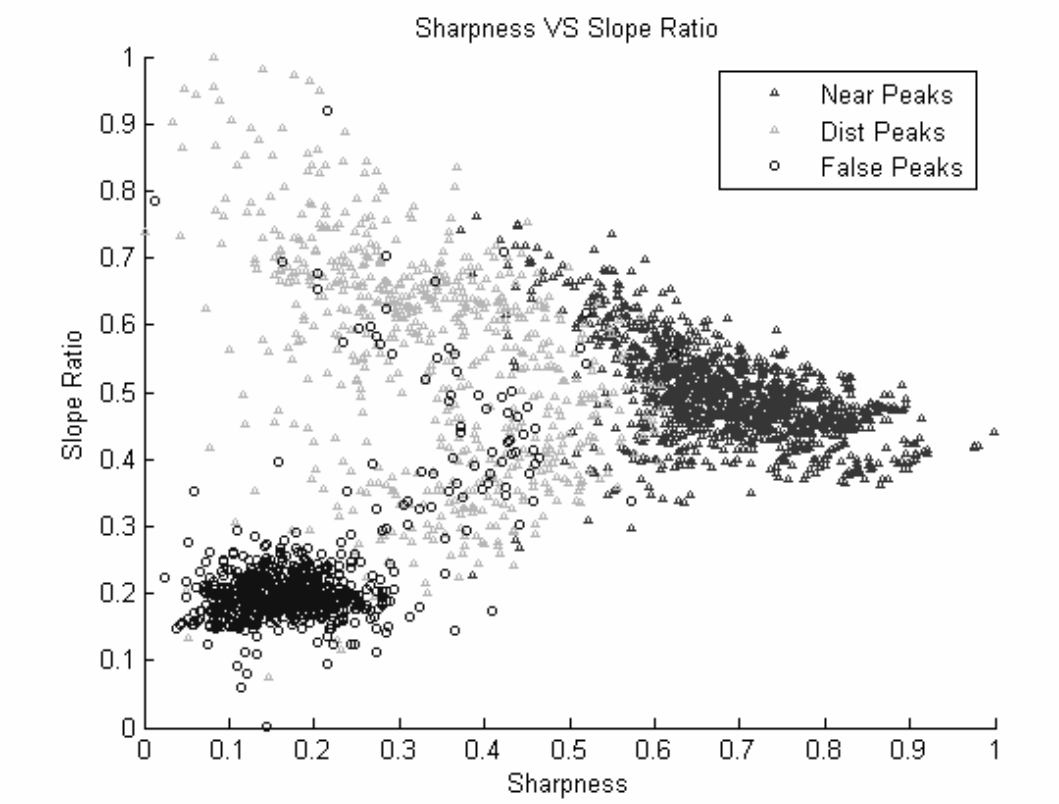

Figure 5.10: A 2-D subspace shows the separability of peaks when normalized by a logarithmic transformation

5.2.3 Classifier Design

As a major part in the PR system design, classifier design includes procedures of model searching and classifier evaluation. For the MFP peak identification problem, no prior knowledge about the data structure model has been given. The nonparametric techniques and linear discriminant classification algorithms were considered, because both of them can learn the data structure from the training data without prior knowledge. The classic linear and quadratic discriminant classifiers (note as LDC and QDC respectively) were compared to the two typical nonparametric techniques: k nearest neighbor (k-NN) and Parzen window algorithms in this thesis. Based on the requirement of this MFP peak recognition problem, the four candidate classifiers were evaluated on accuracy, speed, and algorithm complexity aspects.

5.2.3.1 Linear discriminant classifier (LDC) and quadratic discriminant classifier (QDC)

From [Duda 2000], a linear discriminant function of **x** can be written as a linear combination of the components of **x** as:

$$g(\mathbf{x}) = \mathbf{w}^{\mathrm{T}}\mathbf{x} + w_0,$$

where **w** is the weight vector and w_0 is the bias. For two-category cases, the linear decision boundary $g(x) = 0$ will separate the feature space into two half spaces R_1 where $g(x) > 0$ and R_2 $g(x) < 0$ correspondingly. For multi-category cases like the MFP identification problem, a linear machine was employed. A linear machine divides the feature space into *c* decision regions, which classify **x** to region R_i where $g_i(x)$ being the largest discriminant. The boundary between two contiguous region R_i and R_j are defined by

$$g_i(\mathbf{x}) = g_j(\mathbf{x}).$$

The linear machine generally is most appropriate for the problem with unimodal conditional densities $p(\mathbf{x}|w_i)$, so it was a good choice for the normalized dataset in this study.

The quadratic linear function is an extension of the linear discriminant function created by adding additional terms involving the products of pairs of the components of **x**:

$$g(\mathbf{x}) = w_0 + \sum_{i=1}^{d} w_i x_i + \sum_{i=1}^{d}\sum_{j=1}^{d} w_{ij} x_i x_j \ .$$

The separating surface defined by $g(\mathbf{x}) = 0$ is a hyperquadric surface.

5.2.3.2 k-NN classifier and Parzen window classifier

Both the k-NN and Parzen window techniques are essentially density estimation approaches. The difference between them is that the later uses a hypercube window with optimized size to estimate the density, while the former adopts cells whose volume is decided by the training data. They both do not require any prior knowledge, thus are suitable for estimating any density theoretically. As classifiers, the number of cells of the k-NN approach or the smoothing parameter of the Parzen windows method has to be provided. In this study, these two parameters were optimized by leave-one-out or Jackknife cross validation on a training dataset. Though these optimized parameters are dataset dependent, they are reliable if the training dataset suitably represents real data.

5.3 EXPERIMENTS

5.3.1 Simulated Data Sets

Three datasets with different levels of difficulty were created to investigate the performance of the four classifiers. The easiest dataset is shown in Table 5.1 and is defined based on the criteria described in equation (5.1). This is the most separable dataset. The moderately difficult dataset one is defined as using equation (5.2) and is shown in Table 5.2. The dataset defined using the most difficult criteria defined by equation (5.3) has been listed in Table 5.3.

An isolated acceleration peak is a

$$\begin{cases} \text{"near" peak,} & \text{if it corresponds to a MFP peak and its amplitude} > 7.5\ \text{kV/s}^2; \\ \text{"dist" peak,} & \text{if it corresponds to a MFP peak and its amplitude} < 5\ \text{kV/s}^2; \\ \text{"false" peak,} & \text{if it does not correspond to any MFP peak.} \end{cases} \quad (5.2)$$

Table 5.2: The composition of the simulated '7.5-5' dataset

Classes	Near	Distant	False	Total
Number of data	1280	663	696	2639
Percentage (%)	48.5	25.1	26.4	100

An isolated acceleration peak is a

$$\begin{cases} \text{"near" peak,} & \text{if it corresponds to a MFP peak and its amplitude} > 5\ \text{kV/s}^2; \\ \text{"dist" peak,} & \text{if it corresponds to a MFP peak and its amplitude} < 5\ \text{kV/s}^2; \\ \text{"false" peak,} & \text{if it does not correspond to any MFP peak.} \end{cases} \quad (5.3)$$

Table 5.3: The composition of the simulated '5-5' dataset

Classes	Near	Distant	False	Total
Number of data	1573	663	696	2932
Percentage (%)	53.7	22.6	23.7	100

5.3.2 Procedure

The basic procedure for each experiment was performed as:

data transformation -> feature extraction / selection -> classifier training -> classifier testing -> classification evaluation.

For the nonparametric classifiers, k of k-NN classifier (kNNC) and the smoothing parameter h of Parzen window classifier (ParzenC) were optimized by minimizing the Jackknife error of the training data. For example, k=14, h=0.036 were found by cross validation with the '7.5-5' dataset. Once these parameters were found, the models of the classifiers were fixed for further studies and this optimization procedure was not repeated again.

To make sure that the performances of all classifiers were compared using a consistent index, the leave-one-out (an extreme case of the Jackknife method) error of the whole dataset was calculated for each classifier and weighted averaged by the class frequencies. Confusion matrixes were created by half training and half testing the data of the datasets, for further analysis of error distribution. Meanwhile, the classification time of each data has been recoded for each candidate. (Note it was the testing time rather than the training time recoded, since the training time is not important for an identification system.) Experimental results follow in the next section.

5.3.3 Results

As an example, the decision boundaries of the four classifiers on the moderately difficult dataset '7.5-5' are shown in Figure 5.11. It seems that all four classifiers worked well and none of them was out-performed by the others. However the k-NN classifier and the Parzen window classifier as shown in the subplot (c) and (d) tend to be over- complex for this dataset. Especially the Parzen classifier, its boundary separating distant and false peaks seems overfit to the noisy data.

The confusion matrixes of the four classifiers are listed as Table 5.4 to Table 5.7. As illustrated by the decision boundaries and the confusion matrixes, the results of the four methods do satisfy the unequaled requirement of classification errors. The important false identification errors of classifying false peaks as near ones are all almost 0, and the critical missed identification errors of recognizing near peaks as false ones are quite small. This means the weighting strategy works well from the design perspective for each classifier.

The classification errors for the three datasets are listed in Table 5.8 and shown in Figure 5.12 as well. The performance of each classifier decreased with the increasing difficulty of the different datasets, while the k-NN and Parzen window classifiers yielded relatively fewer errors than LDC and QDC classifiers. However the nonparametric classifiers work very slowly, and tend to over fit the training data, so they are not preferred for the MFP peak recognition problem. Between the two discriminant methods, the LDC had a slightly smaller average, but fails when the data gets more difficult. Based on the comparison performed so far, the QDC is the most appropriate classifier in the four selected classifiers for the three-class classification problem in this chapter.

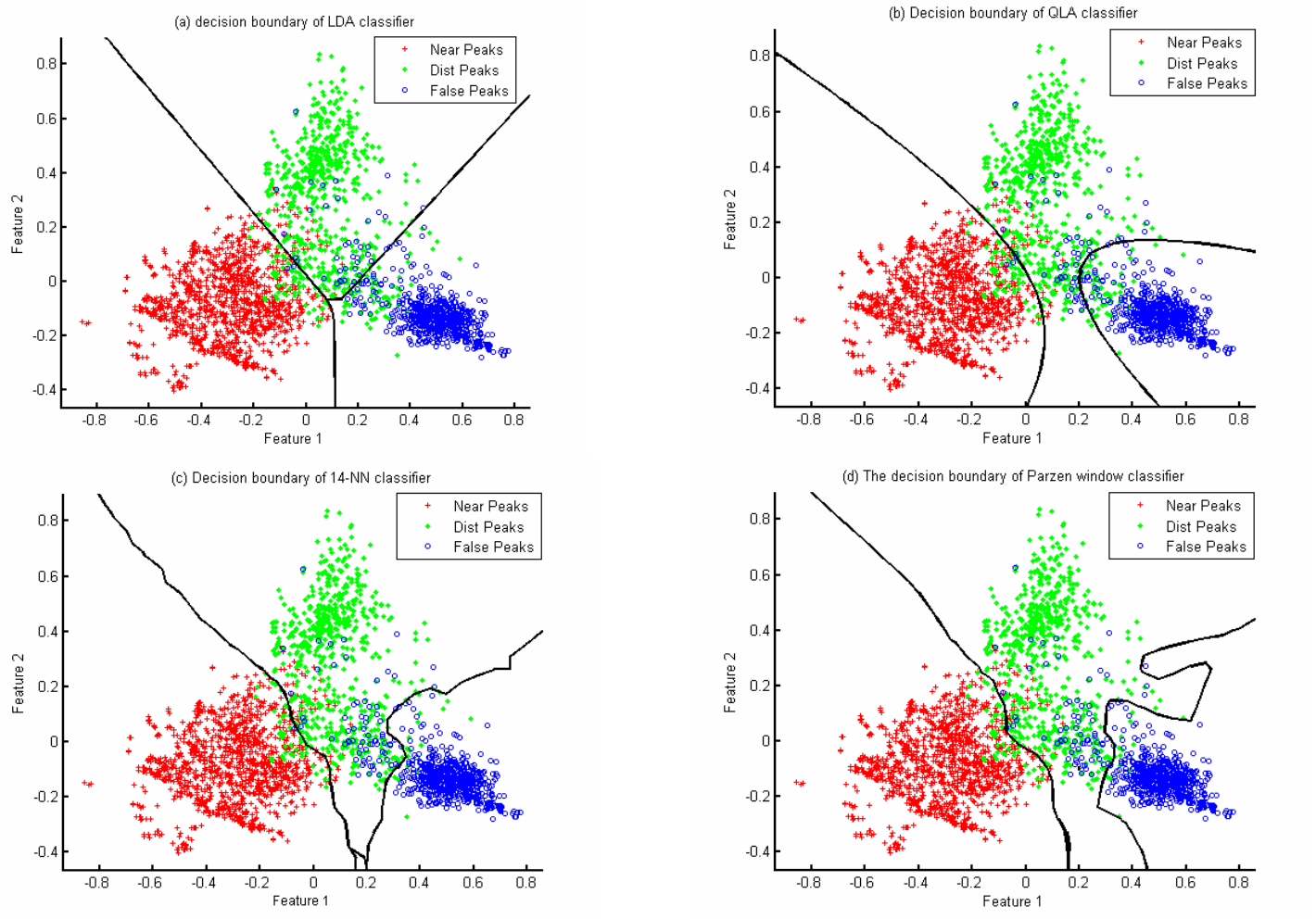

Figure 5.11: The decision boundaries of the four classifiers for the moderately difficult dataset

Table 5.4: Confusion matrix of LDC

True Labels	Estimated labels			
	Dist	False	Near	Total
Dist	265	35	31	331
False	20	327	1	348
Near	20	0	620	640
Total	305	362	652	1319

Table 5.5: Confusion matrix of QDC

True Labels	Estimated labels			
	Dist	False	Near	Total
Dist	277	29	25	331
False	26	322	0	348
Near	20	0	620	640
Total	323	351	645	1319

Table 5.6: Confusion matrix of 14-NN classifier

True Labels	Estimated labels			
	Dist	False	Near	Total
Dist	297	10	24	331
False	41	306	1	348
Near	30	0	610	640
Total	368	316	635	1319

Table 5.7: Confusion matrix of Parzen classifier

True Labels	Estimated labels			
	Dist	False	Near	Total
Dist	299	8	24	331
False	30	317	1	348
Near	25	0	615	640
Total	354	325	640	1319

Table 5.8: The experimental results of four classifiers on three datasets

Classifier	Dataset	Ave Weighted Test Error of Jackknife Estimation (%)	Ave Classify Speed (ms/data)
LDC	'7.5-2.5'	6.79	0.013
	'7.5-5'	7.92	0.012
	'5-5'	9.79	0.010
	Average	8.17	0.012
QDC	'7.5-2.5'	7.03	0.000
	'7.5-5'	8.34	0.012
	'5-5'	9.48	0.000
	Average	8.28	0.004
k-NN (k = 14)	'7.5-2.5'	6.34	0.530
	'7.5-5'	6.74	0.665
	'5-5'	8.36	0.618
	Average	7.15	0.604
ParzenC (h = 0.036)	'7.5-2.5'	6.18	0.505
	'7.5-5'	7.28	1.101
	'5-5'	8.53	0.618
	Average	7.33	0.741

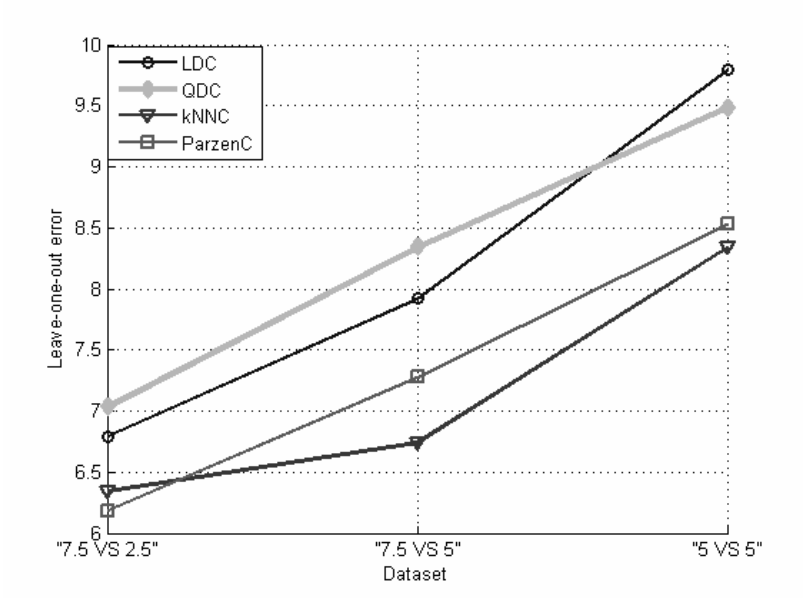

Figure 5.12: The error of four classifiers on three datasets

5.4 CONCLUSIONS AND DISCUSSIONS

A pattern recognition system was designed for the MFP peak recognition problem. Three major tasks of data collection, feature selection, and classifier design were carried out. Six measurements were taken to represent each data, and two features were selected to characterize each detected peak. Given no prior knowledge of the data distribution, the nonparametric techniques and linear discriminant methods were adopted to classify the MFP peaks in the reduced feature space. Two nonparametric classifiers (k-NN and Parzen window) and two discriminant methods (LD and QD) were compared with respect to the classification accuracy, computability, and simplicity for the practical problem. Leave-one-out or Jackknife cross validation was employed to evaluate the performance of the classifiers. Errors were weighted averaged over three classes by the class priors. Based on the experimental results, a simple PR system was chosen and could be implemented as shown in Figure 5.13. According to the experiments on synthetic datasets, the classification error for the finial system is expected to be around 10%.

All the work done till now is only the first loop of the design cycle as shown in Figure 5.2. Adjustment of each step has to be made to improve the performance of the recognition system. For instance, the lognormal density fitting has to be checked using more datasets, noise and outlier data of the false peak class should be removed

since they are the main cause of classification error. Other classifiers or methods improving classification performance such as support vector machine (SVM) and boosting, can also be tried. In fact, since features are almost all Gaussian distributed after the logarithmic transformation, the MFP peak data is essentially Gaussian. Therefore, we do not need more powerful techniques for this classification problem since linear discriminant classifiers can find an optimal solution for 2-D normal distributed data in theory. Actually, LDC is good enough to classify false and true MFP peaks, and it works even better than QDC in some circumstances, though QDC may be more powerful and be the best choice for classifying three types of peaks in this Chapter. However, the weights of error should be adjusted, and an ROC curve could be used for classification evaluation and design. Real data must be applied to the final designed system. When results on real data are suitable, the whole system will be simplified and integrated as part of a clinical EMG signal decomposition system for measuring jitter or fiber density in the future.

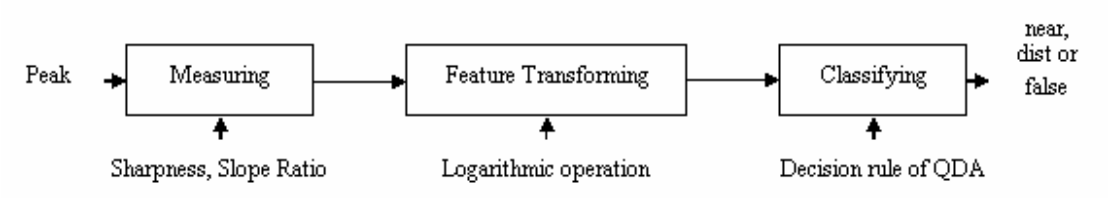

Figure 5.13: The final designed PR system for MFP peak recognition

Chapter 6

Measuring Jitter from Detected Near MFP Contributions to Isolated MUPs in an MUPT

After SUP-MUPs are excluded and near MFPs are recognized, jitter can be finally measured from the near MFP pairs contributed to ISO-MUPs in a train.

6.1 Introduction

As explained in Chapter 2, neuromuscular jitter is the measurement of the variability of inter-potential intervals (IPIs) within MUPs created by consecutive discharges of an MU. To measure jitter in MUPs, individual MFP pairs have to be found precisely and consistently across an MUPT. After the steps described in Chapter 4 and Chapter 5, ISO-MUPs and their significant MFP contributions can be detected accurately and robustly. The final step for the automated jitter measurement system, measuring jitter from near MFP contributions to ISO-MUPs in a train, is discussed in this chapter. The whole procedure for this step can be divided into three functional sections: tracking near MFPs across all ISO-MUPs in a train, selecting proper MFP pairs, and calculating jitter. Since jitter calculation from a selected MFP pair is straightforward, the focus of this chapter is on the first two sections.

6.2 Serial MFP Tracking and Selection Algorithm

6.2.1 Basic Idea

As emphasized in Chapter 3, MFPs of at least one pair of near muscle fibers have to be detected correctly and consistently for measuring jitter. Now since near MFPs of ISO-MUPs have been identified, the key problem described in this chapter is how to determine which near MFPs are created by the same muscle fiber. In this thesis, MFPs created by one muscle fiber are called serial MFPs and the corresponding problem was called serial MFP tracking. Essentially, this tracking problem can also be dressed as a pattern recognition problem and solved by a classification system like the system

described in chapter 5. However, the philosophy behind this problem is a simple fact that MFPs created by the same muscle fiber are temporally located at approximately the same position relative to MUPs in an MUPT because of the relatively consistent activation times of muscle fibers in an MU. So serial MFPs can be tracked by their locations in each MUP in a train, which allows us to generate a simple classification rule directly:

- If two MFPs are detected almost at the same position of two ISO-MUPs in an MUPT, they belong to one series of MFPs.

After the tracking process, MFP pairs can be selected from those series of MFPs which are consistently detected across the MUPT. Neuromuscular jitter can then be calculated based on each pair of MFPs.

6.2.2 Challenges

The principles of the finial jitter measurement step are straightforward and nothing intricate. Nevertheless, the effect of biological variations and instrumentation noise on detected MFPs and MUPs make the process easier said than done in practice. For serial MFP tracking, the waveforms of ISO-MUPs are not exactly identical and the locations of a series of MFPs may differ a lot from each other, especially when jitter is large. Meanwhile, as neuromuscular jitter increases, blocking appears more frequently which means some near MFPs may not be detected in some MUPs when the corresponding NMJ fails. Moreover, besides the residual SUP-MUPs falsely detected by the preprocessing step, the superposition of multiple MFPs (SUP-MFPs in short) in one MUP is also a challenge for tracking. Compared to the SUP-MUPs, the number of SUP-MFPs goes up with increasing jitter and can be a more serious problem for jitter measurement. In addition, simulated MUP data used in this research were sampled at 31.25 kHz (i.e., sampling time interval of 32 μs), which does not satisfy the time resolution for measuring jitter since it normally ranges from 5 to 50 μs and requires a time resolution of at least 1 μs. In conclusion, only stable, smooth, and non-bifurcated near MFP contributions are qualified for jitter measurement. Therefore, the shapes of detected near MFP peaks have to be analyzed as well as their locations, and compared to the expected features (or 'typical' features in [Ma 2003, Wang 2005]) of the serial MFPs to make assignment decisions.

6.2.3 Method

In Ma's thesis, the expected number, occurrence times and amplitudes of serial MFPs were determined based on a preliminary set of filtered MUPs and by some arbitrary threshold [Ma 2003]. The MST algorithm was applied to detect individual MFP contributions belonging to the same series of MFPs, because ISO-MUP identification and near MFP peaks recognition had not been carried out previously and independently before jitter measurement. In this research, most of the SUP-MUPs have been excluded from MUPTs by the preprocessing step, and only near and a few distant MFP peaks have been recognized using the designed PR system. Therefore, MFP peaks for jitter measurement can be tracked and selected simply based on the similarity of their location and amplitude to those expected values.

Following the work of Ma and Wang [Ma 2003, Wang 2005], the first positive peak in each filtered MUP was aligned as a reference, the expected number, occurrence times and amplitudes of near MFP contributions were then determined based on the ISO-MUPs template. The average amplitude of the baseline noise was also considered to determine amplitude assignment thresholds for tracking serial MFPs.

As for blocking, it has to be separately processed since the blocking rate is also an important clinical reference of NMJ transmission. A blocking will be recognized once no similar MFP peak has been found in the searching interval around the expected peak. MUPs with any blocked MFP contribution are excluded for jitter calculation of that series of MFPs, but they are counted to measure the corresponding blocking rate.

To deal with the problem of superposition, the amplitude of each MFP peak is checked along with its location during tracking, since the sharpness and slope ratio of a MFP peak has been verified as described in Chapter 5. If the NMJ axial positions of two muscle fibers in an MU are so close that most of their detected MFP peaks across an MUPT are completely overlapped with each other, the two serial MFPs can not be distinguished by MFP detection and serial MFP tracking. Therefore, a further inspection of such kind of superposition is carried out during the MFP selection process. An MFP peak is actually superimposed by two MFPs if a bifurcation of its peak has been detected. Once a bifurcation has been found, the whole series of MFPs has to be excluded for jitter calculation, because the bifurcated MFP series actually carries variations of two or more NMJs and can not be estimated as one MFP.

However, the criterion defining a bifurcation has to be robust to reduce the effects of noise and some accidental superposition, e.g., the amplitude of these bifurcating peaks should both be much larger than the expected amplitude of the noise.

In order to enhance the time resolution of measured jitter, a suitable interpolation must be applied to the detected MUPs. The cubic spline interpolation technique introduced by Ma [Ma 2003] with increased sampling rate of 967.5 kHz was also applied in this research to obtain a time resolution of exactly 1 μs.

6.2.4 Procedure

To meet the challenges of serial MFP tracking and selection, the whole procedure of the final jitter measurement step can be summarized by the flowchart shown in Figure 6.1. To evaluate the procedure in this chapter, simulated data was created with different expected jitter values. Note that neuromuscular jitter actually is a test corresponding to each NMJ, so the jitter calculated based on each pair of available near MFPs were calculated as one result. The details of the jitter measurement procedure are introduced in the following sections.

6.2.4.1 Tracking of a Serial MFP across all ISO-MUPs in an MUPT

To resist to the inevitable distortion of MFPs caused by the errors left by previous processes, biological variability like jitter, or instrumentation noise, robust tracking of serial MFPs with additional amplitude checking was designed. The searching interval for an expected MFP was determined by the expected location of this MFP and the IPIs between it and other MFPs, e.g. 'expected location +/- coefficient × IPI'. The acceptable range of amplitude was a robust range around the amplitude of the expected MFP, which was controlled by the average amplitude of all expected MFPs and the root mean square (RMS) of the baseline noise. Considering the average amplitude was to make the checking range more resistant to the slight superposition of MFPs, while the RMS of the baseline noise was taken into account to eliminate the effect of noise. Because of the joint checking of location and amplitude of a MFP, both thresholds can be more relaxed and robust to the variability of MFPs caused by slight superposition or noise. One example is shown in Figure 6.2, where different markers stand for different serial MFPs tracked.

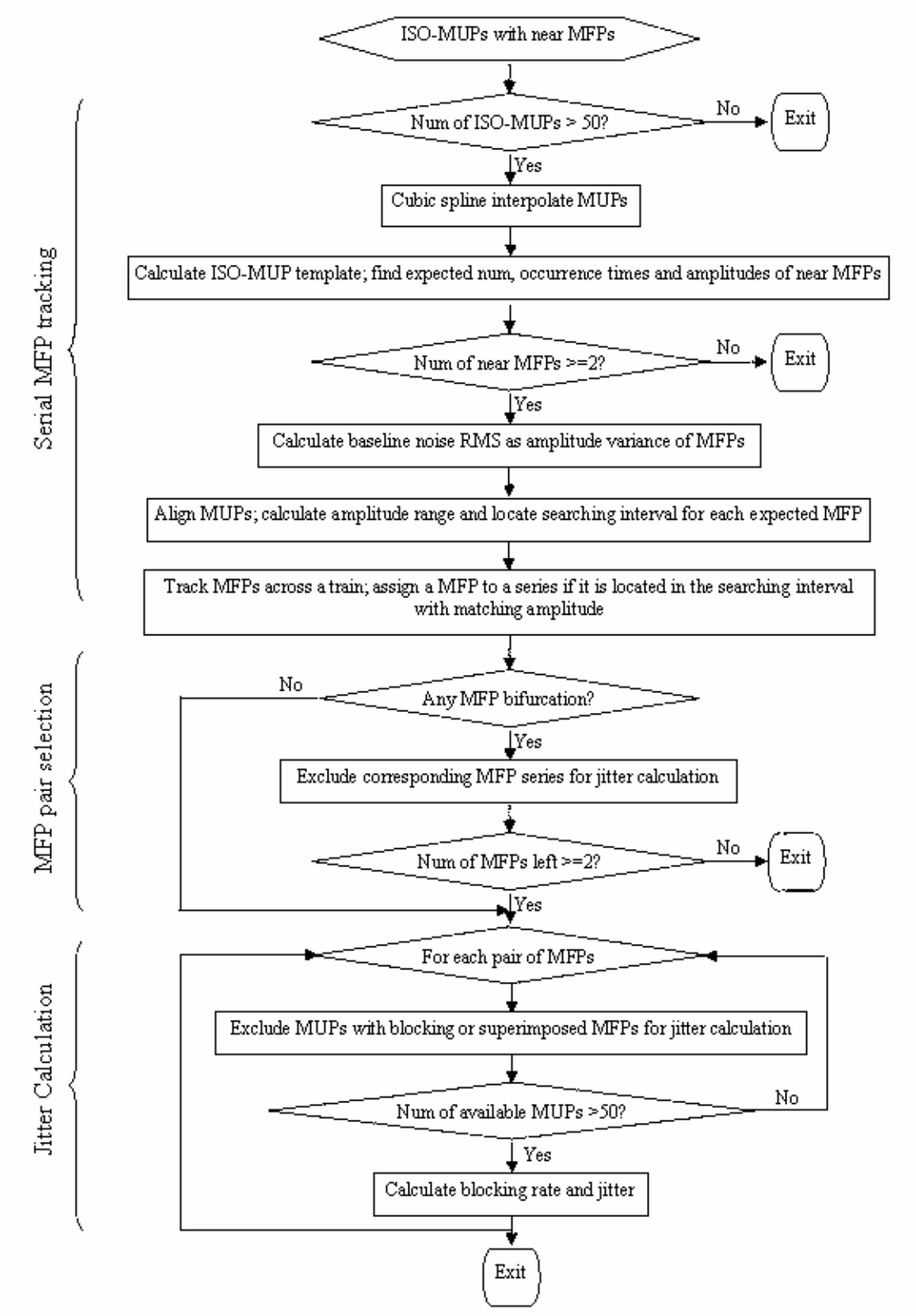

Figure 6.1: Flowchart of jitter measurement from near MFPs of ISO-MUPs in a train

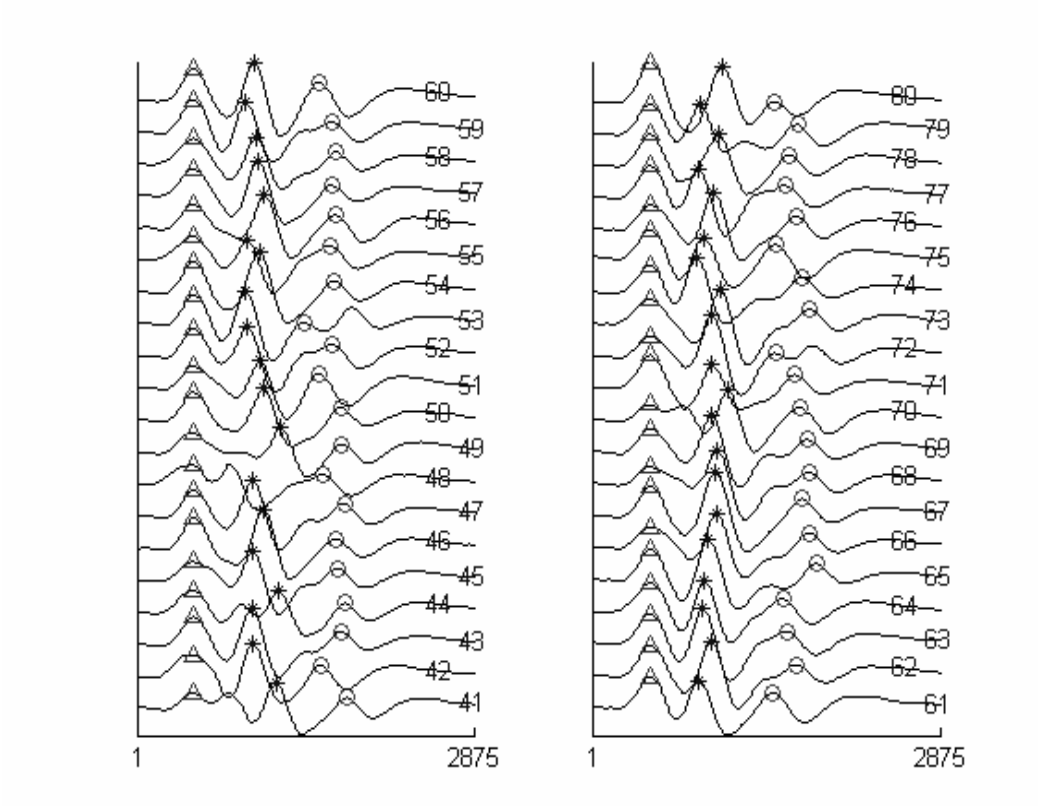

Figure 6.2: An example raster showing serial MFP tracking results of one MUPT with three near MFPs and an expected jitter value of 50 us (Note different MFP series are marked using different markes)

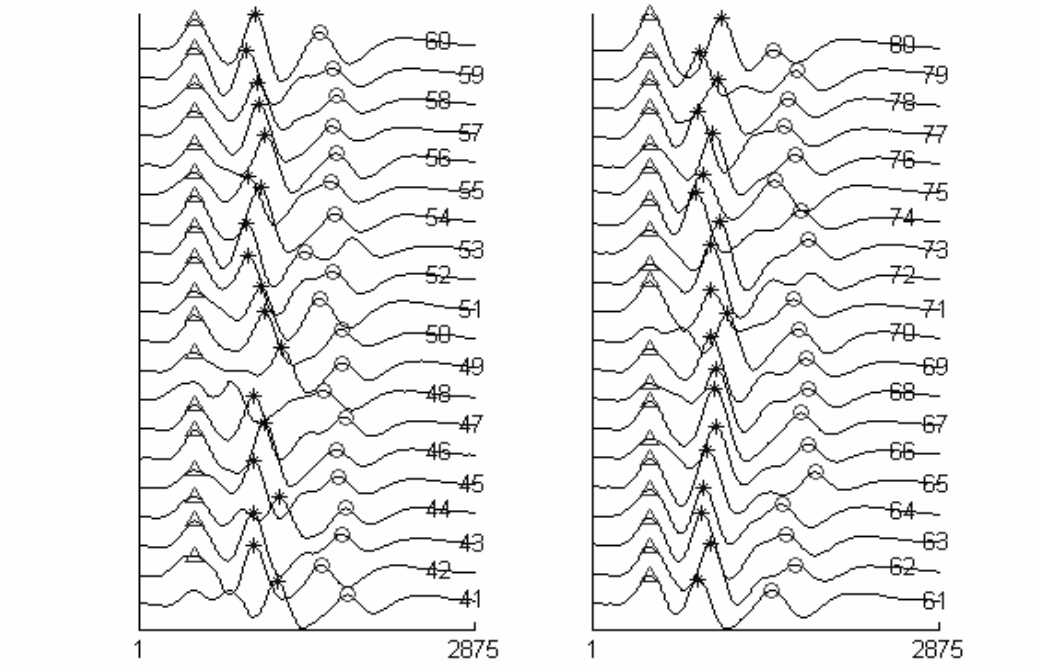

Figure 6.3: MFP Selection Result for the same MUPT in Figure 6.2. Unmarked peaks are not selected for jitter measurement.

However, a medium to complete superposition of MFPs may still not be distinguished by tracking, e.g., when two MFPs are almost completely overlapped across the MUPT except the small bifurcations of a few detected peaks. Therefore, in order to eliminate the effect of MFP superposition, a MFP selection process is necessary.

6.2.4.2 Typical MFP Pair Selection

The tracked MFPs have to be further selected to exclude the medium to complete superposition of MFPs. When two near muscle fibers have similar axial NMJ locations, some of their detected MFPs may be temporally overlapped to some extent and their detected peaks may be smoother and blurred due to the superposition. This kind of superposition is categorized as medium superposition in this thesis. A serial MFP with some medium SUP-MFPs can still be used for jitter measurement after removing these superimposed ones. However, if two MFPs are so close in time that most of their firings are detected as one MFP peak except a few bifurcated peaks, they are almost not distinguishable by corresponding MFP peaks, and have to all be excluded from jitter measurement. Therefore, to measure jitter accurately and robustly, bifurcation and superposition of MFPs have to be processed separately. When two (or more) MFPs are tracked within one searching interval with proper amplitudes, they are defined as a superposition of MFPs if their occurrence interval is relatively large; otherwise they are recognized as a bifurcation. For example, if two peaks are detected within a time interval of 500 μs but longer than 350 μs, they are recognized as medium SUP-MFPs; or bifurcated MFPs if their time interval is smaller than 350 μs, where 500 and 350 μs are empirical thresholds. For both situations, the amplitudes of both peaks also have to be larger than a threshold of baseline noise so that the noise on a MFP peak does not cause the detection of two peaks (i.e., a bifurcation).

The MFP selection result for the same MUPT shown in Figure 6.2 is shown in Figure 6.3, where the first MFP peaks of MUPs NO. 41, 48, 70 and the third peak of MUP NO. 72 are SUP-MFPs and not selected for jitter measurement. Note that not all SUP-MFPs are recognized since the interfered MFP peak may be detected as another individual MFP or may not even be detected. For example, the fourth peak of MUP NO. 53 was recognized as an individual MFP; the small peak before the third one of MUP NO. 69 was actually not detected as a peak.

6.2.4.3 Blocking Identification and Jitter Measurement

If no matched positive peak is found in a corresponding searching interval, a blocking is identified. The percent blocking is calculated by the ratio of the number of detected blockings to the total number of MUPs.

Neuromuscular jitter is calculated using the MCD statistic (see Chapter 2 for details). To calculate the jitter of a MFP pair, at least 50 MUPs are required [Sanders 1996]. Jitter measurements were evaluated using a synthetic MUPT that modeled signals detected using CN electrodes during voluntary muscle contraction (level 5% MVC). In addition, the percentage of blocking was also measured as the larger one between two blocking rates of the two serial MFPs of the pair.

6.3 Independent Experiment

6.3.1 Simulated Data

To evaluate the jitter measurement step independently, a typical simulated EMG signal was generated repeatedly with different jitter values. Instead of being determined by the near MFP peak recognition system, the expected number and occurrence times of near MFPs were input manually after visually checking. Since visually checking results can be considered as a gold standard, the influences of previous procedures were eliminated. However, in order to investigate the performance of the jitter measurement step under the same conditions as in the whole system, proper amounts of errors were kept in the simulated EMG signal, e.g., a relatively low SUP-MUP ratio, which stands for the false identification error of ISO-MUP from the preprocessing step, and some peak detection error representing the error of the near MFP recognition process.

The simulator employed in this thesis provides an optional function for jitter evaluation that models enormous fibers at known locations close to the detection surface of the electrode. Although the ‘super’ MUPs created are based on an unnatural layout of a muscle, the simulated MUPs consist of multiple near MFP contributions which are especially useful for the evaluation of jitter measurement. A typical MUPT composed by three near MFPs and two distant MFPs was employed as example data to evaluate the jitter measurement procedure in this chapter. All data were generated at a contraction level 5% MVC with a signal to noise ratio of 25. The templates of this

MUPT with two different jitter values were compared in Figure 6.4, where the peaks with larger jitter values tends to be smaller and noisier than the one with lower jitter due to the increasing variability of the MUPs.

6.3.2 Results

Jitter measurement results of the example train are listed in Table 6.1 and 6.2 with different ways of treating bifurcated MFPs, i.e., removing MFP series with bifurcated MFPs or excluding bifurcated MFPs, where the percentage error is calculated by:

$$\text{Percentage Error} = \frac{\sum_{i=1}^{n} \left| \text{Measured Jitter}_i - \text{Expected Jitter} \right|}{n \cdot \text{Expected Jitter}} \times 100\%,$$

where n is the number of MFP pairs.

Table 6.1: Experiment Result Excluding the Superimposed MFPs and Bifurcated MFP serials

Expected Jitter (us)	Num. of SUP-MUPs based on Gold Standard	Num. of SUP-MFPs Detected	Num. of Bifurcated MFPs Detected	MFP Pair 1 (1 and 2)		MFP Pair 2 (1 and 3)		MFP Pair 3 (2 and 3)		AVE. Error of Jitter (%)
				Jitter (us)	Blocking Rate (%)	Jitter (us)	Blocking Rate (%)	Jitter (us)	Blocking Rate (%)	
25	7	1	0	24.7	0	30.9	0	29.6	0	14.5
50	14	1	0	50.3	0	61.6	0	57.0	0.4	12.6
75	8	8	2	66.8	0					11.0
100	9	23	0	93.9	0	118.0	0	113.3	2.6	12.5
125	3	42	2							
150	10	75	4							

Table 6.2: Experiment Result Excluding the Superimposed (including Bifurcated) MFPs

Expected Jitter (us)	Num. of SUP-MUPs based on Gold Standard	Num. of SUP-MFPs Detected	Num. of Bifurcated MFPs	MFP Pair 1 (1 and 2)		MFP Pair 2 (1 and 3)		MFP Pair 3 (2 and 3)		AVE. Error of Jitter
				Jitter (us)	Blocking Rate (%)	Jitter (us)	Blocking Rate (%)	Jitter (us)	Blocking Rate (%)	
25	7	1	0	24.7	0	30.9	0	29.6	0	14.5%
50	14	1	0	50.3	0	61.6	0	57.0	0.4	12.6%
75	8	8	2	66.8	0	93.9	0	74.6	1.8	12.2%
100	9	23	0	93.9	0	118.0	0	113.3	2.6	12.5%
125	3	42	2	108.0	0.4	121.3	0	118.0	6.6	7.4%
150	10	75	4	123.9	1.3	185.7	0	147.0	4.4	14.4%

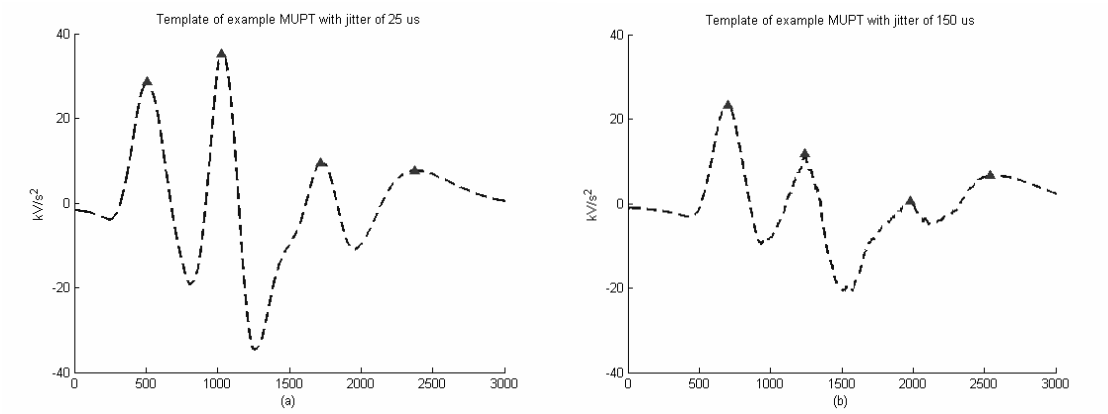

Figure 6.4: Templates of the experimental MUPT with jitter of (a) 25 us and (b) 150 us. The triangles mark the detected peaks. The first and third peak is a superposition of one near MFP and one distant MFP, and the last peak is a false peak.

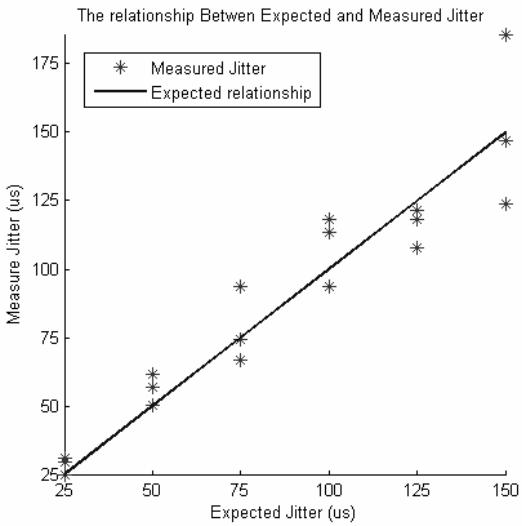

Figure 6.5: The expected jitter value and measured jitter value of results in Table 6.2

Table 6.1 and 6.2 show that the number of detected SUP-MFPs is not affected by the relative low false ISO-MUP identification errors, but directly related to the expected jitter. This is reasonable since the probability of MFP overlapping goes up with increasing jitter, while the slight superposition by another MUP may not affect the MFP peaks. The number of detected bifurcated MFPs also does increase with jitter as expected. Though muscle fibers created by the simulator never block, blocking was still recognized when a MFP was canceled by other MFPs, i.e., a negative superposition. The relationship between expected and measured jitters is shown in Figure 6.5.

From the comparison of Table 6.1 and Table 6.2, one can find that excluding the whole serial MFP in which one or more MFPs bifurcate can eliminate errors in jitter measurement caused by the corresponding superpositions. Meanwhile, jitter may be immeasurable due to the reduced number of available MFP series. The balance between accuracy and measurability has to be considered in real clinical testing, though the strategy described in Table 6.1 was applied to the system designed in this thesis.

6.4 System Experiment

To evaluate the whole jitter measurement system, the simulated database introduced in Chapter 4 (see Table 4.1), which is called Data Base 1, could be used. However, since that data base was created for evaluation of identification of ISO-MUPs, almost all MUPs only have one near MFP, and the only train which is composed of multiple near MFPs has bifurcation problems. Therefore, a new database was created for evaluating the whole jitter measurement system. A Data Base 2 was created taking advantage of the 'super' muscle fiber generation option of the simulator. The two data bases have the same structure except that the contraction levels of 17.5% and 20% MVC are not considered in the system experiment since these levels of intensity are never expected during clinical testing. The acceleration threshold of 7.5 kV/s^2 was used to define near MFP peaks in Data Base 2. The general information and the ISO-MUPs identification errors of Data Base 2 are listed in Table 6.3. Note that the optimal parameters for the MST-based two-phase clustering algorithm were changed because the acceleration of the MUPs (or filtered MUPs) would be used instead of the raw MUP waveforms. (The raw signal is used wider in EMG signal decomposition system, so the ISO-MUP identification algorithm in Chapter 4 was evaluated based on it.) The empirical optimal parameters applied to the ISO-MUP identification step is CAT: 1 and COV_3: 4. The final jitter measurement results are shown in Table 6.4 as well as the blocking rate.

Observed from Table 6.4, the blocking rates measured were quite low since the simulator does not generate MUPs with blocking. Most jitter values measured matched the expected ones except those large ones at relative high contraction level. This is because some MUPs differ a lot from others in an MUPT due to the variation caused by large jitter so that they may be excluded as SUP-MUPs during the ISO-

MUP identification step, i.e., the missed errors of the preprocessing step cause underestimation of jitter. Some other measured jitter values shifted from the expected ones when they are small because of the false detection of MFP peaks. For example, one MUPT with expected jitter of 25 μs and measured jitter of 43 μs at a contraction level 15% MVC is partly shown in Figure 6.6. The first peak of each MUP is not sharp enough to be accurately detected, so its location is severely affected by noise. This kind of peak should be recognized as a distant peak in the peak detection step, and not used for measuring jitter. In practice, peaks without enough amplitude would not be counted as near MFP peaks, so that such types of errors can be avoided in a real implementation.

Table 6.3: Errors of Iso-MUP identification of filtered MUP in Data Base 2

Data Set	Contr. Level / Intensity (pps)	Num. of Trains	Sup-MUP Ratio (%)	Missed Error Rate (%)		False Error Rate (%)		Error Cost (%)	
				Maximum	Average	Maximum	Average	Maximum	Average
1	5.0 / 16.8	2	4.6	2.9	1.5	3.6	1.7	2.2	1.6
2	7.5 / 27.9	3	7.9	3.4	2.2	3.3	1.8	2.3	2.0
3	10.0 / 47.2	5	14.4	3.4	2.4	8.3	4.2	4.7	3.2
4	12.5 / 70.1	7	21.3	4.5	3.5	9.6	5.3	6.8	4.3
5	15.0 / 90.1	8	27.9	4.6	3.4	11.5	6.8	7.0	4.9

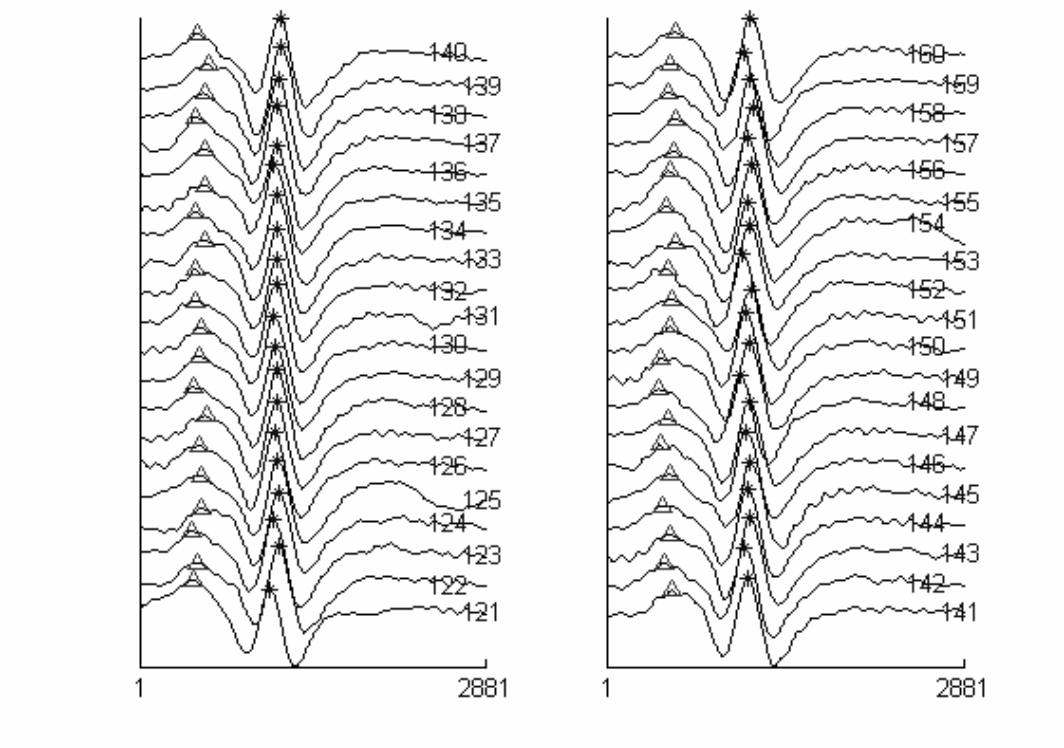

Figure 6.6: Raster of an MUPT with overestimated jitter

Table 6.4: Test results of Data Base 2

Contr. Level / Intensity (p.p.s.)	Num. of Trains	Expected Jitter (us)	Num. of Avail. MFP pairs	Measured Jitter				Blocking Rate		
				Jitter (us)	Mean	MAD	Percent Error (%)	Blocking Rate (%)	Mean	MAD
5.0	2	25	4	31 26 29 24	27	2.5	9.1	0 0 0 0	0	0
		50	4	57 46 60 46	52	6.2	4.0	0 0 0 0.5	0.1	0.2
		75	1	83	83	0	11.1	0	0	0
		100	1	105	105	0	5.4	0	0	0
16.8		150	0							
7.5	3	25	4	37 31 38 30	34	3.6	35.9	0 0 0 0	0	0
		50	2	51 53	52	0.8	3.4	0 0	0	0
		75	2	76 69	73	3.9	3.3	0 0	0	0
27.9		100-150	0							
10.0	5	25	5	39 35 36 33 41	37	2.8	47.5	0 0 0 0 0	0	0
		50	2	52 63	57	5.4	14.7	0 0	0	0
		75	1	66	66	0	11.6	0	0	0
		100	1	100	100	0	0.4	0.5	0.5	0
47.2		125	1	94	94	0	25.1	0.7	0.7	0
		150	0							
12.5	7	25	4	42 34 40 35	38	3.4	52.1	0 0 0 0	0	0
		50	2	52 56	54	2.1	8.6	0 0	0	0
		75	2	71 77	74	3.4	1.3	0 0	0	0
70.1		100-150	0							
15.0	8	25	4	37 35 43 37	38	2.6	53.0	0 0 0 0	0	0
		50	2	50 58	54	4.0	7.3	0 0	0	0
		75	3	68 78 80	75	5.0	0.3	0 0.9 0	0.3	0.4
		100	5	86 83 94 97 105	93	6.8	7.3	0 0.9 1.6 1.6 1.6	1.2	0.6
		125	1	107	107	0	14.3	3.4	3.4	0
90.1		150	0							

Totally, only 51 MFP pairs were selected from Data Base 2. In order to thoroughly evaluate the jitter calculation step as well as the whole automated jitter measurement system, further experiments need to be done using simulated data and real data with a gold standard for jitter measured using the SF-EMG technique.

6.5 Discussions

Although the principle of jitter measurement is straightforward, the operation has to be tolerant of the errors created by previous steps, the biological variability inherent in an EMG signal and instrumentation noise. A robust procedure composed by three functional sections was described in this chapter, where the peak amplitude of a MFP

was employed for serial tracking along with the occurrence time and superpositions and bifurcations were excluded for MFP selection.

Since the designed procedure is stable and just sensitive to changes of jitter values, one typical MUPT was simulated with different jitter values to exemplify and evaluate the jitter measurement step independently. The designed jitter measurement procedure is robust to errors created by the previous steps to some extent. As long as the errors are kept in the proper range as discussed in pervious chapters, the whole jitter measurement system can be accurate and robust. However, some details of the design of the last step could be further discussed. For example, amplitude threshold could be adjusted to eliminate the effect of falsely recognized peaks which causes the overestimation as shown in Figure 6.6. The underestimation of jitter when the expected value is large can be reduced by making the serial MFPs tracking range adaptive to the jitter. In addition, the definition of bifurcation and superposition of MFPs should be reconsidered carefully for the trade of accuracy and measurability. Finally, experiments on real EMG signals need to be carried out for validation in the future.

Preliminary experiments using a small synthetic data base of 'super' MUPs were done for evaluating the whole jitter automated measurement system. The result showed that most of the measured jitter values match the expected ones. Compared to the reported average error of jitter measurement 8.37% at contraction level 5% of MVC in [Ma 2003], the corresponding error of the whole system tested by the small data set was 7.40%. The system designed in this thesis is also aimed to measure jitter under different muscle firing intensities which has not been studied by former researchers. Since the algorithms were fundamentally developed and each step of the whole procedure was evaluated by simulated data, further refinement and adjustment should be carried on using a large simulated data base and real data. Furthermore, the designed system will be evaluated using real data with a gold standard and compared to the traditional SFN EMG method. Ultimately, the system will be integrated into the DQEMG system for clinical testing in the future.

Chapter 7
Conclusions, Contributions and Future Work

In order to facilitate the study of neuromuscular disorders using disposable routine electrodes, an automated jitter measurment system based on the decomposition of CN detected EMG signals was developed and preliminarily evaluated in this thesis. The designed system comprises three functional modules for excluding SUP-MUPs, identifying near MFPs and calculating jitter, which are described separately in three chapters in this thesis.

In addition to being a preprocessing step of the jitter measurement system, identifying ISO-MUPs is also important for detailed EMG signal decomposition. The proposed MST-based two-phase clustering algorithm demonstrates higher accuracy, robustness and stability than the MST clustering algorithm or the template-based algorithm. A simulation experiment obtained results with missed error rates less than 5% and false rates less than 15% simultaneously.

After preprocessing, the near MFP contributions to an ISO-MUP can be recognized by properly filtering the MUP and classifying the detected peaks using the proposed quadratic discriminant classifier (QDC). A pattern recognition system was employed for the classifier design, and the weighted average error obtained was less than 10%. In practice, the QDC can be simplified as a linear discriminant classifier (LDC) if only true and false MFP peaks have to be distinguished.

Finally, jitter can be measured from the near peaks detected from ISO-MUPs in an MUPT, though the practical process also has to be robust to biological variation, errors from previous steps and instrumentation noise. The flowchart of this step is divided into three sections: serial MFP tracking, MFP pair selection and jitter calculation. A preliminary experiment using simulated data demonstrated the efficiency of the designed system.

The performance of each step was evaluated independently using simulated data as well as the whole system. The measurement results suitably matched the expected values based on the simulation experiments. The measurement error principally

resulted from the effects of noise and overlapping of individual MFPs. Compared to the initial algorithm created by Ma and Wang [Ma 2003, Wang 2005], in which the three functional modules are interactive and iterative, the designed system proposed in this thesis is well modularized which allows each step to be modified, evaluated, and reused in other applications independently. Furthermore, the proposed system demonstrated an improved performance over a variety of EMG signals compared to the initial algorithm, e.g., average jitter measurement error of 7.40% versus 8.37% at contraction level of 5% of MVC. In addition, the effect of muscle contraction level on jitter measurement was also studied in this thesis, which was not previously investigated. Ma and Wang worked on the basic idea of measuring jitter based on decomposed CN-EMG signal; the work done in this thesis created algorithms and a scheme for practical application. For example, the MST clustering algorithm is improved for ISO-MUPs identification, the optimal classifier for near MFP recognition is implemented, and a complete procedure for jitter calculation using detected MFPs is suggested.

However, due to time constraint, the last step of the jitter measurement system is not fully developed, i.e., the serial MFP tracking and typical MFP pair selection parts can be improved by adjusting the thresholds iteratively. The parameters can be further adjusted and optimized for each step using a large simulated data base and real data. Last but not least, the system has not been fully validated, especially using the real data that is difficult to collect. To implement the automated jitter measurement system clinically, the optimization of each step as well as the whole system should be carried out using real EMG data and compared to reference values measured using SF-EMG techniques. In addition, the degree of MFP superposition or minimal IPI which can be tolerated for measuring jitter accurately could be investigated in detail.

Although the system designed in this thesis has not been fully validated, the algorithms and the whole scheme are demonstrated to be powerful enough for jitter measurement based on decomposed CN-EMG signals. The three functional modules can also be applied to other application areas in EMG signal processing, e.g., the MST-based two-phase algorithm has been implemented in DQEMG to remove superimposed MUPs for calculating MUP templates. The system can also be used to measure jitter based on decomposed MN-EMG signals, or even calculate fiber density once the MFPs for an MU can be clearly counted from the decomposed MUPs.

Bibliography

[1] Antoni L, Stalberg E, and Sanders D. Automated analysis of neuromuscular 'jitter'. *Computer Programs in Biomedicine* 1983; 16: 175-188.

[2] Benatar M, Hammad M, and Doss-Riney H. Concentric-needle single-fiber Electromyography for the diagnosis of Myasthenia Gravis. *Muscle Nerve* 2006; 34: 163-8.

[3] Barnes RJ, Dhanoa MS, and Lister SJ, Standard Normal Variate Transformation and De-trending in Near-Infrared Diffuse Reflectance Spectra, *Applied Spectroscopy* 1989; 43 (5): 772-777.

[4] Basmajian JV and Deluca CJ. *Muscles Alive: Their Functions Revealed by Electromyography (5th edition)*. Williams and Wilkins, Baltimore, MD. USA, 1985.

[5] Boron WF and Boulpaeq EL. *Medical Physiology: a Cellular and Molecular Approach* (1st edition), Philadelphia, PA. USA, 2003.

[6] Brown WF. *The Physiological and Technical Basis of Electromyography*. Butterworth Publishers, Stoneham, MA. USA, 1984.

[7] Buchman A Garratt M. Determining neuromuscular jitter using a monopolar electrode. *Muscle Nerve* 1992; 15: 615-9.

[8] Clarke S and Eisen A. Electromyographic jitter measured using a monopolar electrode. *Neurology* 1985; 35 (Suppl): 69.

[9] Duda RO, Hart PE, and Stork DG, *Pattern Classification*, Wiley, Second Edition, 2000.

[10] Dumitru D, Zwarts MJ, and Amato AA. *Electrodiagnostic Medicine (2nd edition)*. Hanley & Belfus, Philadelphia, PA. USA, 2002.

[11] Eatas M, Baslo MB, Yildiz N, et al. Concentric needle electrode for neuromuscular jitter analysis. *Muscle Nerve* 2000; 23: 715-719.

[12] Etawil H and Stashuk DW, Resolving superimposed motor unit action potentials, *Med. & Bio. Eng. & Comput.* 1996; 34: 33-40.

[13] Guiheneuc P, Calamel J, Doncarli C, et al. Automatic Detection and Pattern Recognition of Single Motor Unit Potentials in Needle EMG. *Computer-Aided Electromyography (progress in clinical neurophysiology 1983; 10: 73-127)*. Karger, Basel, NY. USA, 1983.

[14] Hamilton-Wright A and Stashuk DW. Physiologically based simulation of clinical EMG signals. *IEEE Transactions on Biomedical Engineering* 2005; 52 (2): 171-183.

[15] Hastie T, Tibshirani R, and Friedman J, *The Elements of Statistical Learning*, Springer, New York, NY, USA, 2001.

[16] Juszczak P, Learning to recognise A study on one-class classification and active learning, *PhD thesis* 2006, Delft University of Technology.

[17] Kandel ER, Schwartz JH, and Jessell TM. *Principles of Neural Science (4th edition)*, McGraw-Hill, USA, 2000.

[18] King JC, Dumitru D, Nandedkar S. Concentric and single fiber electrode spatial recording characteristics. *Muscle Nerve* 1997; 20 (12): 1525-1533.

[19] Kruskal JB, On the shortest spanning subtree of a graph and the traveling salesman problem. *Proc. Amer. Math. Soc.* 1956; 7: 48-50.

[20] Loof Yngve. Improving Electromyographic Jitter Measurements by Analysis of the Firing Pattern. *IEEE Transactions on Biomedical Engineering* 1990; 37 (11): 1105-1114.

[21] Ma Sh. Measuring Neuromuscular Jitter in Motor Unit Potentials. *Master Thesis*, University of Waterloo, Waterloo, Ontario, 2003.

[22] McGill K. A method of quantitating the clinical electromyogram. *PhD Thesis*, Stanford University, Stanford California, 1984.

[23] Merletti R and Parker PA. *Electromyography: Physiology, Engineering, and Noninvasive Application*. IEEE/John Wiley & Sons, Hoboken, NJ. USA, 2004.

[24] Payan J. The blanket principle: a technical note. *Muscle Nerve* 1978;1:423-426.

[25] Sarrigiannis PG, Kennett RP, Read S, et al. Single-fiber EMG with a concentric needle electrode: validation in Myasthenia Gravis. *Muscle Nerve* 2006; 33: 61-5.

[26] Sanders DB and Stalberg E, AAEM Minimonograhp #25: single-fiber electromyography. *Muscle Nerve* 1996; 19:1069-1083.

[27] Sankar KP and Pabitra M, Pattern Recognition Algorithms for Data Mining, *Boca Raton: Chapman & Hall / CRC*, 2004, Ch. 1.

[28] Slawnych M, Laszlo C, and Hershler C, Motor unit estimates obtained using the new "MUESA" method, *Muscle & Nerve* 1996; 19: 626-636.

[29] Stalberg E, Ekstedt J, Broman A. The electromyographic jitter in normal human muscles. *Electroencephalography and Clinical Neurophysiology* 1971; 31(5): 429-438.

[30] Stalberg E and Antoni L. Computer-Aided EMG Analysis. *Computer-Aided Electromyography* (progress in clinical neurophysiology 1983; 10: 186-234). Karger, Basel, NY. USA, 1983.

[31] Stalberg E and Trontelj JV. The study of normal and abnormal neuromuscular transmission with single fibre electromyography. *J Neurosci Methods* 1997; 74: 145-154.

[32] Stalberg E. Measuring jitter with concentric needle electrodes. *Clinical Neurophysiology* 2006; 117 (S1): S6.

[33] Stashuk DW. Simulation of electromyographic signals. *Journal of Electromyography and Kinesiology* 1993; 3: 157-173.

[34] Stashuk DW. Decomposition and quantitative analysis of clinical electromyographic signals. *Medical Engineering & Physics* 1999a; 21: 389-404.

[35] Stashuk DW. Detecting single fiber contributions to motor unit action potentials. *Muscle Nerve* 1999b, 22: 218-229.

[36] Stashuk DW. EMG signal decomposition: how can it be accomplished and used? *Journal of Electromyography and Kinesiology* 2001; 11: 151-173.

[37] Stewart CR, Nandedkar SD, Massey JM, et al. Evaluation of an automatic method of measuring features of motor unit action potentials. *Muscle Nerve* 1989; 12: 141-8.

[38] Tutkavul K, Baslo MB, Ertas M, et al. Evaluation of neuromuscular transmission by using monopolar needle electrode. *Acta Neurol Scand* 2006; 114: 340-345.

[39] Tvrdon M, Stashuk DW, and Ali A. The measurement of neuromuscular junction jitter using a concentric needle electrode: a simulation study. 1995 *IEEE-EMBC and CMBEC Neuromuscular Systems/Biomechanics*; 1325-1326.

[40] Tang J, Chen ZhX, Fu AW, and Cheung DW, Capabilities of outlier detection schemes in large datasets, framework and methodologies, *Knowledge and Information Systems*, 2005, 00: pp. 1-41.

[41] Wiechers DO. Single fiber electromyographyu with a standard monopolar electrode. *Arch Phys Med Rehabil* 1985; 66: 47-48.

[42] Wang X. Automatically Measuring Neuromuscular Jitter. *Master Thesis*, University of Waterloo, Waterloo, Ontario, 2005.

[43] Webb AR, *Statistical Pattern Recognition*, Arnold, New York, NY, USA, 1999.